Graduation Report Applied Mathematics

Magnetic Behaviour of a Steel Ellipsoid

Author:
Henk Jongbloed

Supervisors:
Prof. dr. ir. Arnold Heemink
Dr. ir. Eugene Lepelaars
ir. Aad Vijn

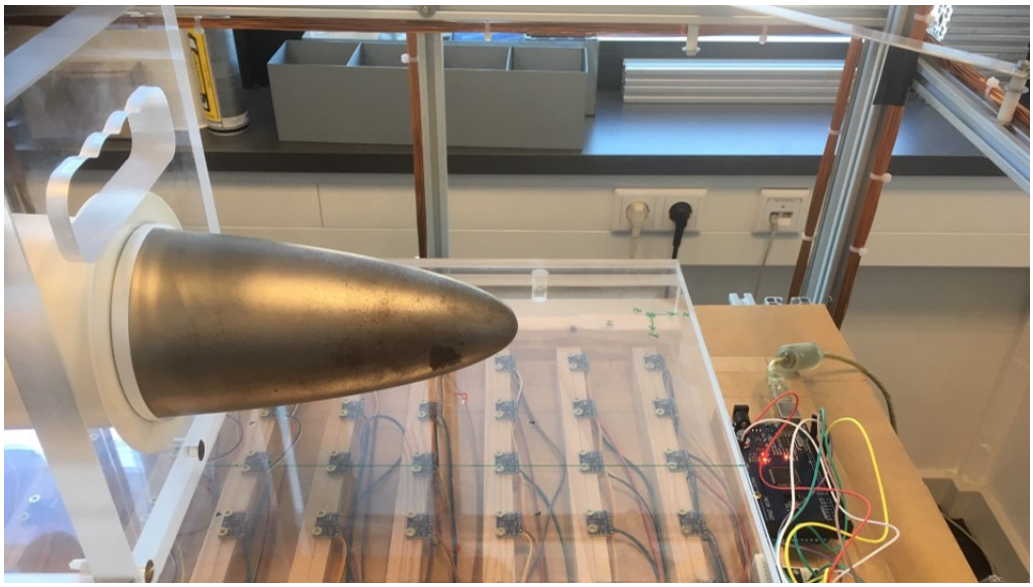

TU Delft TNO

December 16, 2019

Abstract

Context Reliable and efficient modelling of magnetic hysteresis in inhomogeneous and anisotropic media is an important step in developing a state-of-the-art closed-loop degaussing system for naval ships and submarines, to be developed by TNO and to be used by the Royal Netherlands Navy in an updated generation of naval vessels and submarines. Different models have been proposed to describe the nonlinear and history-dependent nature of ferromagnetic hysteresis at a material level.

With a focus on three key differing aspects of models, namely *linear* versus *nonlinear* (hysteresis), *isotropic* versus *anisotropic* and *homogeneous* versus *inhomogeneous*, we attempt to discriminate between the performance of models on the basis of these criteria. More specifically, with increasing model complexity, we have combined Maxwell's equations with four different hysteresis models within the context of a prolate steel ellipsoid, whose ferromagnetic properties evolve under the influence of a uniform applied background field. Among other aspects, the hysteresis models differ in terms of physical motivation, complexity and parameter spaces. In this research, we have analysed four hysteresis models in more detail: The *Induced - Permanent magnetization* model, The *Rayleigh* model, the *Jiles-Atherton* model and an *Energy-Variational* model, based on energy balances.

The thus derived forward models have subsequently been inverted in order to estimate material hysteresis parameters. With increasing complexity also, twin experiments have been performed. This increasing complexity *temporally* stems from the fact that the hysteresis models named previously, are stated in increasing order of complexity, and can all be modified in order to model anisotropic material by generalizing model parameters to tensors. *Spatially*, the increase in complexity is caused by the fact that in special cases, namely of uniform ellipsoid magnetization, an analytical formula relating the magnetic field, the background field and the ellipsoid magnetization exists by solving the Poisson partial differential equation on an infinite domain using direct computation with Green's functions.

When the problem conditions are relaxed by not requiring a uniform magnetization to be present inside the ellipsoid, this analytical result fails and one has to resort to numerical techniques. Using the Finite Element Method, we have approximated the solution to this non-uniform problem and formulated model inversions that provide a framework to both estimate the non-uniform magnetization distribution and the hysteresis parameters of the non-uniform or inhomogeneous ellipsoid model. Our iterative-based models allow for the material hysteresis parameters to also be location and time-dependent and provide a possibility for perhaps stochastic error analysis, data assimilation and in the end, a closed-loop degaussing algorithm. However, these last three elements have not been implemented yet.
Moreover, using a physical measuring device setup CLAViS located at TNO Oude Waalsdorperweg, different models have been fitted to a real-world steel ellipsoid, providing experimental validation of our models.

Results Using genetic algorithms, three out of four homogeneous hysteresis models, with the exception of the Energy-Variational model, have been successfully fitted to measured data. We have quantified the prediction error that was made by approximating the magnetic behaviour of the real ellipsoid by our simplified models. The homogeneous models, which have the property of only requiring time integration, are able to describe the ellipsoid magnetization only up to a uniform level. On the one hand, this makes estimating the magnetization 'distribution' very straightforward and overdetermined, on the other hand, it induces a larger prediction error, since measurements indicate that the magnetization of the experimental ellipsoid is not uniform. Using a signature-based mean squared error optimization algorithm, we have been able to estimate the optimal ellipsoid parameters in several different models, although more measurements are required to solidify our conclusions about these estimated parameters.
Resorting to the inhomogeneous models, which are able to describe non-uniform magnetization distributions and their signatures, one has considerably more freedom to estimate the realistic magnetization distribution, yielding a lower prediction error. By using a heuristic method of regularization that effectively drastically reduces the number of unknowns but nevertheless is able to model a wide range of magnetization distributions, we have estimated the magnetization distribution through time that minimizes the global squared signature error. The hysteresis parameters of inhomogeneous models have not been estimated and will be subject of further research.

Conclusions and Recommendations From our results, we can conclude that the ellipsoid exhibits all three aspects that were a priori established as interesting variations of models. This is concluded on the basis of the signature prediction error decreasing with model complexity increasing; indeed, the more flexible the model is in terms of both spatial and temporal range, the more accurately it can describe the very complex behaviour of the experimental steel ellipsoid. It is interesting to note that the **IP**homogeneous model has the smallest signature error of the homogeneous models by far, while being a relatively simple model. Since the hysteresis parameters of the inhomogeneous model have not been estimated, we cannot draw conclusions on the performance of these models in a temporal sense. However, we can conclude that homogeneous magnetization estimation is, in a certain sense, a subset of inhomogeneous magnetization estimation. Therefore, it is the case that inhomogeneous models have a much lower static inversion error than the simple homogeneous models. One might need to employ inhomogeneous hysteresis parameter distributions to approximate the behaviour of the real, measured ellipsoid optimally. Thereafter, data assimilation by combining the inverse magnetization distribution simultaneously with the temporal hysteretic evolution, yields a much more complete description and prediction of the ellipsoid magnetization evolution. Lastly, an outlook to closed-loop degaussing can be made by applying certain derived discretized operators to non-uniform applied magnetic background fields, which together with the prospect of data assimilation, yield hopeful thoughts about the future of the prolate steel ellipsoid and our understanding of it.

Notation

This section defines the notation in the current report. Please note that this section only lists general notation conventions. In case of deviation from these conventions, it will always be indicated.

General conventions

In general, the following conventions are used for the notation of scalars, vectors, tensors and matrices, as depicted in the table below. By 'physical vector' we always mean a vector from $\mathbb{R}^3$, for example a location vector or a magnetic field. By 'mathematical vector', we mean a vector of parameters or a solution to a system of equations in a finite element sense, for example.

Table 1: General notation conventions

x, μ_0	scalar	italic small or capital character
$\mathbf{x}$, $\mathbf{H}$	physical vector	bold-faced, straight, small or capital character
$\boldsymbol{x}$, $\boldsymbol{\phi}$	mathematical vector	bold-faced, italic, small character
$\underline{\boldsymbol{x}}$, $\underline{\boldsymbol{\alpha}}$	tensor	underlined bold-faced small character
$\underline{\mathrm{X}}$, $\underline{\Lambda}$	matrix	straight, underlined capital character

In the field of mathematical modelling, different ideas are often denoted by the same symbols. For someone working in a specific discipline, this can be self-explanatory, depending on the context. However, in the research discussed in this report, a physical problem is analysed using a variety of techniques and tools. For example, the magnetostatic scalar magnetic potential Φ is, strictly speaking, a function $\Phi : \mathbb{R}^3 \to \mathbb{R}$. In literature however, this value may refer to a vector quantity related to the actual potential, it may refer to the numerical approximation of the potential, or maybe a solution to a system of equations. All these notions are intimately related to the magnetic potential, but in order to avoid confusion, we have chosen to refer to different concepts by different symbols as much as possible.

List of Abbreviations

For magnetic quantities, we follow the standard work by Jackson [2]. In describing the various hysteresis models, the notation of original papers [24, 21, 39] has been used as much as possible, with some deviations which are indicated. The vectorial generalisations of these models are all parametrised by vectors and tensors, which causes the model notation to differ from their original introduction. The notation when discussing the Finite Element formulation of the problem and related notions, are mostly taken from [18]. Some general abbreviations are used throughout the report, explained below:

- **IP**: The induced - permanent magnetization model, which is somewhat linear in nature;
- **RA**: The Rayleigh hysteresis model;

- **JA**: The Jiles-Atherton hysteresis model;
- **EV**: The Energy-Variational hysteresis model;
- FEA : Finite Element Analysis;
- FEM : Finite Element Method;
- ODE : Ordinary Differential Equation;
- PDE : Partial Differential Equation;
- BC : Boundary Conditions;
- HOM : Homogeneous ellipsoid model;
- LIH : Forward linear, isotropic, homogeneous ellipsoid magnetization model;
- LAH : Forward linear, anisotropic, homogeneous ellipsoid magnetization model;
- nLIH : Forward nonlinear, isotropic, homogeneous ellipsoid magnetization model;
- nLAH : Forward nonlinear, anisotropic, homogeneous ellipsoid magnetization model;
- LIiH : Forward linear, isotropic, inhomogeneous ellipsoid magnetization model;
- LAiH : Forward linear, anisotropic, inhomogeneous ellipsoid magnetization model;
- nLIiH : Forward nonlinear, isotropic, inhomogeneous ellipsoid magnetization model;
- nLAiH : Forward nonlinear, anisotropic, inhomogeneous ellipsoid magnetization model.
- i-LIH : Inverse linear, isotropic, homogeneous ellipsoid magnetization model;
- i-LAH : Inverse linear, anisotropic, homogeneous ellipsoid magnetization model;
- i-nLIH : Inverse nonlinear, isotropic, homogeneous ellipsoid magnetization model;
- i-nLAH : Inverse nonlinear, anisotropic, homogeneous ellipsoid magnetization model;
- i-LIiH : Inverse linear, isotropic, inhomogeneous ellipsoid magnetization model;
- i-LAiH : Inverse linear, anisotropic, inhomogeneous ellipsoid magnetization model;
- i-nLIiH : Inverse nonlinear, isotropic, inhomogeneous ellipsoid magnetization model;
- i-nLAiH : Inverse nonlinear, anisotropic, inhomogeneous ellipsoid magnetization model.

In order to completely specify a model, often notation such as 'nLAiH - **EV**' is used. In this case, we refer to the forward nonlinear, anisotropic, inhomogeneous ellipsoid model, where the hysteresis phenomenon is modelled using the energy-variational model.
In addition to the above list of abbreviation, a list of symbols should be included. However, the authors think that all variables are clear from their respective context.

Preface

It was December 2018, when a Skype conversation between The Hague and Waterloo (Canada) established the first connection between ellipsoids and me. During this call, Eugene Lepelaars, Aad Vijn and I talked about the possibility of doing my graduation project at TNO Oude Waalsdorperweg, unit Defence, Safety and Security, at the department of Electronic Defence. After some contemplation, we decided that is was a good match and two months after, the research started. During the ten-month internship at the Oude Waalsdorperweg, it was my task to improve existing models on the magnetic behaviour of a steel prolate ellipsoid. More specifically, it was my task to quantify the influence of *nonlinearity, anisotropy and inhomogeneity* in the magnetic evolution of a real, physical steel prolate ellipsoid located at the Oude Waalsdorperweg, with the help of a *magnetic signature* measuring device called CLAViS, built by Eugene. The availability of such a real, existing object can be quite threatening to a mathematician, but in reality it is a great blessing, making the connection between the idealised but possibly non-conforming world of mathematics, to the physical reality we inhabit. Accordingly, 'fitting mathematical models to data' is a deeply mysterious undertaking, the effectiveness of which is not at all facile to predict beforehand. But, to quote a famous paper by Eugene Wigner [1], the *'unreasonable effectiveness of mathematics in the natural sciences'*, proves again and again that it can be done. But it is often a slow and laborious undertaking, where rewards might only be found at the end.

The past ten months consisted of firstly conducting a literature study. The field of magnetic modelling is extensive and consists of many different viewpoints and approaches. Different notation exists to describe the same physical quantities. It requires time to distinguish between ideas and formulations of ideas. However, it is very interesting to see how the sciences progress, by often small steps and discussions, until a new model is introduced or certain bridges are built between two seemingly unrelated concepts. This has taught me a lot.

After doing the three-month literature study, I started implementing different simplified models, describing the magnetic evolution of the steel ellipsoid under the influence of an applied background field. Together with my supervisors, we formulated and implemented ellipsoid models of increasing complexity, in order to be able to describe the ferromagnetic behaviour and signature (that what can be *measured* about the ellipsoid behaviour) increasingly well. This process required many iterative steps of model revision and re-implementation because of new insights and flaws surfacing. Roughly speaking, we have looked at four different hysteresis models (the 'nonlinear' part of the research objective), which can have anisotropic parameters, describing anisotropy. When the ellipsoid *magnetization* is assumed uniform throughout the material, the magnetic evolution can be modelled by solving three coupled nonlinear ordinary differential equations. When the assumption of uniformity is loosened, the analytical result underlying the homogeneous/uniform case can no longer be used. To analyse this case of inhomogeneity, we have used the Finite Element Method, which is able to efficiently model local variations in materials. The static, spatial Finite Element formulation then is combined with the nonlinear, temporal aspect of hysteresis, yielding the most flexible formulation of the *for-*

ward ellipsoid model, in the sense that the magnetic signature is generated by applying known parameters, initial conditions and boundary conditions.

Thereafter, the various forward models are inverted, by which we mean that the initial condition of the forward models and the material parameters, need to be estimated on the basis of signature data. The more complex the forward model is, the more *ill-posed* the inverse model will become, requiring advanced mathematical modelling techniques to solve.

In the end, we thus combined the theory of electromagnetic physics with measurements to contribute to a larger project: The development of a closed-loop degaussing system to be used by the Royal Netherlands Navy, which purpose it is to firstly model the magnetic signature of naval vessels, thereafter estimate the magnetization distribution in the vessel, and thereafter to actively monitor and even control the signature. In that context, I follow in the footsteps of many researchers at TNO, as well as my daily PhD-supervisor Aad Vijn and the the fellow TU Delft students Olivier Baas, Marianne Schaaphok and Adia Lumadjeng.

All in all, the project at TNO was very challenging, both in the mathematical realm and in the personal sphere, but extremely rewarding, again both in terms of being the apotheosis of my six-year period of studying Applied Mathematics (and a bit Applied Physics) in Delft, as well as one of the biggest personal challenges in my life.

This brings us to some personal comments. Doing academic research at this scale was quite new to me. More specifically, working at an external location outside a university environment, while simultaneously enjoying lots of freedom in approach and direction, required a steady vision and determination. It is now clear to me that the inhomogeneous (in effectiveness), nonlinear (in time) and anisotropic (in direction) progression of academic research can only be traced afterwards. This observation entails a big learning point for me personally: Often, one has to make a leap of faith into the unknown, to pick one approach over the other. One has to have sufficient *courage* to pursue such an idea, to keep one's nerves and to be flexible in case of setbacks. Perhaps this aspect of the graduation project has taught me the most. Moreover, discipline and determination is absolutely necessary, which is a harsh lesson to learn, but a necessary one in life. I have made many mistakes during the project in this respect, from which I have hopefully learned my lessons, realizing that lessons have to be learned continuously in life. For one thing, my mind was often very distracted during the project. I have not been able to figure out why, by in some sense, the whole past MSc period of more than two years have felt like I was only taking part in it, and not owning it. This is a very surreal experience and was even more intense during the graduation project. I resorted to certain philosophers and existential or even nihilistic ideas to justify my experiences, which sometimes caused my mind to run ever more chaotic. This has impacted my research in a negative way, causing many changes of plans, reductions of goals and personal dissatisfaction. I want to sincerely apologise to the people I have let down during the previous period, but have come to the conclusion that, regardless of the objective, measurable outcome of the mathematical part of my graduation, it has *in the end* been a thoroughly *good* time in all aspects of my life.

Luckily, the research was far from solitary and my supervisors were extremely supportive. I would like to thank dr. ir. Eugene Lepelaars greatly for supervising me from TNO. We have had many great conversations, not only about the project but also about life and the future. He was always very supportive and generous in commenting on my draft versions of the current report. Our weekly meetings taught me a lot, as well as his general stance and humility in life. On the same note, I would like to thank my PhD supervisor ir. Aad Vijn for always being

ready to answer my (sometimes) confused questions and for keeping an eye on my progression. He has taught me a lot and was very generous to include me on a paper that was presented at the Marelec conference in Boston, for which I am very grateful. He was very supportive and included me also in his experience as a PhD candidate by discussing the reality of a life as a PhD candidate. I am very grateful to have known him better over the course of the last ten months. Finally, I would like to thank the chair of the group Mathematical Physics and my official supervisor Prof. dr. ir. Arnold Heemink for his professional and always positive leadership. I always enjoyed the meetings with him and the discussions we had on several areas of life. I am very grateful to have had him as my head supervisor.

Secondly, I would like to thank the professors and researchers that I had several meetings with during the project. Among others, dr. ir. Fred Vermolen has helped me to formulate the FEM framework of the current research, for which I would like to thank him greatly. Dr. ir. Martin van Gijzen and dr. ir. Johan Dubbeldam, who contribute to the larger TU Delft - TNO cooperation in the context of the degaussing project, have also commented on my progress in several meetings, for which I would like to thank them. Prof. dr. ir. Mark Veraar has taught me a lot on theoretical results concerning the Poisson equations which was encountered in the current report, for which I thank him. Also, several TNO researchers shared their thoughts with me over the course of the project, among others Bart Jan Peet and Reinier Tan, for which I thank them. In a broader context, I also thank TNO and the department of Electronic Defence for the pleasant working environment that was offered to me, which consisted of very friendly colleagues, awesome activities and great fellow interns. I would recommend an internship at TNO to anybody, given the possibility.

Moreover, I am grateful for Arnold, Eugene, Fred and Aad to be part of my thesis committee.

Lastly, I would like to thank my family, my father Geurt and mother Simone and my brother Willem and two sisters Heidi and Brenda, as well as my grandma and uncles and aunts, for being such a good and supportive family. I am very blessed in that respect. I would also like to thank my dear roommates for supporting me, as well as my friends and a very special girl that has come into my life during the last stages of the project, for which I am very grateful. Especially during the finalisation of the project, you have all been of great help to me. Lastly, I want to thank God for blessing me in this life.

Delft, December 13th, 2019
Hendrik Jongbloed

Contents

Chapter 1

Introduction

1.1 Research Motivation

In order to minimize the risk of being detected in war situations, it is of the utmost importance to minimize the signature of naval ships and submarines. The *signature* of such a vessel is the set of all detectable physical quantities that differ with the presence of the vessel, relative to the unperturbed situation without the vessel. Formulated this way, one can view the signature of a ship as a source - perturbation problem: The signature of a vessel is a consequence of the internal 'production' of physical effects, such as engine noise, but also a consequence of the interplay between the vessel and surrounding media, such as in the case of the slow magnetization of a submarine in the Earth's magnetic field. Today's advanced mines are equipped with a variety of sensors in order to measure the slightest changes in different physical quantities: acoustic waves, electric fields, magnetic fields, pressure changes, temperature changes, to name a subset of signature aspects. Upon measuring a certain set of deviations from the unperturbed situation, the mine will detonate, causing great destruction, possibly of human lives. Since an advanced mine is, however expensive in its own right, orders of magnitude cheaper than a state-of-the-art modern naval vessel, stealth technology, signature monitoring and minimization is both an important and necessary frontier in current Defence research.

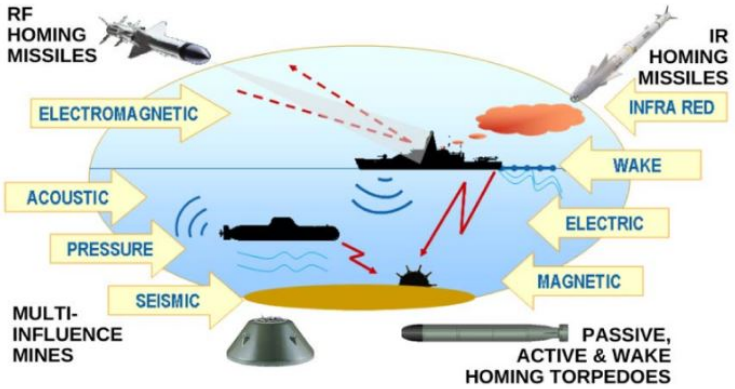

Figure 1.1: A schematic depiction of many possible physical effects that make it possible to detect a naval vessel or submarine. This figure was cropped from the thesis of Aad Vijn [80].

As can be observed from Figure 1.1, there exist many signature-generating mechanisms. A good question could be: 'Can all of those effects be minimized to a satisfactory degree?'. In order to do this, one has to firstly *predict* or measure the signature accurately. However, measuring the signature of a naval vessel sounds easier than it is. It is often an expensive and time-consuming operation. Even when restricted to only the *magnetic signature*, the subject of

the current research, measuring the signature is quite a challenge. This is why reliable physical models have to be formulated in order to extrapolate relatively easy-to-get data, for example from within the vessel, to the outside of the ship's hull.

1.2 The magnetic signature of a vessel

Steel naval ships and submarines perturb the Earth's magnetic field locally. Their ferromagnetic properties induce a perturbation field, detectable by advanced modern mines using magnetic sensors. This perturbation field is known as the *magnetic signature* of the ship and ultimately is a function of the interplay between the ship's steel properties, geometrical configuration, the local Earth's magnetic field, the motion of the ship and the electrical currents and phenomena present in and around the ship. In order to minimize the risk of being detected in war situations, it is vital to minimize the magnetic signature of these ships. An advanced system of electric coils on board is able to do just that: by Ampere's law, electric coils generate a magnetic field aimed to cancel the magnetic signature of the ship. This is known as a *degaussing system*: a (partially) self-regulating system, monitoring the motion and position of the ship continuously and controlling the current through degaussing coils by means of an algorithm. One encounters some complexities in this process. Firstly, in practice it is difficult and expensive to accurately measure the magnetic signature *outside* the ship, especially if it is large. Another difficulty in this paradigm is the complexity of accurately determining which part of the magnetization of the ship's hull is permanent (not influenced by the Earth's magnetic field), and which part is induced (and thus, possibly nonlinearly, influenced by the Earth's field), furthermore, sensors measuring the actual magnetic field are inside the ship, while the relevant minimization of the signature is at the location of expected mines. Moreover, the field generated by degaussing coils *also* influence the magnetization of the ship's steel. Underlying these problems is the fact that it is very difficult to model the magnetic behaviour of steel.

This is where the present project comes in. Due to the non-linear magnetic behaviour of ferromagnetic steel, the ship's degaussing system will decrease in performance after some time, *if* the system is designed with the assumption of *linearly reacting steel*. Indeed, the present systems use a *linear* approximation of the magnetic behaviour of the ship's hull, while the actual behaviour is non-linear and even history-dependent, a phenomenon known as *hysteresis*. Now, commissioned by Royal Netherlands Navy, TNO is currently developing a *closed-loop degaussing system* as part of a much larger project of procuring new naval ships and submarines, including this nonlinear hysteresis component. A closed-loop degaussing system is, in some way, the perfection of a sequence of consecutively more advanced systems in magnetic stealth technology: Deperming, open-loop degaussing and closed-loop degaussing. Deperming has been done for many years in history, and refers to a static procedure to remove permanent magnetization from a naval vessel, visualized in the figure below.

Figure 1.2: A naval vessel is being depermed at a harbour.

1.3 Towards ellipsoid modelling

Having discussed the broader context of the present research in terms of naval warfare and signature minimization, we are ready to focus on the particular. As discussed above, it is often very difficult to *model* the magnetic behaviour of a vessel's steel, because of its nonlinear and inhomogeneous (location-dependent) nature. As is often the case in science and applied mathematics, *experiments, data and observations* must be included in the description and modelling of these complicated phenomena. Combining models with data, opens up a whole new horizon of techniques, theory and tricks. In combining physical models with data, one encounters the notion of *inverse modelling* rather frequently. This is the case, because in a multitude of realistic situations, one cannot directly observe the quantities of interest. Rather, one assumes that measured data are generated by some pre-derived forward model. This forward model must thereafter be inverted in order to draw conclusions about the quantities of interest. In formal notation, let observed data be denoted by a vector $\boldsymbol{y}$, let a (known) parameter vector be given by $\boldsymbol{\theta}$ and let physical quantities of interest (which, confusingly, may also contain quantities that could be named 'parameters') be denoted by the vector $\boldsymbol{x}$. These are related formally by the forward model $\mathcal{F}$:

$$\boldsymbol{y} = \mathcal{F}(\boldsymbol{x}, \boldsymbol{\theta}) \tag{1.1}$$

which can be loosely described as the data one observes, given the hidden quantity $\boldsymbol{x}$ and the model parameters $\boldsymbol{\theta}$. The *inverse* problem is then roughly to estimate the hidden variables $\boldsymbol{x}$ from the data $\boldsymbol{y}$. Often times, there are many more unknowns to be estimated than knowns, yielding an ill-posed inverse problem (here, we do not give a precise definition). Numerically, this fact is often related to notions of high condition number, which in turn is related to high noise-sensitivity and so on, resulting in the often very complex nature of inverse problems. For example, in his MSc thesis, Aad Vijn [80] analysed inversion algorithms to estimate the

magnetization distribution in a real-life steel specimen, which is certainly non-trivial.
This was before the CLAViS was built at TNO. The CLAViS, built by Eugene Lepelaars, is a small-scale magnetic signature monitoring device that makes use of Helmholtz coils to generate an uniform applied field. Inside the CLAViS, there is space to place an object above a sensor array, providing the means to measure the effect of an uniformly applied background field on that object.

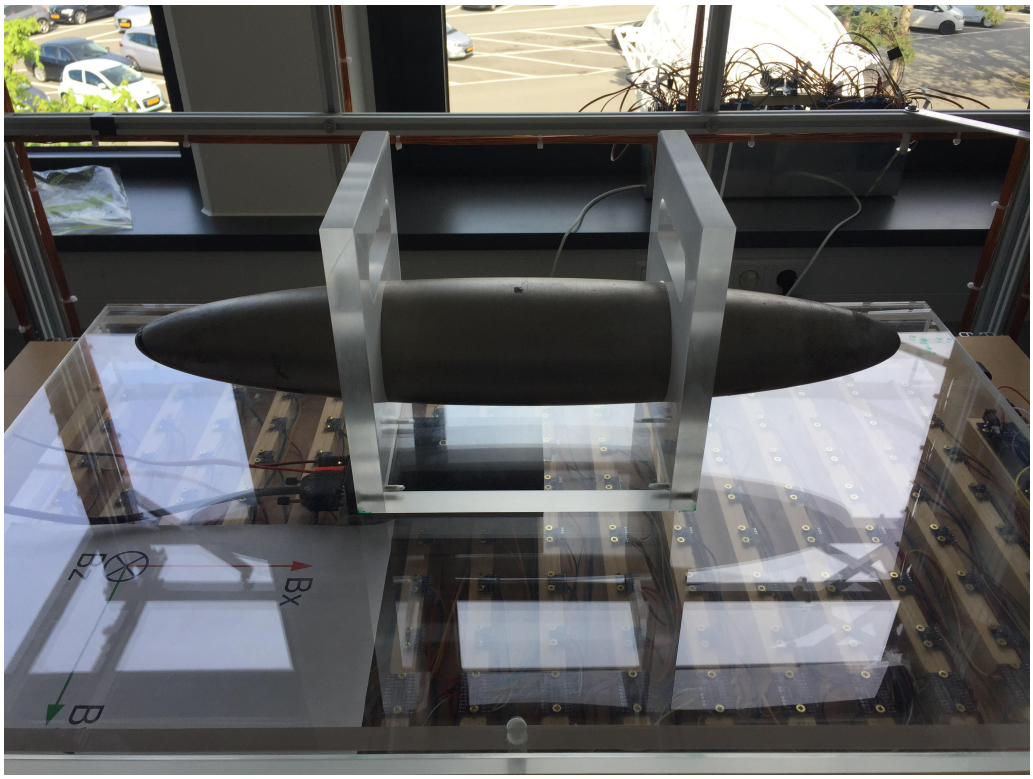

Figure 1.3: The CLAViS with our ellipsoid inside.

Once the CLAViS was built to perform small-scale signature measurements on miniature ferromagnetic objects, a great variety of possible experiments was made possible at once, motivating new research projects within the context of magnetic signature modelling and prediction. For example, Marianne Schaaphok has performed research using the CLAViS at TNO, looking into real-time data-driven model for magnetostatics. This allows us to now move from general naval ships and submarines, towards a more manageable object that is easier to analyse using measurements: A prolate steel ellipsoid located at TNO, Oude Waalsdorperweg.

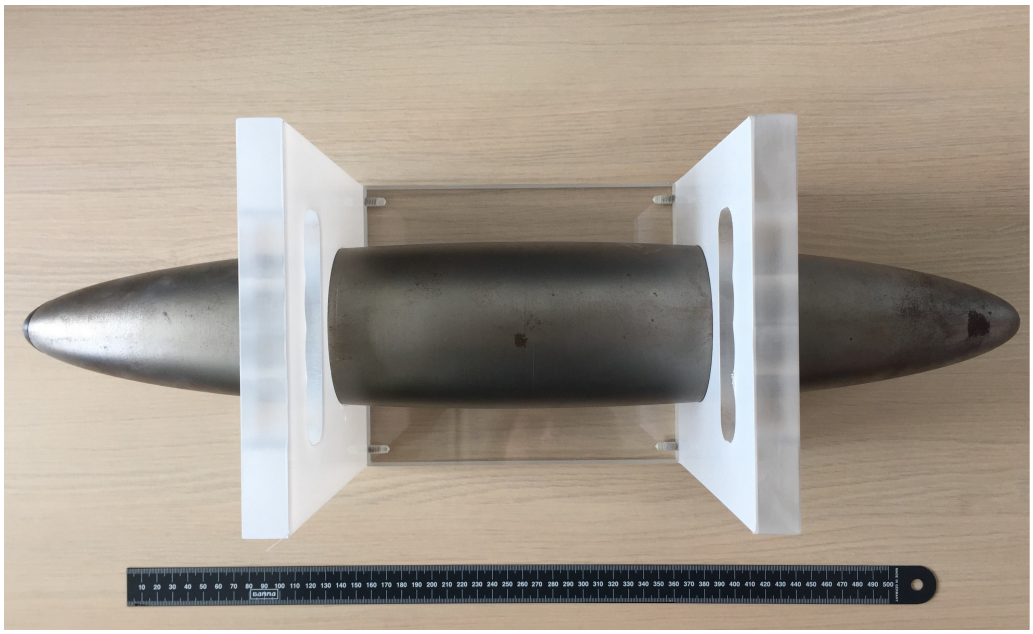

Figure 1.4: The prolate steel ellipsoid that was analysed during our research.

An ellipsoid is remotely comparable to, for example, a submarine, although many aspects differ. This makes ellipsoids interesting objects from a far-field perspective. The main inspiration for the current research is formed by an observation in the thesis by Olivier Baas [74], who also conducted research at TNO during his graduation project. He eventually focussed his research on a steel plate, and investigated the influence of external fields and stress on the magnetization distribution of that plate. He also looked into the prolate steel ellipsoid that is the focus of the current research, but did not fully analyse it. Baas conjectured that the magnetization inside the ellipsoid has a non-uniform permanent component; this would explain the measured discrepancy between the measured signature and theoretical results assuming a uniform magnetization. Later, Eugene Lepelaars and Aad Vijn formulated the current project, to analyse the prolate steel ellipsoid and focus specifically on three aspects, discussed below.

1.4 Research Goals

Using the prolate solid steel ellipsoid, owned by TNO, the goal of the project is to investigate and quantify the significance of nonlinearity, anisotropy and inhomogeneity of the steel constituting the ellipsoid; this is done by employing different models of nonlinear hysteresis. These models differ, among other things, in terms of the number of parameters and physical motivation. Using and comparing different hysteresis models has a number of benefits. A forward model can be employed to generate artificial data, whereafter another model can be used to be fitted to these data. In that way, a correspondence between different models can possibly be created. The material hysteresis models are able to describe material non-linearity and anisotropy, whereas the inhomogeniety in the ellipsoid itself is reflected in either assuming non-uniform magnetization and initial conditions, or varying model parameters throughout the ellipsoid, on a macro scale. Accordingly, the main research goal of this graduation project can be formulated as follows:

'Formulate, motivate, design, implement, verify and improve a model of the magnetic behaviour of a ferromagnetic steel ellipsoid, taking into account hysteresis, anisotropy and inhomogeneity, moreover, quantify the impact of these three aspects.'

We hope to achieve this goal by formulating the following sub-goals.

- Develop a flexible and general forward model
- Identify and understand the physical and mathematical significance of model parameters
- Investigate a flexible, general and reliable method of model inversion and parameter estimation
- Quantify the impact of hysteresis, (an)isotropy and (in)homogeneity

From the subquestions above, it is essentially our main task to go from sensor data to magnetization prediction and estimation in time, roughly depicted in the figure below:

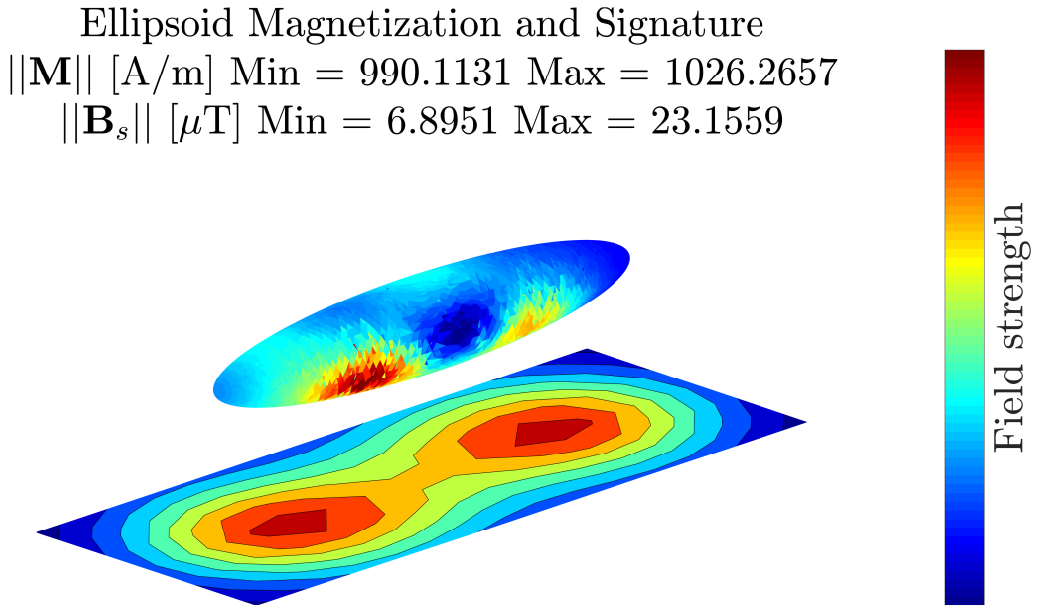

Figure 1.5: Our task is to go from the ellipsoid, to the sensor array, back to the ellipsoid. Will it work out as planned in nonlinear, anisotropic and inhomogeneous circumstances, and are we able to quantify relevant aspects?

1.5 Report structure

The structure of the report is as follows.
Firstly, we will present a short overview of the basic theory of electromagnetism, which is then directed towards equations describing the field of magnetostatics. The resulting partial differential equation, a nonhomogeneous Poisson equation with nonlinear coupling between its solution and its nonhomogeneous term, is presented. Thereafter, we apply the obtained equations to a general steel ellipsoid. Prolate spheroidal coordinates are introduced and the forward and inverse model are defined. At this point, only spatial aspects have been considered. However, in order to model the quasi-static evolution of the situation at hand, we need to describe the behaviour of a magnetizable object in a changing magnetic field in time. This is where material hysteresis models come in. The four material hysteresis models **IP**, **RA**, **JA**, and **EV**are introduced and resulting equations are derived.
The second part of the report is concerned with modelling the magnetization evolution and corresponding signature of the steel ellipsoid under one specific assumption: *Homogeneity*. In this case, an analytic expression called *'The Ellipsoid Formula'* can be derived as a solution to the magnetostatic Poisson equation. This expression is of great importance and forms the

basis of the homogeneous ellipsoid model. A nonlinear ordinary differential equation is capable of describing the magnetic evolution of the system. The four hysteresis models are coupled with this ODE in an incremental, iterative manner. Having derived the homogeneous forward model, we proceed by inverting the model using a genetic algorithm. The influence of measurement noise is analysed, though not too extensively.
Thirdly, we consider the Poisson equation derived in the first part of the report *without* the assumption of homogeneity. The magnetostatic solution is analysed using a combination of the analytic, homogeneous solution and the usage of *finite element analysis*.The finite element matrices and vectors are derived and a specific Dirichlet solution method is described. An incremental procedure is proposed to describe the evolution of both the magnetic field and the magnetization inside the ellipsoid, coupled by the underlying hysteresis model. Subsequently, the resulting stepping scheme is inverted by considering the measurement data as input to the inverse model. This yields an ill-conditioned system of linear equations at each time step. Using regularization, the magnetization distribution inside the ellipsoid is estimated. Thereafter, the hysteresis parameters of the inhomogeneous ellipsoid are estimated using genetic algorithms. Lastly, the influence of noise is considered.
The fourth part of the report is devoted to results, discussion, conclusions and recommendations. Results of both forward and inverse simulations are given with the help of noise-perturbed twin experiments. A comparison of all discussed models is made on the basis of criteria such as region of validity, computational cost and stability. Some of the assumptions underlying the different models are analysed by comparing models of different complexity. Finally, the models are fitted to real measurement data, obtained using the CLAViS at TNO. These results are then discussed, conclusions are formulated and recommendations are given.
Finally, the appendices of the current report consist of more results and figures, more equations involved in modelling hysteresis and more equations involving the finite element method. Lastly, the list of consulted literature is provided.

1.6 Software

Throughout the research, we have made use of the familiar scientific computing tool `Matlab`. We have implemented our own ODE solvers to be able to enjoy an optimal degree of customization and understanding. After generating a Finite Element mesh using the software `Comsol`, we have imported these different meshes automatically in `Matlab`. Thereafter, we have used our own derived Finite Element matrices to compute the forward and inverse inhomogeneous model results. For the inverse estimation of hysteresis parameters, we have made use of the built in `ga()` function, an implementation of a genetic algorithm.

Part I

Magnetostatics, Hysteresis and Ellipsoid Models

Chapter 2

Magnetostatics

The current chapter will be foundational for the rest of the present research. The equations governing different magnetic concepts will be stated, accompanied by short discussions on their derivations and assumptions. The chapter is mainly based on Jackson [2], Coey [5], Jiles [8] and Feynman [9].

2.1 What is Magnetism?

This section aims to get the reader familiar with the idea of magnetism. We will focus specifically on magnetostatics: Temporal effects will not be discussed. For example, electromagnetic waves as solution of the Maxwell equations will not be touched upon.
From a historic point of view, magnetic phenomena have been studied for at least as long as electric phenomena. Ever since the classical age, naturally magnetised objects known as lodestones were studied; the 6th century Greek philosopher Thales of Miletus (624 B.C. - 546 B.C.) is believed to have been one of the first figures in written history to have discovered the permanent magnetic properties of these naturally occurring materials.

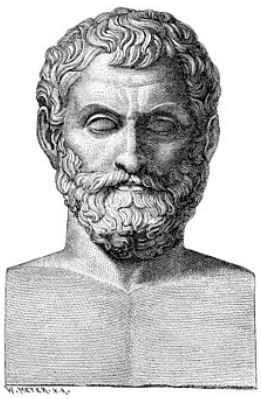

Figure 2.1: Thales of Miletus (624 B.C. - 546 B.C.)

In fact, the name 'magnet' may come from lodestones found in Magnesia, Anatolia. The magnetic compass is a very old invention and has been an indispensable tool for millennia. The Earth has been regarded as a giant magnet for centuries. However, the physical laws governing and describing the mysterious phenomenon of magnetism were discovered not so long ago; with great difficulty and determination, the behaviour of magnetic phenomena was described. It required the combined genius of many different great scientists, both experimentally and theoretically, to arrive at the theory of magnetism presented in this chapter. In electrostatics, the discovery of governing laws was more straightforward. This has to do with a fundamental

difference between the two: In contrast to electric charges such as the elementary electron, *there are no free magnetic charges*. Even so, it can be useful to use the concept of magnetic charge mathematically. But one simply cannot make a piece of material, possessing a certain magnetic charge. How then to study magnetism? In this literature study, we have chosen to take the classical approach to defining the relevant concepts. The reader must keep in mind that equivalent concepts can be derived and defined, for example, by fundamental principles of thermodynamics or solid state physics. More on this approach can be found in Dunning-Davies [16] (for the thermodynamic/energetic approach) or Simon [13](for the solid state physics/quantum mechanical approach). The basic entity in the study of magnetic phenomena was the magnetic dipole, relating rotational force to a measure of 'magnetic strength', which will be rigorously defined later:

$$\boldsymbol{\tau} = \mathbf{m} \times \mathbf{B}. \tag{2.1}$$

This fundamental relation contains the quantities torque $\boldsymbol{\tau}$[N m], magnetic dipole moment $\mathbf{m}$[A m^2] and the *magnetic flux density* $\mathbf{B}$[T]. We will take this as our definition for the $\mathbf{B}$-field, which is also sometimes called the *magnetic induction field*. Please note that this is an idealised situation involving a perfect dipole: its own field is assumed to not influence the applied magnetic flux density. Derived from this elementary magnetic moment, is the Magnetization $\mathbf{M}$[A m^{-1}], which is defined as the volume average over all microscopic magnetic moments in a material.

2.2 Maxwell's Equations and Constitutive Relations

One of the great scientific breakthroughs in science was achieved in the nineteenth century, by the brilliant Scottish scientist James Clerk Maxwell (1831 - 1879).

Figure 2.2: James Clerk Maxwell (1831 - 1879)

He managed to combine the previously seemingly unrelated and mysterious phenomena of electricity, magnetism and (what is now known as) electromagnetic radiation together in a very elegant theory [20]. Four coupled partial differential equations, known as Maxwell's Equations,

describe the behaviour of electric and magnetic fields in both vacuum and matter [2]:

$$\nabla \cdot \mathbf{D} = \rho \tag{2.2}$$

$$\nabla \cdot \mathbf{B} = 0 \tag{2.3}$$

$$\nabla \times \mathbf{E} = -\frac{\partial \mathbf{B}}{\partial t} \tag{2.4}$$

$$\nabla \times \mathbf{H} = \mathbf{J} + \frac{\partial \mathbf{D}}{\partial t}. \tag{2.5}$$

In these fundamental equations, the *electric field* $\mathbf{E}$ [$\mathrm{V\,m^{-1}}$] and magnetic flux density $\mathbf{B}$ are furthermore related by charge, motion and force. A particle of charge q [C], moving at a velocity of $\boldsymbol{v}$ [$\mathrm{m\,s^{-1}}$] experiences a Lorentz force given by

$$\mathbf{F} = q(\mathbf{E} + \boldsymbol{v} \times \mathbf{B}) \tag{2.6}$$

which gives a fundamental recipe of determining both the electric field and magnetic flux density in space. One observes two extra vector fields in the differential formulation of Maxwell's equations. These so-called *auxiliary field*s take *physical matter* into effect and are defined as follows:

$$\mathbf{D} = \epsilon_0 \mathbf{E} + \mathbf{P} \tag{2.7}$$

$$\mathbf{H} = \frac{1}{\mu_0}\mathbf{B} - \mathbf{M}. \tag{2.8}$$

The auxiliary fields are excellent tools for the macroscopic analysis of electromagnetic phenomena in matter. The *electric displacement* field $\mathbf{D}$ [$\mathrm{C\,m^{-2}}$] is non-trivial in case of matter in which the *polarization* $\mathbf{P}$ [$\mathrm{C\,m^{-2}}$] is non-trivial. Analogously, the *magnetic field* $\mathbf{H}$ [$\mathrm{A\,m^{-1}}$] is an important field in ferro-, para- or diamagnetic matter. Here, we encounter the previously defined magnetization $\mathbf{M}$, then defined as volume-averaged dipole moments. Although the following equation may seem like a rewriting of the previous one, the emphasis is different:

$$\mathbf{B} = \mu_0(\mathbf{H} + \mathbf{M}). \tag{2.9}$$

This equation always holds, per definition of $\mathbf{H}$. The subtle connotation is found in the fact that many in a wide class of problems, (partial differential) equations yield solutions in terms of $\mathbf{M}$ and $\mathbf{H}$, whereafter the $\mathbf{B}$-field is computed by (2.9). The magnetostatic time-independent Maxwell equations then reduce to the macroscopic equations

$$\nabla \cdot \mathbf{B} = 0 \tag{2.10}$$

$$\nabla \times \mathbf{H} = \mathbf{J}. \tag{2.11}$$

Combining (2.9) with (2.10) and (2.11) yields an almost complete description of the magnetic behaviour of matter. What is missing however, is a relationship between $\mathbf{B}$ and $\mathbf{H}$, $\mathbf{B}$ and $\mathbf{M}$ or $\mathbf{H}$ and $\mathbf{M}$ (thereafter, (2.9) can be applied to compute the third quantity). For the sake of the present discussion, let us relate $\mathbf{M}$ to $\mathbf{H}$ inside a material. This constitutive relation is material-specific, which originates in quantum mechanical and microscopic effects in matter. This is where the concepts of *magnetic permeability*, *magnetic susceptibility* and *hysteresis* come in. Indeed, in general, one can describe the nonlinear relation between the magnetic quantities locally as

$$\begin{cases} \mathbf{M} = \mathcal{M}[\mathbf{H}] \\ \mathbf{B} = \mathcal{B}[\mathbf{H}] \\ \mathcal{B}[\mathbf{H}] = \mu_0(\mathbf{H} + \mathcal{M}[\mathbf{H}]) \end{cases} \tag{2.12}$$

where the square brackets indicate a complicated relationship, in general involving the history of the magnetic field inside the material as well as highly specific and local material parameters. It is therefore not trivial to formulate the domain of these operators $\mathcal{M}$ and $\mathcal{B}$, so we will leave it at here. Let us look at some examples of these operators.

Linear materials For linear materials, both $\mathcal{M}$ and $\mathcal{B}$ are linear mappings of the following form

$$\begin{cases} \mathbf{B} &= \mathcal{B}[\mathbf{H}] = \underline{\boldsymbol{\mu}}\mathbf{H} \\ \mathbf{M} &= \mathcal{M}[\mathbf{H}] = \underline{\boldsymbol{\chi}}\mathbf{H} \end{cases} \tag{2.13}$$

where $\underline{\boldsymbol{\mu}}$ is, in general, a second-rank tensor, called the *magnetic permeability* [$\mathrm{N\,A^{-2}}$]. The *volume magnetic susceptibility* (often simply called magnetic susceptibility) $\underline{\boldsymbol{\chi}}$ of a material is a dimensionless quantity. Combining the various expressions above, yields the relation

$$\underline{\boldsymbol{\mu}} = \mu_0(\underline{\mathbf{1}} + \underline{\boldsymbol{\chi}}) \tag{2.14}$$

and via the constitutive relation (2.9), one obtains the expression of the *relative magnetic permeability*, a dimensionless quantity:

$$\underline{\boldsymbol{\mu}}_r := \frac{1}{\mu_0}\underline{\boldsymbol{\mu}} = \underline{\mathbf{1}} + \underline{\boldsymbol{\chi}} \tag{2.15}$$

For linear, isotropic materials, $\underline{\boldsymbol{\mu}} = \mu\underline{\mathbf{1}}$, where $\mu \in \mathbb{R}$ and $\underline{\boldsymbol{\delta}}$ is the unit tensor. Already encountered a few equations ago, the permeability of free space is given by $\mu_0 := 4\pi \times 10^{-7}\,\mathrm{N\,A^{-2}}$. So in free space, $\underline{\boldsymbol{\mu}}_r = \underline{\mathbf{1}}$ and thus $\underline{\boldsymbol{\chi}} = \underline{\mathbf{0}}$

$$\begin{cases} \mathbf{B} = \mu_0\underline{\mathbf{1}}\mathbf{H} = \mu_0\mathbf{H} \\ \mathbf{M} = \underline{\boldsymbol{\chi}}\mathbf{H} = \mathbf{0} \end{cases} \tag{2.16}$$

Nonlinear ferromagnetic materials For nonlinear ferromagnetic media, the relations Equation 2.12 are more complicated. However, one can still speak of *differential* permeability and susceptibility derived from the local linear approximation of the mappings $\mathcal{M}$ and $\mathcal{B}$. Indeed, we then define these two quantities by the respective Jacobians

$$\begin{cases} \underline{\boldsymbol{\mu}}^d_{ij} &:= \left(\frac{\partial\mathcal{B}[\mathbf{H}]}{\partial\mathbf{H}}\right)_{ij} \\ \underline{\boldsymbol{\chi}}^d_{ij} &:= \left(\frac{\partial\mathcal{M}[\mathbf{H}]}{\partial\mathbf{H}}\right)_{ij} \end{cases} \tag{2.17}$$

where $1 \leq i, j \leq 3$ represent the dimensions. Note that these quantities only make sense locally, since the mappings $\mathcal{B}$ and $\mathcal{M}$ are no functions. Although the previous expressions are somewhat loosely defined, they become clear in the application. In order to be mathematically rigorous, one would have to define what 'the history of the system' really is, which is beyond the scope of this research.

2.3 Solving problems in magnetostatics

Let us look at solving the magnetostatic Maxwell equations in the presence of material configurations and under bound current-free conditions ($\mathbf{J} = \mathbf{0}$), namely

$$\nabla \cdot \mathbf{B} = 0 \tag{2.18}$$

$$\nabla \times \mathbf{H} = \mathbf{0} \tag{2.19}$$

$$\mathbf{B} = \mu_0(\mathbf{H} + \mathbf{M}). \tag{2.20}$$

$$\mathbf{M} = \mathcal{M}[\mathbf{H}] \tag{2.21}$$

Let us now consider a volume $\Omega \subset \mathbb{R}^3$. Since we are in a setting of physics in this research, we do not have to worry about fundamental mathematical aspects of geometry and manifolds; we assume 'everything works'. The interested reader is referred to literature on functional analysis and partial differential equations. At the boundary of the object Ω, we can apply a 'pill box' method to deduce the boundary conditions on $\mathbf{B}$ and $\mathbf{H}$. In the absence of bound currents,

$$(\mathbf{B}_2 - \mathbf{B}_1) \cdot \mathbf{n} = 0 \tag{2.22}$$

$$\mathbf{n} \times (\mathbf{H}_2 - \mathbf{H}_1) = \mathbf{0}. \tag{2.23}$$

Solving equations (2.10) and (2.11) together with the relation (2.9) and boundary conditions (2.22) and (2.23) can be very difficult and is often analytically impossible due to the complexity of geometrical configurations or a complicated relationship between $\mathbf{B}$ and $\mathbf{H}$. Depending on these factors, Jackson provides three main lines of strategy [2]. We will only discuss one of them: solving the magnetostatic Maxwell equations using the scalar magnetic potential.

2.3.1 The Scalar Potential Φ

Let us specifically look at the equation

$$\nabla \times \mathbf{H} = \mathbf{0}. \tag{2.24}$$

Now, this law allows for introducing the *magnetic scalar potentia*l $\Phi : \mathbb{R}^3 \to \mathbb{R}$, defined by

$$\mathbf{H} = -\nabla\Phi, \tag{2.25}$$

since substituting the above equation in Equation 2.24 yields, using formal determinant notation

$$\nabla \times \mathbf{H} = -\nabla \times \nabla\Phi \tag{2.26}$$

$$= -\begin{vmatrix} \hat{\mathbf{x}} & \hat{\mathbf{y}} & \hat{\mathbf{z}} \\ \frac{\partial}{\partial x} & \frac{\partial}{\partial y} & \frac{\partial}{\partial z} \\ \frac{\partial\Phi}{\partial x} & \frac{\partial\Phi}{\partial y} & \frac{\partial\Phi}{\partial z} \end{vmatrix} \tag{2.27}$$

$$= \mathbf{0}. \tag{2.28}$$

The last step follows from the differentiability conditions of Φ. Again, one could make this more precise using function spaces, strong and weak forms. For example, one can see that we have not proven $\Phi \in C^2(\mathbb{R})$ which would make the step Equation 2.28 to be immediate. Surely, there are technical difficulties involved when boundaries are present or when geometric bodies exhibit nonsmooth behaviour. Again however, we will not focus on these mathematical details.

2.3.2 The Poisson Equation

The introduction of the scalar potential allows one to derive the Poisson equation. This PDE describes the local, spatial relation between $\mathbf{H}$ and $\mathbf{M}$ in space and will be the fundamental equation in the current research. Taking the divergence of the constitutive equation Equation 2.9 yields

$$0 = \nabla \cdot \mathbf{B} = \mu_0 \nabla \cdot (\mathbf{H} + \mathbf{M}) \tag{2.29}$$

$$= \mu_0(\nabla \cdot \mathbf{H} + \nabla \cdot \mathbf{M}) \tag{2.30}$$

$$= \mu_0(-\Delta\Phi + \nabla \cdot \mathbf{M}). \tag{2.31}$$

And so, one obtains the Poisson equation

$$\Delta\Phi = \nabla \cdot \mathbf{M}. \tag{2.32}$$

The solution to the Poisson equation is widely discussed in all kinds of physical and mathematical literature. In the following, let us now prescribe certain mathematical properties to the equation above. Defining

$$f(\mathbf{r}) = (\nabla \cdot \mathbf{M})(\mathbf{r}) \tag{2.33}$$

we obtain the standard Poisson equation $\Delta\Phi = f$. Now, assuming the smoothness of f, the Poisson equation has an analytic solution that can be obtained by Green's function theory. Examples of Green's functions on different computational domains can be found in many textbooks.

Chapter 3

Modelling the Magnetic Ellipsoid using the Maxwell Equations

The previous chapter was devoted to the introduction of the Maxwell equations, which unify electricity and magnetism. The concept of magnetization was introduced as an averaged distribution of nanoscale dipoles. Constitutive relations were derived, whereafter the local Poisson equation was derived.

$$\Delta\Phi = \nabla \cdot \mathbf{M} \tag{3.1}$$

This equation can be integrated using theory of Green's functions, yielding an integral form, allowing for the direct calculation of the magnetic field in the presence of a magnetization distribution. In the current research however, we firstly attempt to solve the above Poisson equation by means of a direct analytic treatment using simplifying assumptions, and later using the Finite Element Method. But firstly, let us consider the properties of the above equation in different circumstances.

3.1 Analysing the Poisson equation

Suppose one has a magnetization distribution in space, $\mathbf{M} = \mathbf{M}(\mathbf{r})$, and let us suppose that for all $\mathbf{r} \in \mathbb{R}^3$ we have $\mathbf{M}(\mathbf{r}) = \mathbf{M}(\mathbf{r})\mathbb{1}_{\Omega_e}(\mathbf{r})$, where Ω_e is some closed and bounded subset of $\mathbb{R}^3$. This means that the nonzero magnetization distribution is limited to the set Ω_e. We want to compute the magnetic field $\mathbf{H} = \mathbf{H}(\mathbf{r})$, such that the Maxwell equations are satisfied. As discussed before, we need to find a scalar potential $\Phi(\mathbf{r})$, which solves the Poisson equation. However, in concrete ferromagnetic situations, the terms Φ and $\mathbf{M}$ are interrelated, because $\mathbf{H}$ and $\mathbf{M}$ are interrelated. Therefore, although the Poisson equation is linear (the Laplace operator is a linear operator on certain function spaces), the resulting PDE is nonlinear in general. Using the formal hysteresis relation $\mathbf{M} = \mathcal{M}[\mathbf{H}]$ (which can be highly nonlinear and often implicit), the original Poisson equation

$$\Delta\Phi = \nabla \cdot \mathbf{M} \tag{3.2}$$

is formally given by

$$\Delta\Phi = \nabla \cdot \mathcal{M}[-\nabla\Phi] \tag{3.3}$$

where the (generalized) boundary conditions have not been specified yet.

Example 3.1.1. *To see that the Poisson equation with hysteresis is 'very difficult' in general, let us look at a relatively simple (but unphysical) expression for $\mathcal{M}$, namely, one that is nonlinear but history-independent. Suppose $\mathbf{M} = \mathcal{M}[\mathbf{H}] = \mathcal{M}(\mathbf{H}) = \gamma \|\mathbf{H}\|^2 \mathbf{H}$ for some $\gamma > 0$.*

Then the equation to solve is given by the nonlinear Laplace equation

$$\nabla \cdot \left(\left(1 + \gamma \left\| \nabla \Phi \right\|^2 \right) \nabla \Phi \right) = 0 \tag{3.4}$$

and the treatment of this equation is beyond the scope of the current research.

As the previous example shows, one cannot expect to derive an analytic solution to the Poisson equation without making some simplifying assumptions. A common and highly simplifying modelling choice is given by assuming the situation to be linear, isotropic and homogeneous, in which case one has $\mathbf{M} = \chi \underline{\boldsymbol{\delta}} \mathbf{H} = -\chi \nabla \Phi(\mathbf{r})$ for $\mathbf{r} \in \Omega_e$, equivalently $\mathbf{M}(\mathbf{r}) = -\chi \mathbb{1}_{\Omega_e}(\mathbf{r}) \nabla \Phi = -\chi(\mathbf{r}) \nabla \Phi$ with $\chi(\mathbf{r}) = \chi \mathbb{1}_{\Omega_e}(\mathbf{r})$ and thus

$$f(\mathbf{r}) = \nabla \cdot \mathbf{M} = -\nabla \cdot (\chi(\mathbf{r}) \nabla \Phi). \tag{3.5}$$

Accordingly, the Poisson equation reduces to the Laplace equation with relatively simple 'diffusion coefficient' $\mu_r(\mathbf{r}) = 1 + \chi(\mathbf{r})$

$$\nabla \cdot (\mu_r(\mathbf{r}) \nabla \Phi) = 0 \tag{3.6}$$

Now, we are tempted to go into many details concerning theoretical properties, existence and uniqueness of solutions to the above equations. We could go as far as analyzing the space of solutions and so on, as can be done following Hunter [87]. However, let us just conclude that the above equation is very difficult to solve in general and one has to employ numerical techniques relatively quickly when contemplating it.

Now we have stated some properties of the simplified Poisson magnetostatic boundary value problem, further categories of modelling choices will be made clear in the following section.

3.2 Classification of modelling choices

We distinguish eight different modelling choices, based on the three aspects of linearity, isotropy and homogeneity of the material. These three aspects will by expanded upon further in the current report. Roughly speaking, (non)linearity and (an)isotropy refer to the hysteresis operator $\mathcal{M}$ and the parameters therein, whereas the notion of (in)homogeneity refers to the spatial distributions of magnetic quantities within the material in the broadest sense.

Linearity The assumption of **linearity** is defined by letting the magnetization operator take a very specific form, namely

$$\mathbf{M}(\mathbf{r}) = \mathcal{M}[\mathbf{H}(\mathbf{r})] = \underline{\boldsymbol{\chi}}(\mathbf{r}) \mathbf{H}(\mathbf{r}). \tag{3.7}$$

where $\underline{\boldsymbol{\chi}}$ only depends on the spatial coordinate. Clearly, $\mathbf{M}$ is linear in $\mathbf{H}$. A material is nonlinear if it is not linear, that is, if the $\mathbf{M} - \mathbf{H}$ relation cannot be written in the form above.

Isotropy The assumption of **isotropy** is concerned with direction-dependent effects inside materials, caused by molecular crystalline properties. Isotropic material can be modelled by using scalar parameters, whereas anisotropic material requires using tensor parameters. The parameter vector $\boldsymbol{\theta}$ consists of only scalar parameters in the isotropic case. Moreover, there are different gradations in anisotropy. One has uniaxial anisotropy, in which hysteresis parameters take the form of diagonal tensors. Fully anisotropic materials exhibit cross-directional behaviour and are modelled by full second-rank tensors.

Homogeneity The assumption of **homogeneity** has to do with the geometric nature of the model. It may be the case that in the manufacturing process or during other events, the steel of the ellipsoid was affected inhomogeneously. On the other hand, the material parameters may be constant in space, but the magnetization distribution may be non-uniform in space. This is the difference between homogeneity and uniformity. However, as we shall see in the following, a slightly confusing deviation from this convention is used in the current report.

3.3 Physical Geometry: Applying the Poisson equation to the ellipsoid

3.3.1 Defining the ellipsoid

Let us now describe the situation to be modelled in full detail. Consider three-dimensional space $\mathbb{R}^3$. Centered at the origin, an ellipsoid is located, denoted by Ω_e as a subset of $\mathbb{R}^3$. The ellipsoid used throughout the whole of the current research, is prolate. In words, this means that the ellipsoid has two equal semi-diameters, whereas the third semi-diameter is greater than the other two. For convenience, we choose the three-dimensional axes parallel to the axes of the ellipsoid and the x-axis parallel to the major axis of the ellipsoid. $\Omega_e \subset \mathbb{R}^3$ is then described by

$$\Omega_e := \{(x, y, z) \in \mathbb{R}^3 : \frac{x^2}{a^2} + \frac{y^2 + z^2}{b^2} \leq 1\} \tag{3.8}$$

where a is the long semi-diameter, and b the small semi-diameter. Without axes, the ellipsoid that was analyzed in our present research, is depicted below in one of our result figures.

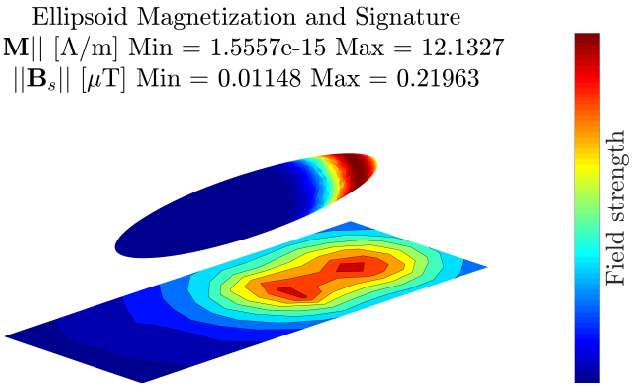

Figure 3.1: An inhomogeneously magnetized ellipsoid, with signature on the sensor array.

3.3.2 Prolate Spheroidal Coordinates

An important tool in deriving analytical expressions for idealized situations involving magnetic fields and prolate ellipsoids are prolate spheroidal coordinates [90]. In a Cartesian coordinate system, one introduces the ellipsoid center point $\mathbf{r}_c = (x_c, y_c, z_c)$ and the focal length $2f > 0$. The ellipsoid focal points are thus located at

$$\mathbf{f}_\pm = \mathbf{r}_c \pm f\mathbf{u}_x. \tag{3.9}$$

An arbitrary position vector $\mathbf{r} = (x, y, z)$ can now be described using prolate spheroidal coordinates (ξ, η, ϕ), where $\xi \in [1, \infty)$, $\eta \in [-1, 1]$ and $\phi \in [0, 2\pi)$, defined by

$$r_+ = ||\mathbf{r} - \mathbf{f}_+||, \tag{3.10}$$
$$r_- = ||\mathbf{r} - \mathbf{f}_-||, \tag{3.11}$$
$$\xi = \frac{r_+ + r_-}{2f} \tag{3.12}$$
$$\eta = \frac{r_+ - r_-}{2f} \in [-1, 1], \tag{3.13}$$
$$\cos\phi = \frac{y - y_c}{\sqrt{(y - y_c)^2 + (z - z_c)^2}}, \tag{3.14}$$
$$\sin\phi = \frac{z - z_c}{\sqrt{(y - y_c)^2 + (z - z_c)^2}}, \tag{3.15}$$
$$\tag{3.16}$$

Observe that the ellipsoid domain Equation 3.8 is now simply described by

$$\Omega_e := \{(x, y, z) \in \mathbb{R}^3 : \xi(x, y, z) \leq \xi_0\} \tag{3.17}$$

for $\xi_0 > 1$. From the previously defined coordinates, it also follows that the ellipsoid length, diameter and volume are given in both the Cartesian and prolate spheroidal system by

$$\ell = 2a = 2f\xi_0 \tag{3.18}$$
$$d = 2b = 2f\sqrt{\xi_0^2 - 1} \tag{3.19}$$
$$V = 4\pi ab^2/3 = \pi d^2 l/6 = 4\pi f^3 \xi_0(\xi_0^2 - 1)/3 \tag{3.20}$$

With these values obtained, the semi-focal length f and dimensions are related by

$$f = \sqrt{l^2 - d^2}/2 \tag{3.21}$$

Another parameter m is introduced to simplify notation. Let $m = l/d = \xi_0/\sqrt{\xi_0^2 - 1}$, which results in $\xi_0 = m/\sqrt{m^2 - 1}$.
The definition of prolate spheroidal coordinates allows for the derivation of an important equation later on.

3.3.3 Sensor Array

The ellipsoid domain is where the interesting physics and nonlinear processes take place; outside the ellipsoid, the magnetic field is a deterministic quantity which exclusively depends on the location $\mathbf{x} \in \mathbb{R}^3 \setminus \Omega_e$, the applied background field and the magnetization distribution. Moreover, the magnetic field in free space is linear in both the magnetization distribution and background field, as can be observed from the analytical solution to the Poisson equation derived above. The applied magnetic background field $\mathbf{H}_a$ functions as driving force for the magnetization distribution evolution inside the ellipsoid. We will denote the set of sensor locations by Ω_s. In practice, we have 112 sensors that are placed 0.156 m below the ellipsoid and are all capable of measuring the magnetic induction field in all three dimensions.

3.4 The Forward Model

Having defined all relevant quantities, we are ready to define the *Forward Ellipsoid Model*.

Definition 3.4.1 (The Forward Model)**.** The forward model, denoted by $\mathcal{F}$ is the mapping

$$\mathcal{F} : \left(\mathbb{R}^3 \times [0,T], B(\mathbb{R}^3), \boldsymbol{\theta}\right) \to B(\Omega_s \times [0,T]) \tag{3.22}$$

defined by

$$\mathcal{F}(\mathbf{H}_a(t), \mathbf{M}_0, \boldsymbol{\theta}) = \mathbf{B}_s|_{\Omega_s}(t) \tag{3.23}$$

from the applied input signal $\mathbf{H}_a(t)$, the initial magnetization $\mathbf{M}_0(\mathbf{r})$ and the governing vector of parameters $\boldsymbol{\theta} = \boldsymbol{\theta}(\mathcal{M})$, to the output signal $\mathbf{B}_s$, the measured signature (magnetic flux density) at the sensor locations Ω_s.
One has

$$\mathbf{B}_s|_{\Omega_s}(t) = -\mu_0 \nabla \Phi|_{\Omega_s}(t) \tag{3.24}$$

where Φ is a solution to the formal Poisson equation Equation 3.3.

Schematically, the forward model is depicted by moving from the top picture to the bottom (in space) and subsequently in time (via a nonlinear hysteresis model).

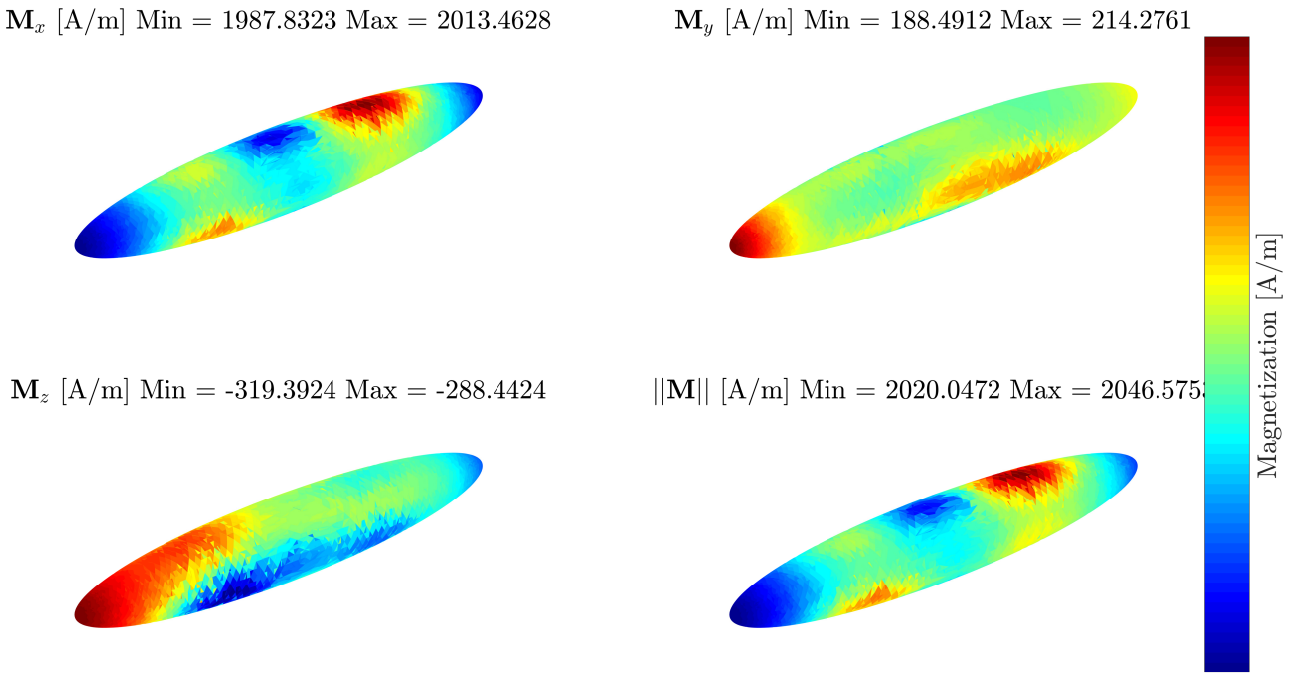

Figure 3.2: An inhomogeneously magnetized ellipsoid. In our formulation, the magnetization of the ellipsoid functions as input to the forward, spatial model.

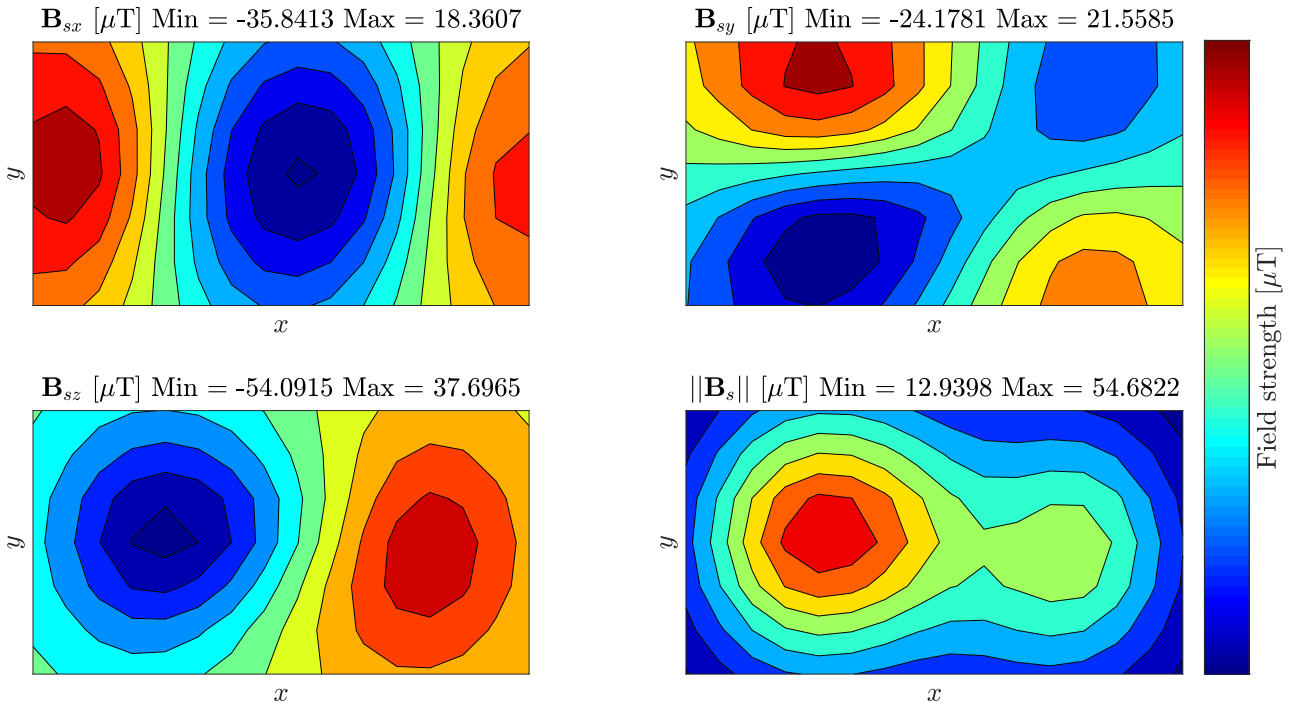

Figure 3.3: The sensor signature, produced by the magnetized ellipsoid of the previous figure.

3.5 The Inverse Model

Definition 3.5.1 (The Inverse Model)**.** Estimation of the hysteresis parameter vector $\boldsymbol{\theta}$ as well as the magnetization distribution $\mathbf{M}(\mathbf{r})$, based on knowledge of $\mathbf{H}_a(t)$, and data $\mathbf{B}_s|_{\Omega_s}(t)$.

Chapter 4

Material Hysteresis Models

In a previous chapter on basic electromagnetic theory, three basic magnetic quantities were discussed. These three vector fields are related by the defining constitutive relation

$$\mathbf{B} = \mu_0(\mathbf{H} + \mathbf{M}). \tag{4.1}$$

Usually, only one of these fields is known. In order to model a physical situation, one thus needs another relation to be able to uniquely determine the three fields. Throughout this report, the second relation is called the *hysteresis relation*, and is most often noted by the operator $\mathcal{M}$. The domain and codomain of this operator depends on the context. Also, a closed-form expression is often impossible to give, since the outcome of the (in general) nonlinear operator $\mathcal{M}$ depends on the 'history'. In general, one can write

$$\mathbf{M} = \mathcal{M}_H[\mathbf{H}, \theta], \tag{4.2}$$

where θ denotes a vector of all relevant material parameters, and the square brackets denote the 'history-like' character of the equation. The subscript H is used to denote the different hysteresis models.
The current chapter consists of brief derivations and vectorial generalizations of four common hysteresis models discussed in literature:

- The Induced-Permanent Model (**IP**), with one permanent magnetization component and one linear parameter χ;
- The Rayleigh Model (**RA**), with 2 hysteresis parameters: $\{\mu_i, \alpha_R\}$;
- The Jiles-Atherton Model (**JA**), with 5 hysteresis parameters: $\{M_s, a, \alpha, k, c\}$;
- The Energy-Variational Model (**EV**), with $3{+}2N_c$ hysteresis parameters: $\{M_s, a, \alpha, \omega_c, k_c\}$.

4.1 Physics of Ferromagnetic Hysteresis

Let us focus on the non-linear ferromagnetic behaviour of steel. This non-linear behaviour, previously denoted by the relation $\mathcal{F}$, is known as *hysteresis*, derived from a Greek word meaning 'to lag behind'. This name is fitting, since it describes the behaviour of ferromagnetic material in an external field quite well, as can be seen in the following classic hysteresis loop figure. One can see that the magnetization exhibits memory-behaviour: the magnetic field already evolves while the magnetization lags behind.

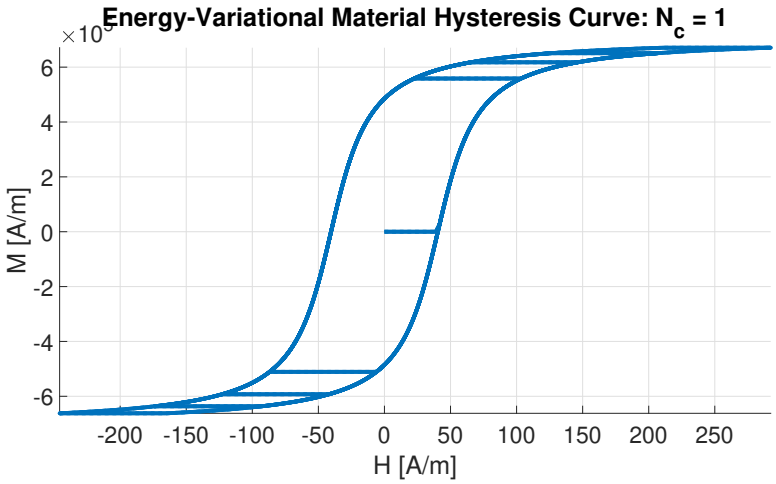

Figure 4.1: A classical hysteresis curve.

The microscopic and mesoscopic origins of hysteresis can be explained by magnetic domain behaviour, which actually can be observed. Details on the material properties giving rise to ferromagnetism may be found in Coey [5] and Chikazumi and Charap [17]. It has to do with specific crystalline structures on the nano- and microscale, giving rise to material anisotropy, whereas the manufacturing process of real-life materials involves complicated and random processes, giving rise to a certain distribution of mesoscopic magnetic domains inside a material. Even more fundamental theory on the occurrence of magnetism may be found in a standard work on solid state physics [13].

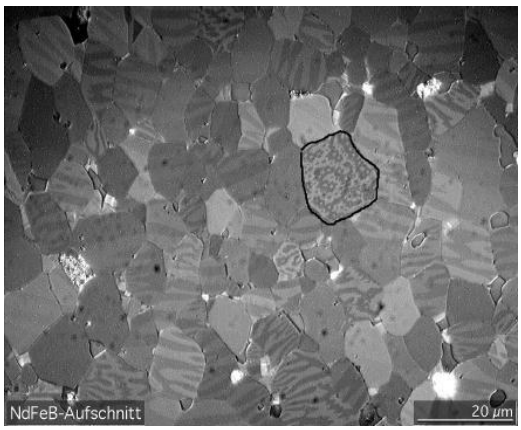

Figure 4.2: Magnetic domains under a microscope.

From these material-specific properties, one has to derive a macroscopic or mean-field description of the relation between different magnetic quantities (technically, even the magnetization $\mathbf{M}$ of a certain material is a wildly varying quantity on a nanoscale). Different hysteresis models exist in literature, all describing a certain relation between $\mathbf{B}$, $\mathbf{H}$ and $\mathbf{M}$ and thus all capable of describing a hysteresis loop as depicted in **??**. We have looked at the models described in their original papers by Rayleigh [23], Preisach [22], Bouc-Wen [25], Bergqvist [37] and Harrison [65]. We will discuss three of these models in more detail, stating the main equations, considerations and (dis)advantages as well as model parameter estimation techniques.

4.2 Hysteresis Modelling

The modelling of magnetic hysteresis can be approached from different angles. Some models are purely aimed at describing observed data as well as possible, often requiring elaborate expansions and approximations. Other models start from the laws of physics and try to find a reasonable set of simplifications to reach a formulation that is both capable of capturing hysteresis behaviour as well as being relatively simple to use. In that respect, one can classify the four hysteresis models by the following set of statements:

- The **IP**model is based on a first-order expansion of the magnetization as function of **H**;
- The **RA**model is a parabolic approximation to observed hysteresis curves;
- The **JA**model works from splitting the magnetization in a reversible and an irreversible part and by using an anhysteric function;
- The **EV**model also works with a 'mean' anhysteric function, but is built up from energy balances by splitting up the magnetic field in a reversible and an irreversible component.

The vectorial generalization of the Rayleigh and Jiles-Atherton model is aimed to incorporate a number of things:

- It must be able to describe anisotropy;
- It must reduce to the scalar case if isotropic and one-dimensional material is modelled;
- It must show intuitive and reasonable behaviour, which can be made more rigorous when compared to intrinsically vectorial hysteresis models.

The vectorial Jiles-Atherton model was firstly described by Bergqvist [40], but vectorial generalizations of the Rayleigh model have not been found in literature. The Energy-Variational model is intrinsically multidimensional. Let us now discuss the development and aspects of the three nonlinear hysteresis models.

4.3 The Induced-Permanent Hysteresis Model

This model is fully defined by the 'affine linear relation'

$$\mathbf{M} = \mathbf{M}_{per} + \underline{\boldsymbol{\chi}}\mathbf{H} \tag{4.3}$$

and is therefore intrinsically vectorial. Because $\mathbf{M}_per$ cannot be measured directly in many circumstances, it is regarded as a free parameter.

4.4 The Rayleigh Hysteresis Model

Since its original publication by Lord Rayleigh [23], the Rayleigh model has had few modifications or improvements. The essential idea is to approximate the hysteresis loops by two intersecting parabolic curves, valid only for low external field strengths.

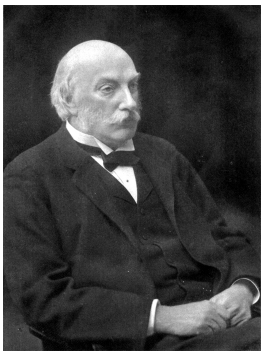

Figure 4.3: Lord Rayleigh

4.4.1 Original Model

The scalar equations of the Rayleigh model as described by Kachniarz and Szewczyk [24] read

$$B_{decr}(H) = \mu_0 \left((\mu_i + \alpha_R H_m) H + \frac{\alpha_R}{2} (H_m^2 - H^2) \right) \tag{4.4}$$

$$B_{incr}(H) = \mu_0 \left((\mu_i + \alpha_R H_m) H - \frac{\alpha_R}{2} (H_m^2 - H^2) \right) \tag{4.5}$$

where the first equation describes the upper, decreasing part of the hysteresis loop, whereas the second equation describes the lower, increasing part.

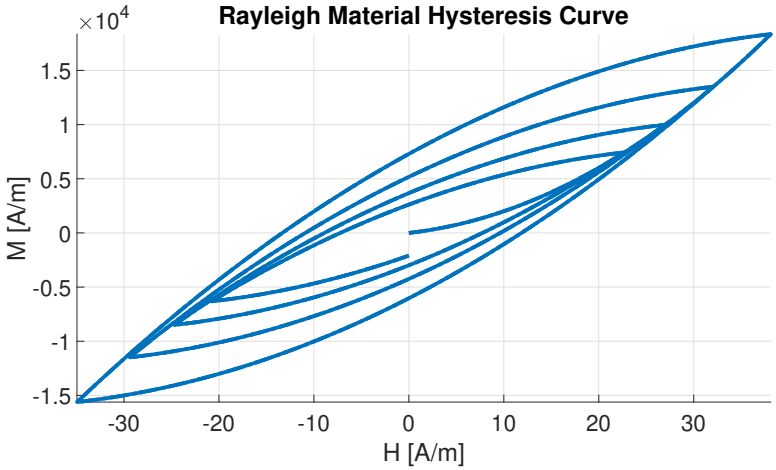

Figure 4.4: Behaviour of the Rayleigh hysteresis model under the influence of a gradually decreasing but alternating magnetic field. One can see that all monotone parts of the curve are parabolas. The extreme end points of these curves are located at specific magnetic field strengths H_m.

Furthermore, the quantity H_m represents the (local) extremal value of the driving magnetic field, in order to connect the two parabolic curves. The virgin curve, obtained when applying an increasing magnetic field to the material starting from a demagnetized state, is described by setting $H_m = 0$ and changing the nonlinear part:

$$B_{virgin}(H) = \mu_0(\mu_i H + 2\alpha_R H^2) \tag{4.6}$$

which results in a connected hysteresis loop when combined with Equation 4.4 and Equation 4.5. The two parameters μ_i (dimensionless) and α_R [$\mathrm{T\,m^2\,A^{-2}}$] are the only parameters in the Rayleigh model, governing the linear and parabolic component of the hysteresis curve,

respectively. Because of its simple and descriptive form, the Rayleigh model allows for the analytical computation of many different magnetic quantities of interest. Among others, this was done by Baldwin [63], who also criticised the Rayleigh relation for very small values of H_m by proposing different logarithmic and exponential terms in the relation. Physical arguments for the Rayleigh model in low field strengths were given by Magni et al. [64], who took a stochastic approach to hysteresis and found a Rayleigh law in the low-field domain.

4.4.2 Vectorial Extension

The scalar Rayleigh model is of the specific form

$$B = B(H, \dot{H}, \theta) \tag{4.7}$$

where θ denotes the Rayleigh parameters. Using the main constitutive relation Equation 2.9, one is able to derive a $M - H$ relation:

$$M = B/\mu_0 - H \quad \Longrightarrow \quad M(H, \dot{H}, \theta) = B(H, \dot{H}, \theta)/\mu_0 - H \tag{4.8}$$

Partially differentiating this expression with respect to H while inserting the Rayleigh $B - H$ relation yields for the increasing-decreasing phase:

$$\frac{\partial M}{\partial H} = \mu_i + \alpha_R H_m \pm \alpha_R H - 1. \tag{4.9}$$

Now, this scalar equation needs to be vectorized. A straightforward choice would be to let all parameters be symmetric tensors. However, one then runs into trouble with matrix and vector dimensions, because one has to provide an interpretation of the square of a vector. We therefore propose the vectorial Rayleigh model in its incremental formulation to be, where $d = x, y, z$:

$$\mathrm{d}\mathbf{M}_d = \begin{cases} (\underline{\boldsymbol{\chi}}\,\mathrm{d}\mathbf{H})_d + (2\underline{\boldsymbol{\alpha}}_R(\sigma(\mathrm{d}\mathbf{H} \otimes \mathbf{H}))\,\mathrm{d}\mathbf{H})_d & \text{if } (\mathbf{H}_m)_d = 0 \\ (\underline{\boldsymbol{\chi}}\,\mathrm{d}\mathbf{H})_d + (\underline{\boldsymbol{\alpha}}_R(\mathbf{H}_m + \sigma(\mathrm{d}\mathbf{H} \otimes \mathbf{H}))\,\mathrm{d}\mathbf{H})_d & \text{if } (\mathbf{H}_m)_d > 0, \end{cases} \tag{4.10}$$

where $\otimes$ denotes the Kronecker or pointwise product between two vectors. $\underline{\boldsymbol{\chi}} = \underline{\boldsymbol{\mu}}_i - \underline{\mathbf{1}}$ can be an anisotropic tensor, and we assume $\underline{\boldsymbol{\alpha}}_R$ to be a diagonal tensor. Furthermore,

$$\sigma(\mathrm{d}\mathbf{H}) := \begin{pmatrix} \mathrm{sgn}(\mathrm{d}\mathbf{H}_x) \\ \mathrm{sgn}(\mathrm{d}\mathbf{H}_y) \\ \mathrm{sgn}(\mathrm{d}\mathbf{H}_z) \end{pmatrix} \tag{4.11}$$

The incremental expression **??** can be used to derive the Rayleigh incremental susceptibility

$$\underline{\boldsymbol{\chi}}^d_{RA} := \frac{\partial \mathbf{M}}{\partial \mathbf{H}} \tag{4.12}$$

which is in turn useful for modelling the magnetic behaviour of the ellipsoid, as will be demonstrated later on.

4.4.3 Visualizing the Rayleigh Model

In order to investigate the behaviour of the vectorial Rayleigh model, a magnetic field $\mathbf{H}(t)$ is prescribed and the incremental formulation **??** is used to obtain a material $\mathbf{M} - \mathbf{H}$-curve. Below, one can observe the behaviour of the Rayleigh model in different settings and varying applied magnetic fields.

4.4.4 Strategies for parameter estimation

In [23], a recipe for the identification of parameters of different materials is proposed on the basis of measuring different pairs of values (H_m, B_m), where

$$B_m = B_{incr}(H_m) = B_{decr}(H_m) = \mu_0(\mu_i + \alpha_R H_m)H_m \tag{4.13}$$

according to the Rayleigh model. Measuring different pairs of (h_m, b_m) (the small letter denotes a measurement of the corresponding capital quantity) and fitting them to (4.13) using a least squares approach, yields estimates for the parameters in the Rayleigh model [24].
Useful strategies for estimating the Rayleigh parameters in the vectorial case could be:

- Employing the approach above, under the assumption of sinusoidal driving field and isotropy.
- Using a gradient and/or adjoint approach to obtain some form of gradient-based error minimization.
- Using a smart genetic algorithm.

Since the Rayleigh model only has a relatively small number of parameters, the second approach could still be feasible. Since the model is also relatively computationally efficient, the genetic-algorithm approach could also result in a useful parameter estimation scheme.

4.5 The Jiles-Atherton Hysteresis Model

The Jiles-Atherton model was proposed by D.C. Jiles and D.L. Atherton in 1984 [21]. It is a scalar model, widely used in modelling magnetic hysteresis over the years. The model is based on already existing ideas of magnetic domain wall motion, including bending (reversible) and translation (irreversible). Concise energetic balances lead to certain conservation equations, giving rise to constitutive relations, as was demonstrated by Melo and Esteves Araujo [36].

Figure 4.5: David Jiles

Figure 4.6: David L. Atherton

The pinning of domain boundaries on certain locations is the cause of hysteresis: without these pinning conditions, a Langevin-type of 'anhysteretic' curve describes the $H - M$-relation. This anhysteretic curve is a fundamental idea of the Jiles-Atherton model. The main result of the model assumptions is an ODE of the form

$$\frac{\mathrm{d}M}{\mathrm{d}H} = f(M, H, dH/dt). \tag{4.14}$$

In that respect, it can be treated in the same way as a differential Rayleigh model. However, the Jiles-Atherton model is more complex in the sense that the change in M is dependent on M itself, while the Rayleigh model only relates it to the magnetic field itself. Moreover, the Jiles-Atherton model makes use of the anhysteric curve, unlike the Rayleigh model but similarly to the Energy-Variational model.
Many modifications, such as vectorial extensions and minor loop adjustments, have been made following the original proposal of the model, which will be briefly discussed in this section. For the total derivation of the Jiles-Atherton model, the reader is directed to the cited papers and books.

4.5.1 Original Model

The original Jiles-Atherton ODE is given by

$$\begin{cases} \frac{dM}{dH} & = \frac{1}{(1+c)} \frac{M_{an}(H_e) - M}{\delta k - \alpha (M_{an}(H_e) - M)} + \frac{c}{(1+c)} \frac{dM_{an}}{dH}, \\ M_{an}(H_e) & = M_s \left(\coth\left(\frac{H_e}{a}\right) - \frac{a}{H_e} \right), \\ H_e & = H + \alpha M \end{cases} \tag{4.15}$$

where the *saturation magnetization* M_s [$\mathrm{A\,m^{-1}}$], the *anhysteric shape parameter* a [$\mathrm{A\,m^{-1}}$], the *mean field parameter* α (non-dimensional), the *pinning energy parameter* k [T] and the *ratio coefficient* c (nondimensional) are the regular parameters in the Jiles-Atherton model. The indicator variable $\delta \in \{-1, 1\}$ is defined as $\delta := \operatorname{sgn}(dH/dt)$. Jiles and Atherton tested and fitted their model to specific materials, which yielded good agreement in case of major loop calculations. In the years following the publication of their paper, the model received some criticism. For example, see Zirka et al. [50], who pointed out some non-physical 'constructions, explanations and patches' in the original Jiles-Atherton model. They point out that the model fails to account for accurate minor loop predictions. Moreover, a non-physical negative susceptibility can be observed in the Jiles-Atherton model in specific situations, which does not occur in nature. Modifications and extensions were proposed in order to make the model more realistic, which can be summarized as 'the susceptibility criterion' and 'the closed-loop criterion'.

Susceptibility Criterion Firstly, in some cases, unphysical negative susceptibility values are observed in the original Jiles-Atherton model. To counter this behaviour, different authors have employed a susceptibility positivity criterion, sometimes reflected in a 'positive part' function, defined by

$$x^+ := \begin{cases} x, \, x \geq 0 \\ 0, \, x < 0, \end{cases} \tag{4.16}$$

and sometimes by introducing an extra parameter $\delta_M \in \{0, 1\}$. This modifies the Jiles-Atherton ODE as encountered in (4.15), as is described by Szewczyk et al. [29].

Minor Loop Dissipation Criterion Leite et al. [41] has proposed to introduce another parameter in the Jiles-Atherton model. This *dissipation factor* R (dimensionless) is a parameter that is not fixed but rather is dependent on the location within the hysteresis loop. It complicates the model but offers the flexibility needed to account for physically realistic minor loops. In the overview paper by Berkman [73], this modification is also discussed.

4.5.2 Vectorial Extension

Secondly, a vectorial Jiles-Atherton model was proposed by Bergqvist [40]. He already notes negative susceptibility issues in the original Jiles-Atherton model. He proceeds by making the parameters c and k from the original ODE symmetric tensors, yielding the vectorial equation

$$\mathrm{d}\mathbf{M} = \frac{\underline{\boldsymbol{\chi}}_f}{||\underline{\boldsymbol{\chi}}_f||}(\underline{\boldsymbol{\chi}}_f \cdot \mathrm{d}\mathbf{H}_e)^+ + \underline{\boldsymbol{c}}\underline{\boldsymbol{\xi}}\,\mathrm{d}\mathbf{H}_e \tag{4.17}$$

where

$$\begin{cases} \underline{\boldsymbol{\chi}}_{\boldsymbol{f}} & := \underline{\boldsymbol{k}}^{-1}(\mathbf{M}_{an}(\mathbf{H}_e) - \mathbf{M}) \\ \underline{\boldsymbol{\xi}}_{ij} & := \frac{\partial \mathbf{M}_{an,i}}{\partial \mathbf{H}_{e,j}} \end{cases} \tag{4.18}$$

and, for example,

$$\mathbf{M}_{an}(\mathbf{H}_e) = M_s \left(\coth \frac{||\mathbf{H}_e||}{A} - \frac{A}{||\mathbf{H}_e||} \right) \frac{\mathbf{H}_e}{||\mathbf{H}_e||} \tag{4.19}$$

From these two equations, any increment in $\mathbf{M}$ can be computed from an increment in $\mathbf{H}$, the driving magnetic field. However, the above equation is implicit in case $\underline{\boldsymbol{\alpha}} \neq \mathbf{0}$. Indeed, since $d\mathbf{H}_e = d\mathbf{H} + \underline{\boldsymbol{\alpha}} d\mathbf{M}$, the quantity of interest $d\mathbf{M}$ appears on both sides of the equation and should be solved in a 'separation of cases' or iterative way. Another approach to a vectorial extension of the Jiles-Atherton model was given by Szymanski and Waszak [51]. Bergqvist does not address anisotropic materials explicitly and only considers uniaxial anisotropic materials. Szewczyk [29] does indeed give expressions for the computation of the fully anisotropic Jiles-Atherton model.

4.5.3 Visualizing the Jiles-Atherton Model

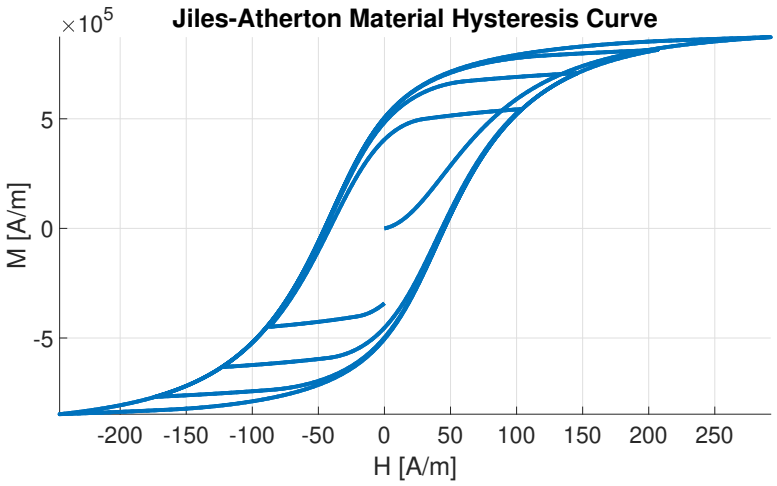

Figure 4.7: A depiction of the material Jiles-Atherton model.

The characteristic shape of hysteresis curves is visible, which has to do with the magnetizing field reaching saturation strengths.

4.5.4 Strategies for parameter estimation

Many different methods of finding the Jiles-Atherton material parameters exist in literature. The earliest parameter identification procedures were devised by Jiles and Atherton themselves. Thereafter, Jiles [48] proposed a parameter estimation method to estimate the parameters

a, α, k and c using readily available material properties. Based on the shape of experimental hysteresis curves, he manages to estimate the parameters with an error of only a few percent. Various intercepts and slopes (incremental susceptibility) were used in determining the parameters. However, this method relies on the choice of anhysteric curve and is only applicable to material-isotropic materials.
Pop and Caltun [49] essentially perform the same procedure, with a very thorough description of their approach. Leite et al. [41] employed a genetic algorithm to obtain the classical Jiles-Atherton parameters. Thereafter, they used a set of inner minor loops to obtain a $R-(H,B)$ relation, which indicates the difficulty of estimating the 'variable' parameter R. They used polynomial regression to obtain good results of the parameter fit.
Three other parameter estimation methods were found in literature. Firstly, a differential evolution algorithm was employed by Biedrzycki et al. [61], which gave good and efficient results, even in the anisotropic, vectorial case with 9 parameters. They describe their method in detail. In his thesis, Olivier Baas [74] has fitted the Jiles-Atherton model to experimental data using the so-called 'Shuffled Frog-Leaping Algorithm', introduced by [62]. This gave very promising results. Lastly, an adjoint method of finding the parameters of the Jiles-Atherton model while incorporating the positive susceptibility criterion was proposed by Zaman et al. in 2016 [52]. This methodology allowed them to efficiently compute the gradient of the cost function with respect to the Jiles-Atherton parameters, and by employing a conjugate gradient-type algorithm, significantly lowered the computational time of arriving at optimal parameters.

4.6 The Energy-Variational Hysteresis Model

The Bergqvist Energy-Variatonal model for ferromagnetic hysteresis was first outlined by Bergqvist in his original paper [37]. By looking at solid-state and thermodynamic energy balances and perturbations in them, he derives a intrinsically vectorial model, reminiscent of dry friction dynamics. For a thorough discussion of the energy balances involved in his model, including notions as Helmholtz and Gibbs free energy, the reader may consult a standard work on thermodynamics [16]. Starting from perturbations in the Helmholtz and Gibbs free energy by applying distributed 'pinning sites' in a ferromagnetic material (akin to the Jiles-Atherton model), he devises a forward algorithm for computing the magnetization in time. Later, he considers an extension of the model by making use of pseudoparticles, an idea also prominent in the Preisach model [22]. Bergqvist successfully fitted the model to different materials. Later research however indicated that the forward step utilised by Bergqvist may introduce systematic errors in the vectorial and especially the anisotropic case [38, 39]. Francois-Lavet et al. [38] therefore proposed an optimization-based approach to find the next magnetization state as function of the applied signal. Prigozhin et al. [39] in turn have improved the optimization scheme by employing some notions of constrained optimization.

Figure 4.8: Leonid Prigozhin

Figure 4.9: Anders Bergqvist

4.6.1 Original Model

The Energy-Variational hysteresis model in its simplest form (without using the effective field or pseudoparticles) consists of a central variational inequality. This inequality is numerically discretized in time, which is thereafter proven to be equivalent to a discretized optimization problem. A (generally unique) minimum is found by Newton's minimization algorithm, using the gradient and Hessian of the function to be minimized. The cost is a function of the (chosen) anhysteretic curve and the previous magnetization of the system only. However, the allowed domain for the new magnetization value is finite and determined by the driving field and friction parameters. Let us quickly describe the derivation of the Energy-Variational model below.

Theoretical Derivation

Consider a ferromagnetic material. The magnetostatic field energy inside a material can be written as the sum of the vacuum field energy plus the material magnetization energy as follows:

$$W = \frac{1}{2}\mu_0\|\mathbf{H}\|^2 + U(\mathbf{M}) \tag{4.20}$$

We now postulate (A1) a time derivative (denoted by $\dot{(...)}$) of the magnetostatic field energy by introducing a dissipative expression:

$$\dot{W} = \mathbf{H}\cdot\dot{\mathbf{B}} - \|r\dot{\mathbf{M}}\| \tag{4.21}$$

where in general, r is a symmetric positive definite matrix with entries determined by the degree of (an)isotropy in the material at hand. r can rightly be interpreted as a friction coefficient matrix. Equating the time derivative of (4.20) to (4.21), we obtain the expression

$$(\mathbf{H} - \mathbf{f}(\mathbf{M}))\cdot\dot{\mathbf{M}} = \|k\dot{\mathbf{M}}\| \tag{4.22}$$

where we have used the chain rule, $k = r/\mu_0$ and $\mathbf{f}(\mathbf{M}) := \frac{1}{\mu_0}\nabla_{\mathbf{M}}U(\mathbf{M})$. We now assume (A2) the $\mathbf{H}$-field to consist of two parts: A reversible part, defined by $\mathbf{H}_r := \mathbf{f}(\mathbf{M})$, and an irreversible part, $\mathbf{H}_i := \mathbf{H} - \mathbf{H}_r$, which transforms the above equation into an equation relating the irreversible magnetic field and the rate of change of magnetization.

$$\mathbf{H}_i\cdot\dot{\mathbf{M}} = \|k\dot{\mathbf{M}}\|. \tag{4.23}$$

Observe that in the isotropic case ($k \in \mathrm{R}^+$), (4.23) is satisfied by imposing the following conditions on $\mathbf{H}_i$ and $\dot{\mathbf{M}}$:

$$\begin{cases} \|\mathbf{H}_i\| \le k & \\ \|\mathbf{H}_i\| < k & \implies \dot{\mathbf{M}} = \mathbf{0} \\ \dot{\mathbf{M}} \neq \mathbf{0} & \implies \dot{\mathbf{M}} \parallel \mathbf{H}_i \end{cases} \tag{4.24}$$

The implication (4.24) $\implies$ (4.23) is trivial in the case of $\|\mathbf{H}_i\| < k$. If $\|\mathbf{H}_i\| = k$ and $\dot{\mathbf{M}} \neq \mathbf{0}$, we have $\dot{\mathbf{M}} = a\mathbf{H}_i$ for some $a > 0$ and thus

$$\mathbf{H}_i \cdot \dot{\mathbf{M}} = a\mathbf{H}_i \cdot \mathbf{H}_i = a\|\mathbf{H}_i\|^2 = ak^2 = |k|\|a\mathbf{H}_i\| = k\|\dot{\mathbf{M}}\| = \|k\dot{\mathbf{M}}\|. \tag{4.25}$$

which proves the implication. The 'dry friction conditions' (4.24) can be cast into a more convenient form with the help of some concepts from analysis.
Firstly, for $n \in \mathbb{N}$ define the $\mathbb{R}^n$-closed ball $\tilde{K} := \overline{B(0,k)} = \{\mathbf{u} \in \mathbb{R}^n : \|\mathbf{u}\| \leq k\}$. Further, define for any convex function $f : \mathbb{R}^n \to \mathbb{R} \cup \{\infty\}$ the *subdifferential set* of f at the point $\mathbf{x} \in \mathbb{R}^n$

$$\partial f(\mathbf{x}) := \{\partial \in \mathbb{R}^n : f(\mathbf{y}) \geq f(\mathbf{x}) + \partial(\mathbf{y} - \mathbf{x}) \ \ \forall y \in \mathbb{R}^n\} \tag{4.26}$$

INCLUDE EXAMPLE
The subdifferential set of any convex function is always closed and convex. The subdifferential set of the 'modified' indicator function on the compact set $\tilde{K}$, defined by

$$I_{\tilde{K}}(\mathbf{x}) = \begin{cases} 0 & \text{if } \mathbf{x} \in \tilde{K} \\ \infty & \text{if } \mathbf{x} \notin \tilde{K} \end{cases} \tag{4.27}$$

is given by

$$\partial I_{\tilde{K}}(\mathbf{x}) = \begin{cases} \{\mathbf{0}\} & \text{if } \mathbf{x} \in \tilde{K}^{\mathrm{o}} = \{\mathbf{x} \in \mathbb{R}^n : \|\mathbf{x}\| < k\} \\ \{a\mathbf{x} : a > 0\} & \text{if } \mathbf{x} \in \partial\tilde{K} = \{\mathbf{x} \in \mathbb{R}^n : \|\mathbf{x}\| = k\} \\ \varnothing & \text{if } \mathbf{x} \in \tilde{K}^C = \{\mathbf{x} \in \mathbb{R}^n : \|\mathbf{x}\| > k\} \end{cases} \tag{4.28}$$

Now, by (4.24) we have $\mathbf{H}_i \in \tilde{K}$. The dry friction law (4.24) can thus be conveniently expressed as

$$\dot{\mathbf{M}} \in \partial I_{\tilde{K}}(\mathbf{H}_i). \tag{4.29}$$

It can be proven [85] that this characterization of the dry friction force follows from basic thermodynamic principles of admissible irreversible fields, which in retrospect justifies our postulation of the specific dry friction conditions (4.24). In the anisotropic case, k denotes a symmetric positive definite matrix, which is invertible. The k-dependent ball $\tilde{K}$ is then generalised to

$$\tilde{K} := \{\mathbf{u} \in \mathbb{R}^n : \|k^{-1}\mathbf{u}\| \leq 1\} \tag{4.30}$$

With the above definition, (4.29) still holds in anistropic material. We postulate the dry friction force conditions as follows:

$$\begin{cases} \|k^{-1}\mathbf{H}_i\| \leq 1 & \\ \|k^{-1}\mathbf{H}_i\| < 1 & \implies \dot{\mathbf{M}} = \mathbf{0} \\ \dot{\mathbf{M}} \neq \mathbf{0} & \implies k\dot{\mathbf{M}} \parallel k^{-1}\mathbf{H}_i \end{cases} \tag{4.31}$$

Using mathematical arguments, this yields the variational inequality, where $\mathbf{M}_p$ is the previous magnetization state:

$$\text{Find } \mathbf{H}_r \in K(t) \ : \ (\nabla S(\mathbf{H}_r) - \mathbf{M}_p) \cdot (\mathbf{u} - \mathbf{H}_r) \geq 0, \ \forall\, \mathbf{u} \in K(t). \tag{4.32}$$

This variational inequality is of certain type discussed in the mathematical paper by Peng [84]. The main theorem states that the above variational inequality is equivalent to an unconstrained minimization

$$\mathbf{H}_r(t) = \underset{\mathbf{u} \in K(t)}{\arg\min}\{S(\mathbf{u}) - \overset{\vee}{\mathbf{M}} \cdot \mathbf{u}\} \tag{4.33}$$

This minimization problem has a unique solution, provided that the derivative $M'_{an} > 0$ on its domain. This is the case for realistic anhysteric curves. Let us look more deeply into the minimization problem (4.33). The unconstrained problem

$$\mathbf{H}_r(t) = \arg\min_{\mathbf{u}\in\mathbb{R}^3}\{S(\mathbf{u}) - \overset{\vee}{\mathbf{M}}\cdot\mathbf{u}\} \tag{4.34}$$

is at a point $\mathbf{u} \in \mathbb{R}^3$ where $\nabla(S(\mathbf{u}) - \overset{\vee}{\mathbf{M}}\cdot\mathbf{u}) = \nabla S(\mathbf{u}) - \overset{\vee}{\mathbf{M}} = \mathbf{0}$. For further reference, we refer to the paper by Prigozhin et al. [39]. Summarizing, the parameters in the Energy-Variational model are the two anhysteric curve parameters M_s [$\mathrm{A\,m^{-1}}$] and A [$\mathrm{A\,m^{-1}}$]. Later on in their paper, the concept of *effective field* $\mathbf{H}_e = \mathbf{H} + \underline{\boldsymbol{\alpha}}\mathbf{M}$ is introduced, bringing about an extra parameter $\underline{\boldsymbol{\alpha}}$. However, the most important parameters in [39] are the dry friction parameters (tensors). In the simplest version of the model ($N = 1$, which means 'no linear superposition of pseudoparticles'), there is just one dry friction tensor $\underline{\boldsymbol{k}}$ [$\mathrm{A\,m^{-1}}$]. For $N > 1$, one obtains the total magnetization of the system as a linear superposition of pseudoparticle magnetizations. Then, N weights $\omega_1, ..., \omega_N$ as well as N pseudoparticle friction tensors $\underline{\boldsymbol{k}}_1, ..., \underline{\boldsymbol{k}}_N$ are needed. Denoting the total magnetization of the model by $\mathbf{M}$, it can be written as

$$\mathbf{M} = \sum_{l=1}^{N} \omega_l \mathbf{m}^l \tag{4.35}$$

where each $\mathbf{m}^l$ is computed according to the minimization procedure, with different friction tensors. The above model description is far from complete. For a more thorough description, one should consult the original paper by Prigozhin et al. [39].

4.6.2 Vectorial Extension

In the EV model, the update is done as follows. One must keep track of several 'friction variables' throughout the entire simulation. The new magnetization at each node is given by:

$$\begin{cases} \mathbf{M}_{new} & = \sum_{l=1}^{N_c} \omega^l \mathbf{M}_c^l = \sum_{l=1}^{N_c} \omega^l \mathbf{M}_{an}(||\mathbf{H}_r^l||)\frac{\mathbf{H}_r^l}{||\mathbf{H}_r^l||} \\ \mathbf{H}_r^l & = \arg\min_{\mathbf{u}\in K^l(t)}\{S(\mathbf{u}) - \mathbf{M}_{c,old}^l\cdot\mathbf{u}\} \\ S(\mathbf{u}) & = \int_0^{||\mathbf{u}||} M_{an}(s)\,\mathrm{d}s \\ K^l(t) & = \{\mathbf{u}\in\mathbb{R}^3 : ||(k^l)^{-1}(\mathbf{u} - \mathbf{H}_{eff}^l)|| \le 1\} \end{cases} \tag{4.36}$$

where the optimization step can be done by gradient descent or Newton minimization, by first writing the problem differently using spherical coordinates. We have implemented this in three dimensions, whereas the authors of the original model have done their derivations and implementations in only two dimensions [39].

4.6.3 Visualizing the Energy-variational model

Below, one can observe the behaviour of the material **EV**model when using a different number of elementary magnetization cells.

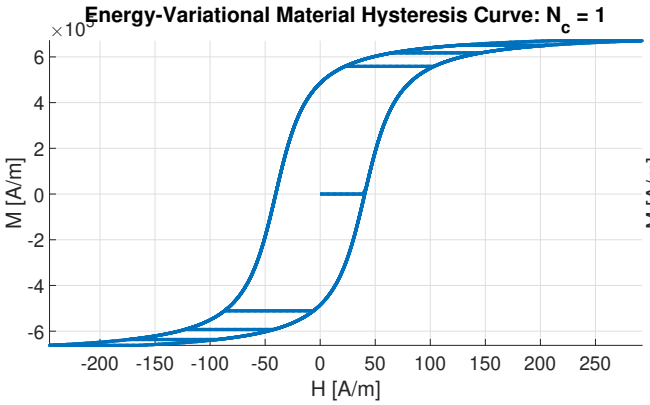

Figure 4.10: The material **EV**model with 1 cell. One can observe quite abrupt behaviour.

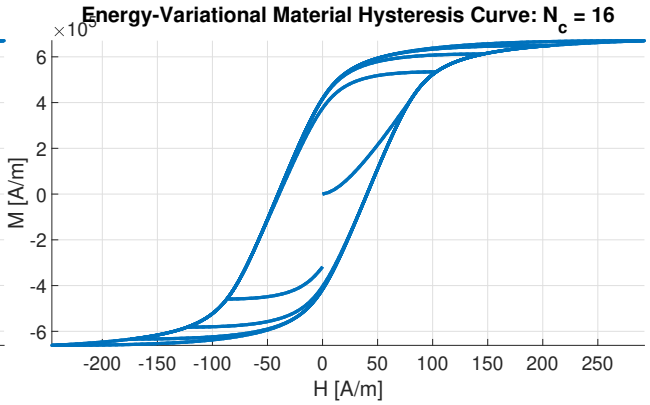

Figure 4.11: The material **EV**model with 16 cells. Smoother model behaviour is visible.

Another interesting fact about the **EV**model is that it is intrinsically vectorial. This can for example be observed in the following figure, which depicts a phenomenon known as 'magnetic leaking', which is actually observed in experiments

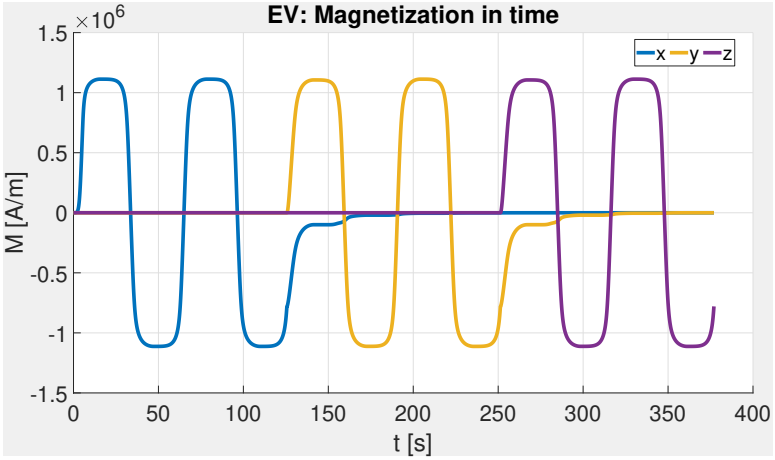

Figure 4.12: The phenomenon of magnetic leaking. Although all parameters are taken isotropic in this simulation, the magnetization changes even when there is no net magnetic field in the direction of change.

4.6.4 Strategies for parameter estimation

In the Energy-Variational model as described by Prigozhin et al. [39], parameter estimation was performed as follows. Under the assumption of material isotropy, a known anhysteric curve and a known distribution of $N = 41$ friction parameters $k_1, ..., k_N$, only the $N = 41$ weights $\omega_1, ..., \omega_N$ had to be estimated. In their procedure, Prigozhin et al. used a cubic spline function as an approximation to the anhysteric function. By performing several experiments, the anhysteric curve and the coupling parameter α could be estimated. Next, a three-level Matlab algorithm was implemented to estimate the weights ω_i. In three nested algorithm steps, a least squares-error was minimized using intrinsic Matlab functions. That way, the anhysteric curve, the value of α and the weights were estimated using a set of experimental 'FORCs' (First-Order Reversal Curves). This is a promising and straightforward approach for parameter estimation, it yielded excellent results on real material [39].

4.7 Comparing the hysteresis models

Looking at the four discussed models, we disregard the **IP**model for now. It is clear that the Energy-Variational model is the most complex out of the three, followed by the Jiles-Atherton model. The Rayleigh model is the simplest, but also the most inflexible; it is furthermore only applicable at low to moderate magnetic field strengths. The Rayleigh and Jiles-Atherton model are both scalar in nature, whereas the Energy-Variational model is vectorial from the start. In terms of parameter estimation, the Rayleigh model is also the simplest. The dissipative R-factor in the modified Jiles-Atherton model poses a difficulty and potentially makes the Jiles-Atherton model less attractive for our purposes, so a choice is made not to include the R-factor in our Jiles-Atherton models. In terms of the exact number of free scalar parameters, the following holds, where d is the number of spatial dimensions:

- The original Rayleigh model has 2 parameters. The multi-dimensional Rayleigh model replaces the two scalar parameters by two (symmetric) tensors, increasing the number of parameters to $d^2 + d$. The number H_m is not really a parameter, but rather a property and consequence of the applied field and the local magnetization.

- The original Jiles-Atherton model has 5 parameters. Not all these parameters are transformed to vectors of tensors in the vectorial case. Bergqvist [40] indicates that in the vectorial case, the parameters α, k and c become symmetric tensors, bringing the total number of parameters to $2 + \frac{3}{2}(d^2 + d)$. Furthermore, the minor loop closure parameter R needs to be estimated for any minor loop, making it a 'pseudo-parameter', comparable to but more complex than H_m in the Rayleigh Model.

- The Energy-Variational model has two anhysteric curve-parameters, just as the Jiles-Atherton model. The effective field parameter $\underline{\boldsymbol{\alpha}}$ introduces another $\frac{1}{2}(d^2+d)$ parameters. When N pseudoparticles are used in modelling the hysteresis behaviour, N weights and $\frac{N}{2}(d^2+d)$ scalar friction parameters are needed, bringing the total number of parameters to $N + 2 + \frac{N+1}{2}(d^2 + d)$.

All three hysteresis models have their advantages and disadvantages. It is useful to make a further practical comparison of the performances of the models, which will be done later on in this research.
In the four previous chapters, we have seen the global overview of the present research, the elementary Maxwell Equations, the geometry of the ellipsoid problem as well as problem definitions, constitutive relations and non-linear dependencies between different magnetic quantities. In cases of high symmetry or easy spatial configurations, one can derive analytic equations as solutions to the Maxwell equations. In rare cases, analytic differential equations describing the non-linear behaviour of ferromagnetic geometrical matter can even be derived (for example, luckily, ellipsoidal bodies) [27]. The previous four chapters thus formed the introduction to the research.
The next two parts will describe how local hysteresis relations and the Maxwell equations are combined to yield a description of the actual inner behaviour of the prolate steel ellipsoid, in increasing levels of complexity and (hopefully) accuracy.

Part II

Homogeneous Ellipsoid Models

Chapter 5

The Ellipsoid Formula

5.1 Demagnetizing Field

Let us consider material that internally reacts to an applied field. As was briefly discussed in the chapter on magnetostatics, ferromagnetic material can be viewed as consisting of a large collection of micro- or mesoscopic magnetic domains. Locally and averaged over time (neglecting Barkhausen fluctuations), the magnetization due to an applied field can be assumed constant over those subdomains. The net magnetization 'creates' small dipoles inside the material, in turn causing a nonzero magnetic field. The magnetic field *inside* a magnetic material, which is thus a consequence of the applied field and magnetization, is in general a complicated function of the geometry of the object, the magnetization distribution and the applied field itself. With this in mind, writing the magnetic field inside a material *locally* as a sum of the applied field $\mathbf{H}_a(\mathbf{r})$ and the 'magnetization-caused' field $\mathbf{H}_M(\mathbf{r})$, which is justified by the superposition principle, one can write

$$\mathbf{H}(\mathbf{r}) = \mathbf{H}_a(\mathbf{r}) + \mathbf{H}_M(\mathbf{M}(\mathbf{r}), \mathbf{r}) \tag{5.1}$$

which always holds true. It is also true that (locally speaking) $\mathbf{H}_M(\mathbf{z}, \mathbf{r}) = \mathbf{z}$. Now, expanding the magnetization-caused field to first order in $\mathbf{M}(\mathbf{r})$ yields

$$\begin{aligned} \mathbf{H}_M(\mathbf{M}(\mathbf{r}), \mathbf{r}) &= \mathbf{H}_M(\mathbf{0}, \mathbf{r}) + \frac{\partial \mathbf{H}_M(\mathbf{0}, \mathbf{r})}{\partial \mathbf{M}} \mathbf{M}(\mathbf{r}) + h.o.t. && (5.2)\\ &= \frac{\partial \mathbf{H}_M(\mathbf{0}, \mathbf{r})}{\partial \mathbf{M}} \mathbf{M}(\mathbf{r}) + h.o.t. && (5.3)\\ & && (5.4) \end{aligned}$$

Defining the *local demagnetization tensor* as

$$\underline{\boldsymbol{N}}(\mathbf{r}) := -\frac{\partial \mathbf{H}_M(\mathbf{0}, \mathbf{r})}{\partial \mathbf{M}}, \tag{5.5}$$

one observes that the magnetic field inside any magnetized material may be written out locally as

$$\begin{aligned} \mathbf{H}(\mathbf{M}(\mathbf{r}), \mathbf{r}) &= \mathbf{H}_a(\mathbf{r}) + \mathbf{H}_M(\mathbf{M}(\mathbf{r}), \mathbf{r}) && (5.6)\\ &= \mathbf{H}_a(\mathbf{r}) - \underline{\boldsymbol{N}}(\mathbf{r})\mathbf{M}(\mathbf{r}) + h.o.t. && (5.7)\\ & && (5.8) \end{aligned}$$

5.2 The Ellipsoid Formula

Having obtained the nomenclature 'demagnetization tensor', the following important result can be stated.

Theorem 5.2.1 (The Ellipsoid Formula)**.** *If a (degenerate) ellipsoidal body is placed in a uniform background field* $\mathbf{H}_a$ *and is uniformly magnetized with magnetization* $\mathbf{M}$*, the demagnetization field* $\mathbf{H}_M$ *is also uniform. Furthermore, the demagnetization tensor is diagonal and constant across the ellipsoid, with elements that can be calculated explicitly from the ellipsoidal dimensions only:*

$$\mathbf{H} = \mathbf{H}_a - \underline{\boldsymbol{N}}\mathbf{M} \text{ (inside ellipsoid)} \tag{5.9}$$

The magnetic field inside the ellipsoid is thus uniform. Also,

$$\mathbf{H}(\mathbf{r}) = A(\mathbf{r})\mathbf{M} \text{ (outside ellipsoid)} \tag{5.10}$$

where $A(\mathbf{r})$ *is a* 3×3 *matrix with entries solely depending on the geometry of the problem and* $\mathbf{r}$*.*

Remark. 1. Relative to the general demagnetization equation Equation 5.8, the above (degenerate) ellipsoid formula is exact (higher order terms vanish), and is moreover *independent* of location inside the ellipsoid. This is a remarkable result and holds true only for (degenerate) ellipsoidal bodies. 2. The word 'degenerate' in the above theorem is understood as follows. A body is said to be degenerate ellipsoidal if one or more of its semi-diameters tend to either zero or infinity. For example, this allows one to compute the magnetic field inside a long rod, a plate or a disk using the general result on demagnetization tensors. The eigenvalues of the demagnetization tensor are known as *demagnetization factors*.

Proof. See Lepelaars [90]. □

5.3 Extending the Ellipsoid Formula

Let us now look at the consequences of the important ellipsoid formula:

$$\mathbf{H} = \mathbf{H}_a - \underline{\boldsymbol{N}}\mathbf{M} \tag{5.11}$$

As is noted in the conditions in the derivation of the ellipsoid formula, this formula strictly holds in the following circumstances: 1. The ellipsoid has to have a uniform magnetization, an can thus be described by only one vector in $\mathbb{R}^3$, and 2. The background field has to be uniform. Thus far, nothing has been said about the interplay between the magnetization $\mathbf{M}$ and the internal magnetic field $\mathbf{H}$. In order to incorporate this relation, linear or nonlinear (hysteresis), one needs to prove that the ellipsoid formula is valid in nonlinear time-dependent cases.

Theorem 5.3.1 (Time-dependent Ellipsoid Formula)**.** *If the material parameters of the magnetizable ellipsoid are constant across the ellipsoid, and the initial/permanent magnetization of the ellipsoid is uniform, application of a continuous uniform background field* $\mathbf{H}_a(t)$ *results in the time-dependent equation*

$$\mathbf{H}(t) = \mathbf{H}_a(t) - \underline{\boldsymbol{N}}\mathbf{M}(t), \tag{5.12}$$

i.e. the magnetization and magnetic field inside the ellipsoid remain spatially uniform in time.

Proof. This is not a mathematical proof in the strict sense, rather, it is a sketch of a possible way of proving the theorem. Looking at the quasi-static case, relaxation effects can be neglected. Suppose one has the homogeneous equilibrium situation

$$\mathbf{H}_0 = \mathbf{H}_{a0} - \underline{\boldsymbol{N}}\mathbf{M}_0 \tag{5.13}$$

Suppose now that the uniform background field of the ellipsoid is incremented by a *small* value of $\delta\mathbf{H}_a$, so

$$\mathbf{H}_{a1} = \mathbf{H}_{a0} + \delta\mathbf{H}_a.$$

Assuming the demagnetization tensor formulation as discussed in the previous chapter, the internal demagnetization relation can be written as

$$\mathbf{H}_1(\mathbf{r}) = \mathbf{H}_{a1} - \underline{\boldsymbol{N}}_1(\mathbf{r})\mathbf{M}(\mathbf{r}). \tag{5.14}$$

Subtracting the starting equation from the above equation, yields the incremental equation

$$\mathbf{H}_1(\mathbf{r}) - \mathbf{H}_0 = \delta\mathbf{H}_a - \underline{\boldsymbol{N}}_1(\mathbf{r})\mathbf{M}_1(\mathbf{r}) + \underline{\boldsymbol{N}}\mathbf{M}_0 \tag{5.15}$$

Now, let us look a the local relationship between $\delta\mathbf{M}(\mathbf{r}) := \mathbf{M}_1(\mathbf{r}) - \mathbf{M}_0$ and $\delta\mathbf{H}(\mathbf{r}) := \mathbf{H}_1(\mathbf{r}) - \mathbf{H}_0$. In order to prove the theorem, we have to prove that $\delta\mathbf{M}(\mathbf{r}) = \delta\mathbf{M}$ and $\delta\mathbf{H}(\mathbf{r}) = \delta\mathbf{H}$, which means that the increments are uniform inside the ellipsoid. As discussed in the previous chapters, this relation is where a hysteresis model comes in. In general, one can write, if the increments are small (linearisation of the hysteresis curve) :

$$\delta\mathbf{M}(\mathbf{r}) = \underline{\boldsymbol{\chi}}^d[\mathbf{r}, \mathbf{H}(\mathbf{r}), \mathbf{M}(\mathbf{r}), \theta]\delta\mathbf{H}(\mathbf{r}) \tag{5.16}$$

where $\underline{\boldsymbol{\chi}}^d$ is the incremental or differential susceptibility, provided by the hysteresis model. Now, using the homogeneity assumptions of the theorem and using the assumption of small increments, one can set

$$\underline{\boldsymbol{\chi}}^d[\mathbf{r}, \mathbf{H}(\mathbf{r}), \mathbf{M}(\mathbf{r}), \theta]\delta\mathbf{H}(\mathbf{r}) \approx \underline{\boldsymbol{\chi}}^d[\mathbf{0}, \mathbf{H}_0, \mathbf{M}_0, \theta] \tag{5.17}$$

which is constant throughout the material. Manipulating Equation 5.15, one obtains

$$(\underline{\mathbf{1}} + \underline{\boldsymbol{\chi}}^d\underline{\boldsymbol{N}}_1(\mathbf{r}))\mathbf{M}_1(\mathbf{r}) = \underline{\boldsymbol{\chi}}^d(\underline{\boldsymbol{N}}\mathbf{M}_0 + \delta\mathbf{H}_a) \tag{5.18}$$

Now, from Newell et al. [79], we can see that the demagnetization tensor in general media and with non-uniform magnetization, is *only* a function of this non-uniform magnetization and the geometric properties of the object. It follows that we have a situation of the form $f(g(\mathbf{r})) = C \in \mathbb{R}^3$, a constant. Now, when looking at Equation 5.18, it is clear that f is not a constant function, therefore, $\mathbf{M}_1(\mathbf{r})$ has to be a constant function for all $\mathbf{r} \in \Omega_e$. By Equation 5.15, $\mathbf{H}_1(\mathbf{r})$ is also constant in space. The result now follows. However, observe that taking limits without careful analysis and using language such as 'small' causes this 'proof' to not be a real mathematical proof, but rather an indication of a possible way of thinking. □

One last ingredient to add to our theoretical foundation for homogeneous ellipsoid models, is the following proposition. Namely

Proposition 5.3.1 (Anisotropic Ellipsoid Formula)**.** *The Ellipsoid Formula can also be used in anisotropic, nonlinear media with uniform magnetization.*

Chapter 6

Forward Homogeneous Ellipsoid Models

The theorem given above, gives one the hope of modelling the temporal evolution of the magnetization of the ellipsoid using relatively simple models. We accordingly define the homogeneous ellipsoid model as follows.

Definition 6.0.1 (Homogeneous Ellipsoid Model)**.** The Homogeneous Ellipsoid Model is defined as the model resulting from combining the Ellipsoid Formula, a hysteresis model and the linear signature mapping to obtain a mapping

$$\mathbf{B}_s(t) = \mathcal{F}(\theta|\mathbf{H}_a(t), \mathcal{M}[\mathbf{M}(t), \mathbf{H}(t)], \mathbf{M}_0) \tag{6.1}$$

Necessary conditions for an ellipsoid model to be called homogeneous are:

1. Both the magnetization and the magnetic field inside the ellipsoid have to be uniform, and can thus be described using only one vector;

2. The material parameters relating $\mathbf{H}$ and $\mathbf{M}$ inside the ellipsoid have to be constant in space across the ellipsoid;

3. Both the initial magnetization $\mathbf{M}_0$ and the (if existing) permanent magnetization $\mathbf{M}_{per}$ have to be uniform inside the ellipsoid.

The above proposition also allows us to obtain a useful incremental formulation of the magnetization evolution inside a homogeneous ellipsoid. Indeed, differentiating the relation with respect to the components of $\mathbf{H}_a$ yields the incremental equation

$$\frac{\partial \mathbf{M}}{\partial \mathbf{H}_a} = \frac{\partial \mathbf{M}}{\partial \mathbf{H}} \frac{\partial \mathbf{H}}{\partial \mathbf{H}_a} \tag{6.2}$$

$$= \frac{\partial \mathbf{M}}{\partial \mathbf{H}} \left(\underline{1} - \underline{\boldsymbol{N}} \frac{\partial \mathbf{M}}{\partial \mathbf{H}_a} \right) \tag{6.3}$$

$$\tag{6.4}$$

where the chain rule for partial differentiation has been used and $\underline{1}$ denotes the identity matrix. Solving for the $\mathbf{M} - \mathbf{H}_a$ Jacobian yields

$$\frac{\partial \mathbf{M}}{\partial \mathbf{H}_a} = \left(\underline{1} + \frac{\partial \mathbf{M}}{\partial \mathbf{H}} \underline{\boldsymbol{N}} \right)^{-1} \frac{\partial \mathbf{M}}{\partial \mathbf{H}} \tag{6.5}$$

Finally, suppose the applied field $\mathbf{H}_a(t)$ is known and differentiable. By the chain rule, the ODE for the uniform magnetization of a (generally) anisotropic ellipsoid becomes

$$\frac{\partial \mathbf{M}}{\partial t} = \left(\left(\underline{1} + \frac{\partial \mathbf{M}}{\partial \mathbf{H}} \underline{\boldsymbol{N}} \right)^{-1} \frac{\partial \mathbf{M}}{\partial \mathbf{H}} \right) \frac{\partial \mathbf{H}_a}{\partial t} \tag{6.6}$$

$$\mathbf{M}(0) = \mathbf{M}_0 \tag{6.7}$$

$$\mathbf{H}(0) = \mathbf{H}_a(0) - \underline{\boldsymbol{N}} \mathbf{M}_0, \tag{6.8}$$

where the second initial condition is often needed to set up the problem correctly in practice. Solving the above system of three coupled ordinary differential equations is a possible way of simulating the homogeneous ellipsoid model. The Jacobian $\frac{\partial \mathbf{M}}{\partial \mathbf{H}}$ is provided for by the hysteresis operator that is chosen in the model. A numerical integration method to solve ODEs can be used to solve the above equations. In our research, we have implemented a number of such integration algorithms, including Euler Forward and Runge-Kutta-type methods. However, the nature of the above equations requires making use of a more stable, but also more expensive type of solving method. This method will be discussed in the following sections. Firstly, let us focus on the homogeneous **IP**model. Since this model is linear, no time integration is needed and given a background field, initial magnetization and material parameters (in this case, only the susceptibility or permeability tensor), the signature can be computed directly.

6.1 Forward Homogeneous Linear Ellipsoid Model

The simplest model of ellipsoid magnetization in an external field is in the case of permanent magnetization, with a linear component superimposed, the **IP**model. It is based on the assumption

$$\mathbf{M}(t) = \mathbf{M}_{per} + \mathbf{M}_{ind}(t). \tag{6.9}$$

Whereas the permanent magnetization component $\mathbf{M}_{per}$ is assumed constant in time, the induced component varies linearly with $\mathbf{H}$:

$$\mathbf{M}_{ind} = \underline{\boldsymbol{\chi}} \mathbf{H} = (\underline{\boldsymbol{\mu_r}} - \underline{1}) \mathbf{H} \tag{6.10}$$

where, importantly, $\underline{\boldsymbol{\mu_r}}$ and $\underline{\boldsymbol{\chi}}$ are independent of location, time and magnetic quantities in the linear material case. Substituting the ellipsoid formula in the above equation yields after rearranging

$$(\underline{1} + \chi \underline{\boldsymbol{N}}) \mathbf{M}(t) = \mathbf{M}_{per} + \underline{\boldsymbol{\chi}} \mathbf{H}_a(t) \tag{6.11}$$

It is convenient to define the *ellipsoidal susceptibility tensor* $\underline{\boldsymbol{\chi}}_a$ as

$$\underline{\boldsymbol{\chi}}_a := \left(\underline{1} + \underline{\boldsymbol{\chi}} \underline{\boldsymbol{N}} \right)^{-1} \underline{\boldsymbol{\chi}} \tag{6.12}$$

which results in the final solution for $\mathbf{M}(t)$, instantaneously caused by $\mathbf{H}_a(t)$:

$$\mathbf{M}(t) = \underline{\boldsymbol{\chi}}_a \left(\underline{\boldsymbol{\chi}}^{-1} \mathbf{M}_{per} + \mathbf{H}_a(t) \right). \tag{6.13}$$

Perhaps contrary to intuition, $\mathbf{M}(t : \mathbf{H}_a(t) = \mathbf{0}) \neq \mathbf{M}_{per}$ in general. This is because a nonzero $\mathbf{M}_{per}$ already implies a nonzero internal magnetic field. Indeed: $\mathbf{M}(t : \mathbf{H}_a(t) = \mathbf{0}) = (\underline{1} + \underline{\boldsymbol{\chi}} \underline{\boldsymbol{N}})^{-1} \mathbf{M}_{per}$. It is important to realize that in the linear model, all magnetic quantities can be expressed explicitly in the known quantities. No forward time integration is required; there exists an explicit relation between the magnetization in time, the geometry, the material parameters, the applied field and the permanent magnetization. This is quite different in the case of nonlinear hysteresis, as the next sections will demonstrate.

6.2 Forward Homogeneous Hysteresis Ellipsoid Models

As was noted two sections before, simply applying an explicit integration method to solve Equation 6.7 numerically, requires very small time steps and even then, stability is not guaranteed. This is mainly due to the demagnetization mechanism. Because of the wildly varying magnitudes of the magnetic field and magnetization that are present in the ellipsoid, forward integration tends to cause numerical instabilities and diverging behaviour in general. We have therefore taken the approach of Prigozhin et al. [39], who used a stabilizing inner loop mechanism to prevent divergence. The differential equation Equation 6.7 is thus solved in a semi-implicit, semi-explicit way, similar to Crank-Nicholson methods. The approach is the same for all three hysteresis models. Firstly, we derive the necessary equations, and thereafter a pseudocode is provided. Lastly, details on the specifics of the hysteresis models that are used, are given.

6.2.1 Incorporating Hysteresis in the Homogeneous model

We are now ready to describe the homogeneous models including hysteresis in more detail. Define the discrete time steps

$$t_n = n\Delta t,\ n \in \mathbb{N} \cup \{0\}, \tag{6.14}$$

and since we are dealing with a quasi-static situation, one can as well take $\Delta t = 1$ (the previous remarks about 'small time steps' actually have to do with small increments in the applied field, not in time per se). An applied background field $\mathbf{H}_{a,n} = \mathbf{H}_a(t_n)$ is associated to every time step. We now attempt to obtain a time-discretized solution

$$\mathbf{M}_n = \mathbf{M}(t_n),\ \ n \in \mathbb{N} \cup \{0\}, \tag{6.15}$$

after which the internal field is given by employing the ellipsoid formula to yield

$$\mathbf{H}_n = \mathbf{H}(t_n) = \mathbf{H}_{a,n} - \underline{\boldsymbol{N}}\mathbf{M}_n,\ \ n \in \mathbb{N} \cup \{0\}, \tag{6.16}$$

Depending on the hysteresis model that is being used, an extra parameter $\underline{\boldsymbol{\alpha}}$ is needed to describe the Weiss effective field, which was discussed in a previous chapter. **RA**does not include such a parameter, but **JA**and **EV**do.
Having stated the relevant magnetic quantities, the effective internal magnetic field is given at every time step by the superposition principle by

$$\mathbf{H}_{eff,n} = \mathbf{H}_{a,n} + \mathbf{H}_{d,n} + \underline{\boldsymbol{\alpha}}\mathbf{M}_n \tag{6.17}$$

where $\mathbf{H}_{d,n}$ is the demagnetization field. In the case of the ellipsoid, the demagnetization field is given by the familiar $\mathbf{H}_{d,n} = -\underline{\boldsymbol{N}}\mathbf{M}_n$, resulting in the relation

$$\mathbf{H}_{eff,n} = \mathbf{H}_{a,n} + (\underline{\boldsymbol{\alpha}} - \underline{\boldsymbol{N}})\mathbf{M}_n \tag{6.18}$$

Hysteresis is incorporated in the above equations by requiring the general hysteresis operator identity to be satisfied:

$$\mathbf{M}_n = \mathcal{M}[\mathbf{H}_{eff,n}], \tag{6.19}$$

where the square brackets again indicate the nonlinear history-dependency of the operator.

6.2.2 Solving the nonlinear system of equations

The situation is now as follows. Having initialised the problem by the conditions

$$\mathbf{M}(0) = \mathbf{M}_0 \tag{6.20}$$
$$\mathbf{H}(0) = \mathbf{H}_a(0) - \underline{\boldsymbol{N}}\mathbf{M}_0 \tag{6.21}$$
$$\mathbf{H}_{eff}(0) = \mathbf{H}(0) + \underline{\boldsymbol{\alpha}}\mathbf{M}_0 \tag{6.22}$$

we have to solve the simultaneous equations

$$\mathbf{H}_{eff,n} = \mathbf{H}_{a,n} + (\underline{\boldsymbol{\alpha}} - \underline{\boldsymbol{N}})\mathbf{M}_n \tag{6.23}$$
$$\mathbf{M}_n = \mathcal{M}[\mathbf{H}_{eff,n}] \tag{6.24}$$

To do this, we employ an idea by Prigozhin et al., who used a iterative inner loop scheme, indexed by the iteration number k. It is based on the linearization of the hysteresis operator around $\mathbf{H}_{eff,n}$:

$$\mathbf{M}_n^{k+1} = \mathcal{M}[\mathbf{H}_{eff,n}^k] + D[\mathbf{H}_{eff,n}^k]\left(\mathbf{H}_{eff,n}^{k+1} - \mathbf{H}_{eff,n}^k\right) \tag{6.25}$$

where $D[\mathbf{H}_{eff,n}^k]$ is the 3×3 matrix of partial derivatives of $\mathcal{M}[\mathbf{H}_{eff,n}^k]$ with respect to $\mathbf{H}_{eff,n}^k$, that is for $\mathbf{u} = \mathbf{H}_{eff,n}^k$:

$$D[\mathbf{u}] := \frac{\partial \mathcal{M}[\mathbf{u}]}{\partial \mathbf{u}} = \begin{pmatrix} \partial_{\mathbf{u}_x}\mathcal{M}_x[\mathbf{u}] & \partial_{\mathbf{u}_x}\mathcal{M}_y[\mathbf{u}] & \partial_{\mathbf{u}_x}\mathcal{M}_z[\mathbf{u}] \\ \partial_{\mathbf{u}_y}\mathcal{M}_x[\mathbf{u}] & \partial_{\mathbf{u}_y}\mathcal{M}_y[\mathbf{u}] & \partial_{\mathbf{u}_y}\mathcal{M}_z[\mathbf{u}] \\ \partial_{\mathbf{u}_z}\mathcal{M}_x[\mathbf{u}] & \partial_{\mathbf{u}_z}\mathcal{M}_y[\mathbf{u}] & \partial_{\mathbf{u}_z}\mathcal{M}_z[\mathbf{u}] \end{pmatrix} \tag{6.26}$$

Now, as one can see from following sections, this derivative is often very difficult to calculate analytically (but certainly not impossible in the case of **RA**and **JA**). We therefore used central differences to approximate the partial derivatives present in the definition of D. This requires six extra evaluations of $\mathcal{M}$ per iteration, but usually shows very stable behaviour. To be clear, D can be approximated numerically column-wise by setting $\delta > 0$ small and computing

$$D[\mathbf{u}] \approx \frac{1}{2\delta}\left(\mathcal{M}[\mathbf{u} + \delta\mathbf{e}_x] - \mathcal{M}[\mathbf{u} - \delta\mathbf{e}_x],\ \ \mathcal{M}[\mathbf{u} + \delta\mathbf{e}_y] - \mathcal{M}[\mathbf{u} - \delta\mathbf{e}_y],\ \ \mathcal{M}[\mathbf{u} + \delta\mathbf{e}_z] - \mathcal{M}[\mathbf{u} - \delta\mathbf{e}_z]\right). \tag{6.27}$$

Now, substituting the linear approximation Equation 6.25 into Equation 6.23, rearranging and solving for $\mathbf{H}_{eff,n}^k$, one obtains the iteration formula for $\mathbf{H}_{eff,n}^k$:

$$\mathbf{H}_{eff,n}^{k+1} = \left(\underline{\mathbf{1}} + (\underline{\boldsymbol{N}} - \underline{\boldsymbol{\alpha}})D[\mathbf{H}_{eff,n}^k]\right)^{-1}\left(\mathbf{H}_{a,n} - (\underline{\boldsymbol{N}} - \underline{\boldsymbol{\alpha}})\left(\mathcal{M}[\mathbf{H}_{eff,n}^k] - D[\mathbf{H}_{eff,n}^k]\mathbf{H}_{eff,n}^k\right)\right). \tag{6.28}$$

These iterations are repeated until convergence of $\mathbf{H}_{eff,n}^k$ with a given tolerance $\varepsilon > 0$. When the iteration converges at the iterate k_{conv}, one sets

$$\mathbf{H}_{eff,n} = \mathbf{H}_{eff,n}^{k_{conv}} \tag{6.29}$$
$$\mathbf{M}_n = \mathcal{M}[\mathbf{H}_{eff,n}^{k_{conv}}] \tag{6.30}$$

to obtain the solution of the problem at time n.
Finally, the following pseudo code contains the procedure to simulate the homogeneous models with different underlying hysteresis models, simulated until a time value T. Choose $\varepsilon, \delta > 0$ small and take a maximum iteration number k_{end}. Then the following procedure yields a numerical approximation to the evolution of the ellipsoid magnetization.

Algorithm 1 Homogeneous Model simulation

procedure NLAH($\mathbf{M}_0$, $\boldsymbol{\theta}$, $\mathbf{H}_a(t_n) : n = 0, 1, 2, ...$)
  $\mathbf{H}_{eff,0} = \mathbf{H}_{a,0} + (\underline{\boldsymbol{\alpha}} - \underline{\boldsymbol{N}})\mathbf{M}_0$
  $\mathbf{H}_0 = \mathbf{H}_{a,0} - \underline{\boldsymbol{N}}\mathbf{M}_0$
  for $1 \leq n \leq T$ **do** ▷ Outer, real-time loop
    $\mathbf{H}^0_{eff,n} = \mathbf{H}_{a,n} + (\underline{\boldsymbol{\alpha}} - \underline{\boldsymbol{N}})\mathbf{M}_{n-1}$ ▷ Initialisation of inner iteration
    for $1 \leq k \leq k_{end}$ **do** ▷ Inner, pseudo-time loop
      $D^k_n = \frac{1}{2\delta} \begin{pmatrix} \mathcal{M}[\mathbf{H}^k_{eff,n} + \delta\mathbf{e}_x] - \mathcal{M}[\mathbf{H}^k_{eff,n} - \delta\mathbf{e}_x] \\ \mathcal{M}[\mathbf{H}^k_{eff,n} + \delta\mathbf{e}_y] - \mathcal{M}[\mathbf{H}^k_{eff,n} - \delta\mathbf{e}_y] \\ \mathcal{M}[\mathbf{H}^k_{eff,n} + \delta\mathbf{e}_z] - \mathcal{M}[\mathbf{H}^k_{eff,n} - \delta\mathbf{e}_z] \end{pmatrix}^T$
      $\mathbf{H}^{k+1}_{eff,n} = \left(\underline{\mathbf{1}} + (\underline{\boldsymbol{N}} - \underline{\boldsymbol{\alpha}})D^k_n\right)^{-1} \left(\mathbf{H}_{a,n} - (\underline{\boldsymbol{N}} - \underline{\boldsymbol{\alpha}}) \left(\mathcal{M}[\mathbf{H}^k_{eff,n}] - D^k_n \mathbf{H}^k_{eff,n}\right)\right)$
      if $\left\|\mathbf{H}^{k+1}_{eff,n} - \mathbf{H}^k_{eff,n}\right\| < \varepsilon \vee k = k_{end}$ **then**
        $k_{conv} = k$
        Exit inner loop
      end if
    end for
    $\mathbf{H}_{eff,n} = \mathbf{H}^{k_{conv}}_{eff,n}$
    $\mathbf{M}_n = \mathcal{M}[\mathbf{H}^{k_{conv}}_{eff,n}]$
    $\mathbf{H}_n = \mathbf{H}^{k_{conv}}_{eff,n} - \underline{\boldsymbol{\alpha}}\mathbf{M}_n$
  end for
end procedure

6.2.3 Proposing the hysteresis operators of the different models

Thus far, we have not touched upon the *concrete definition* of the hysteresis operator $\mathcal{M}$ in different contexts and different hysteresis models. The operators are defined below.

The IPmodel

In the **IP**model, which can in principle be solved exactly, the 'hysteresis' operator $\mathcal{M}_{IP}$ is given by

$$\mathcal{M}_{IP}[\mathbf{H}_{eff}, \boldsymbol{\theta}] = \mathcal{M}_{IP}[\mathbf{H}, \underline{\boldsymbol{\chi}}] = \underline{\boldsymbol{\chi}}\mathbf{H} \tag{6.31}$$

which, when substituted in the procedure above, yields a temporal evolution that is equal to the analytical solution provided before.

The RAmodel

Recall the incremental formulation of the Rayleigh hysteresis model, given in the chapter on material hysteresis models. From this incremental formulation, we obtain an equivalent definition of the hysteresis operator $\mathcal{M}_{RA}$, which takes as input the present magnetic field (there is no Weiss tensor $\underline{\boldsymbol{\alpha}}$), the previous increment of the magnetic field $\delta\mathbf{H}$ and the two tensors $\underline{\boldsymbol{\mu}}_i$ and the diagonal tensor $\underline{\boldsymbol{\alpha}}_R$. The maximum field vector $\mathbf{H}_m$ has to be kept track of throughout the simulation.

$$\mathcal{M}_{RA}[\mathbf{H}_{eff}, \boldsymbol{\theta}] = \mathcal{M}_{RA}(\mathbf{H}, \delta\mathbf{H}, \mathbf{M}_p, \underline{\boldsymbol{\mu}}_i, \underline{\boldsymbol{\alpha}_R}, \mathbf{H}_m) = \mathbf{M}_p + \delta\mathbf{M}. \tag{6.32}$$

where we have to discriminate between the Rayleigh virgin curve and the 'adult' curve on the basis of the value of the elements of $\mathbf{H}_m$. Denoting $d = x, y, z$ as spatial dimensions, we have

the condition to determine the magnetization increment $\delta\mathbf{M}$ as follows. Let $\underline{\boldsymbol{\chi}} = \underline{\boldsymbol{\mu}}_i - \underline{\mathbf{1}}$, then

$$\delta\mathbf{M}_d = \begin{cases} (\underline{\boldsymbol{\chi}}\delta\mathbf{H})_d + (2\underline{\boldsymbol{\alpha}}_R(\sigma(\delta\mathbf{H}\otimes\mathbf{H}))\delta\mathbf{H})_d & \text{if } (\mathbf{H}_m)_d = 0 \\ (\underline{\boldsymbol{\chi}}\delta\mathbf{H})_d + (\underline{\boldsymbol{\alpha}}_R(\mathbf{H}_m + \sigma(\delta\mathbf{H}\otimes\mathbf{H}))\delta\mathbf{H})_d & \text{if } (\mathbf{H}_m)_d > 0, \end{cases} \tag{6.33}$$

where $\otimes$ again denotes the Kronecker (pointwise) product between the two vectors. Substituting this increment in Equation 6.32 yields the expression for the Rayleigh hysteresis operator.

The JAmodel

The incremental susceptibility of the Jiles-Atherton model follows from the incremental formulation, given in the chapter on hysteresis models. Recall that in the Jiles-Atherton model, we have

$$\delta\mathbf{M} = \frac{\underline{\boldsymbol{\chi}}_f}{||\underline{\boldsymbol{\chi}}_f||}(\underline{\boldsymbol{\chi}}_f \cdot \delta\mathbf{H}_{eff})^+ + \underline{\boldsymbol{c}}\underline{\boldsymbol{\xi}}\delta\mathbf{H}_{eff}. \tag{6.34}$$

where

$$\begin{cases} \underline{\boldsymbol{\chi}_f} & := \underline{\boldsymbol{k}}^{-1}(\mathbf{M}_{an}(\mathbf{H}_{eff}) - \mathbf{M}) \\ \underline{\boldsymbol{\xi}}_{ij} & := \frac{\partial \mathbf{M}_{an,i}}{\partial \mathbf{H}_{eff,j}} \end{cases} \tag{6.35}$$

using the anhysteric function

$$\mathbf{M}_{an}(\mathbf{H}_{eff}) = M_s\left(\coth\frac{||\mathbf{H}_{eff}||}{A} - \frac{A}{||\mathbf{H}_{eff}||}\right)\frac{\mathbf{H}_{eff}}{||\mathbf{H}_{eff}||} \tag{6.36}$$

although other possibilities exist for modelling the anhysteric curve. The Jiles-Atherton hysteresis operator is thus given by

$$\mathcal{M}_{JA}[\mathbf{H}_{eff}, \boldsymbol{\theta}] = \mathcal{M}_{JA}(\mathbf{H}_{eff}, \delta\mathbf{H}_{eff}, \mathbf{M}_p, \underline{\boldsymbol{k}}, \underline{\boldsymbol{c}}, M_s, A) = \mathbf{M}_p + \delta\mathbf{M}. \tag{6.37}$$

where we substitute $\mathbf{M}_p$ for $\mathbf{M}$ in Equation 6.35 and substitute the expression of Equation 6.34 in the above equation to arrive at the definition of the operator.

The EVmodel

The Energy-Variational model is of a different character than the linear model (which does not even need time integration if $\mathbf{H}_a$ is known at all times) and the Rayleigh and Jiles-Atherton model, which are treated by means of a differential susceptibility tensor. In contrast, the Energy-Variational model searches for a new value of the magnetization by minimizing internal magnetic energy. The derivation of the EV model has been done in a previous chapter. In the end, we obtained the system of equations

$$\begin{cases} \mathbf{M}_{new} & = \sum_{l=1}^{N_c}\omega^l\mathbf{M}_c^l = \sum_{l=1}^{N_c}\omega^l\mathbf{M}_{an}(||\mathbf{H}_r^l||)\frac{\mathbf{H}_r^l}{||\mathbf{H}_r^l||} \\ \mathbf{H}_r^l & = \arg\min_{\mathbf{u}\in K^l(t)}\{S(\mathbf{u}) - \mathbf{M}_{c,old}^l \cdot \mathbf{u}\} \\ S(\mathbf{u}) & = \int_0^{||\mathbf{u}||} M_{an}(s)\,\mathrm{d}s \\ K^l(t) & = \{\mathbf{u}\in\mathbb{R}^3 : ||(k^l)^{-1}(\mathbf{u} - \mathbf{H}_{eff}^l)|| \le 1\}. \end{cases} \tag{6.38}$$

Since the hysteresis operator framework in the current research was principally motivated by the paper on the **EV**model, the **EV**hysteresis operator now follows simply by setting

$$\mathcal{M}_{EV}[\mathbf{H}_{eff}, \boldsymbol{\theta}] = \mathbf{M}_{new} \tag{6.39}$$

where $\mathbf{M}_{new}$ is given by the **EV**system of equations above.

6.3 Sensor Mapping

As has been noted before, the use of prolate spheroidal coordinates allows for the derivation of an elegant expression to map the ellipsoid magnetization onto magnetic flux density at any point (x, y, z) outside the ellipsoid. This mapping is linear in $\mathbf{M}$ and given by

$$\mathbf{B}(x, y, z) = \mu_0 \xi_0 (\xi_0^2 - 1) \underline{\mathrm{A}}(x, y, z) \mathbf{M} \tag{6.40}$$

where $\underline{\mathrm{A}} \in \mathbb{R}^{3\times 3}$ is a transformation matrix with analytically derived entries, encountered in the derivation and proof of the ellipsoid formula and written out in the Appendix. At any given sensor point (x_s, y_s, z_s) outside the ellipsoid therefore, the relation between the magnetization $\mathbf{M}(t)$, the applied field $\mathbf{H}_a(t)$ and sensor measurement $\mathbf{B}(x_s, y_s, z_s)$ is given by

$$\mathbf{B}(x_s, y_s, z_s, t) = \mu_0 \mathbf{H}_a(t) + \mu_0 \xi_0 (\xi_0^2 - 1) \underline{\mathrm{A}}(x_s, y_s, z_s) \mathbf{M}(t), \tag{6.41}$$

and the magnetic signature of the ellipsoid is therefore given by subtracting the applied signal

$$\mathbf{B}_s(x_s, y_s, z_s, t) = \mu_0 \xi_0 (\xi_0^2 - 1) \underline{\mathrm{A}}(x_s, y_s, z_s) \mathbf{M}(t). \tag{6.42}$$

Let us now consider an actual sensor array. Suppose $\{\mathbf{r}_1, ..., \mathbf{r}_{N_s}\}$ is the set of sensor locations, measuring the external magnetic signature of the ellipsoid, where $\mathbf{r}_s = (x_s, y_s, z_s)$, $1 \leq s \leq N_s$. By defining the matrix $\underline{\Lambda} \in \mathbb{R}^{3N_s \times 3}$ as

$$\underline{\Lambda} = \mu_0 \xi_0 (\xi_0^2 - 1) \begin{pmatrix} \underline{\mathrm{A}}(\mathbf{r}_1) \\ \underline{\mathrm{A}}(\mathbf{r}_2) \\ \vdots \\ \underline{\mathrm{A}}(\mathbf{r}_{N_s}) \end{pmatrix} \tag{6.43}$$

one obtains $3N_s$ equations $\boldsymbol{B}_{s,n} = \underline{\Lambda}\mathbf{M}$. Now, since the forward ellipsoid models described in the four sections above (**IP**,**RA**,**JA**,**EV**) all provide approximations of the magnetization $\mathbf{M}$ at discrete time steps, the end result of applying a discretized signal $\mathbf{H}_a(t_n)$ with $0 \leq n \leq T$ yields

$$\boldsymbol{B}_{s,n} = \boldsymbol{B}_s(t_n) = \underline{\Lambda}\mathbf{M}_n \tag{6.44}$$

which is the temporal evolution of the ellipsoid signature in time.

6.4 Summary and Outlook

In the present chapter, we firstly motivated the 'temporal ellipsoid formula', that is, the ellipsoid formula is still valid in the case of nonlinear temporal incremental evolution under the influence of a uniform applied field. This allowed us to derive a two-loop algorithm to solve for the ellipsoid magnetization in time, where the hysteresis operator $\mathcal{M}$ played a fundamental role. Lastly, the ellipsoid signature was related to the magnetization by a linear transformation, finishing the formulation of the homogeneous forward models.
It is now time to look at inverse homogeneous models: Can we, given a uniform applied field in time, and a measured signature in time, estimate the governing hysteresis parameters? This question will be answered in the following chapter.

Part III

Inhomogeneous Ellipsoid Models

Chapter 7

Forward Inhomogeneous Ellipsoid Models

In the previous chapters, we have formulated the homogeneous ellipsoid model under influence of different material hysteresis models. The essential building blocks of the homogeneous ellipsoid models were

1. The Ellipsoid Formula, which comes from the solution of the infinite-domain Poisson Equation assuming uniform magnetization of an ellipsoid, together with the uniform background field potential, which are added by the superposition principle;

2. The choice of a hysteresis model and corresponding parameters;

3. For the quasi static time-stepping formulation, we needed to assume that the material hysteresis parameters were constant in time and space throughout the ellipsoid.

The homogeneous model then was defined as the time evolution of the signature of the ellipsoid at certain external sensor locations, under the influence of a temporally incremented uniform applied field.
Now, assumptions 1) and 3) are not assumed any more in inhomogeneous ellipsoid models. We have chosen to go all the way back to the Poisson equation discussed in **??** and to build our models from scratch using Finite Element theory. Some other methods are often applied to magnetostatic field problems, such as Boundary Element Methods (BEMs), which do not require a meshing of surrounding space, but are harder to combine with the notion of inhomogeneity. This is why we have chosen to use the Finite Element Method (FEM).
Firstly, let us briefly introduce some general concepts of the FEM where we specifically focus on the Galerkin approach. Thereafter, we apply this theory to the Poisson equation at hand.

7.1 Very short introduction to the FEM

The Finite Element Method and more specifically the Galerkin approach, are described in many textbooks. For a functional analysis - perspective, one can consult the lecture notes by Hunter [87] which were used by Veraar, most notably chapter 6.4. For a more accessible monograph, one can consult the book by Vermolen et al. [18]. There also exist many other discussions of the FEM from a specific electromagnetism-perspective, such as [14]. It is a very, very large research field with applications ranging from biology to electromagnetism, with solid foundations in pure mathematics, theory of partial differential equations and approximation theory.

We will suffice here by loosely describing the FEM, which is by no means a sufficient mathematical introduction. Suppose one has a linear PDE of the form

$$\mathcal{L}u = f \tag{7.1}$$

where $\mathcal{L}$ is a linear differential operator acting on a certain function space Σ with functions defined on a certain 'nice' domain Ω. Boundary conditions for u must also be provided. In that case, several deep mathematical theorems such as the Riesz Representation and Lax-Milgram Theorem, shed a light on the existence and uniqueness of solutions. Energy (norm) estimates of the solution can be given, dependent on the function f and the form of the linear operator $\mathcal{L}$.
Now, associated to the operator $\mathcal{L}$ there (often, but not always, in our case it does) exist a bilinear form such that the *weak form* of the above PDE can be written as: For all η in a certain function space Σ_2, we have

$$a(u, \eta) = (f, \eta) \tag{7.2}$$

where $(\cdot, \cdot)$ denotes a type of inner product, which of course makes conditions on f necessary. This is called the weak form, since the conditions on u are much more relaxed in order for Equation 7.2 to make sense.
Now, one can choose a N-dimensional linear subspace of the space Σ, denoted by Σ_N, wherein one wishes to approximate the sought $u \in \Sigma$ by some linear combination of 'basis functions' for the space Σ_N, in some norm that is associated to Σ. Indeed, now one wishes to find $u_N \in \Sigma_N$ such that for all $\eta_N \in \Sigma_{2,N}$ we have

$$a(u_N, \eta_N) = (f, \eta_N) \tag{7.3}$$

Now, the FEM approaches finding u from a standpoint of a finite number of 'elements', subdividing the domain Ω. That is, the approximants $u_n \in \Sigma_N$ are often defined on a small number of elements. The Galerkin approach is then to expand u in functions of Σ_N, substitute this expansion in the weak form Equation 7.2 and also take η to be one of the basis functions from Σ_N. This way, one obtains a system of linear equations, with the possibility of boundary conditions to cause extra terms. The linear system is solved in order to obtain optimal coefficients that minimize $\|u - u_N\|_\Sigma$. This way, the FEM solution u_N is a finite dimensional projection of u on the finite dimensional subspace Σ_N. This whole paradigm can also be viewed in the context of approximation theory, whereby the PDE Equation 7.1 is firstly written as a minimization problem. Under certain conditions, these approaches are equivalent.

7.2 Applying FEM theory to the magnetostatic equation at hand

The situation in this section is as follows. Using the Galerkin method, we aim to solve the forward, magnetostatic problem to find the magnetic field $\mathbf{H}(\mathbf{r})$ from the non-uniform ellipsoid magnetization $\mathbf{M}(\mathbf{r})$. Our strategy is to firstly solve for the scalar potential $\Phi(\mathbf{r})$ and thereafter deduce the magnetic field in both the ellipsoid and the surrounding air, in particular the sensor locations.

7.2.1 Formulating the Poisson problem on a bounded domain

Firstly, we choose a FEM bounding box $\Omega = [-L, L]^3 \subset \mathbb{R}^3$ to define the scalar potential boundary conditions on. This choice will be commented upon later on, but it is good to

know that a great corpus of knowledge exists in literature on how to model essentially infinite-domain problems by employing strategies to either map the infinite domain onto a finite one, or to create a number of matching layers to create the impression of working on an infinite domain. For examples, see CITE. However, one can also choose a number of relatively simple different boundary condition formulations to model the static forward inhomogeneous problem, most notably Dirichlet, Neumann and mixed-type or Robin boundary conditions. To model the influence of the 'incident' applied field $\mathbf{H}_a$ in the case of the bounded airbox, where taking the limit $\|\mathbf{r}\| \to \infty$ does not make sense, we have chosen to take inhomogeneous Dirichlet boundary conditions. For $\mathbf{r} \in \partial\Omega$, we require

$$\Phi(\mathbf{r}) = -\mathbf{H}_a \cdot \mathbf{r}, \tag{7.4}$$

where $\mathbf{H}_a$ is the applied background field. Our main reason for employing these boundary conditions is as follows. As we will see later on in this chapter, choosing Dirichlet boundary conditions yields a dramatic decrease in condition number of the system to be solved, since we are effectively adding many 'knowns' to the linear system. Moreover, choosing exactly these boundary conditions gives rise to a 'perturbation-interpretation' of the problem at hand. Indeed, choosing $\mathbf{M}(\mathbf{r}) = \mathbf{0}$ in the Poisson equation, yields the Laplace equation with inhomogeneous Dirichlet boundary conditions, with solution $\Phi(\mathbf{r}) = -\mathbf{H}_a \cdot \mathbf{r}$, which exactly yields the correct solution $\mathbf{H}(\mathbf{r}) = \mathbf{H}$ by taking minus the gradient of the potential. Now, letting $\mathbf{M}(\mathbf{r})$ take a nontrivial value, perturbs the solution to the equation, which in turn perturbs the resulting magnetic field. Finally then, we end up with the equation to solve using the FEM:

$$\begin{cases} \Delta\Phi(\mathbf{r}) = \nabla \cdot \mathbf{M}(\mathbf{r}) \\ \Phi|_{\partial\Omega} = g(\mathbf{r}) \end{cases} \tag{7.5}$$

with

$$g(\mathbf{r}) = -\mathbf{H}_a \cdot \mathbf{r}|_{\partial\Omega} \tag{7.6}$$

7.2.2 Deriving the weak form

We are now ready to follow the Galerkin procedure (which we do not comment fully upon, but will be discussed critically later on in the recommendations) as follows. Multiplying the Poisson equation by -1, a test function $\eta(\mathbf{r}) \in H_0^1(\Omega)$ and integrating over Ω yields

$$-\int_\Omega (\Delta\Phi)\eta \,\mathrm{d}\Omega = -\int_\Omega (\nabla \cdot \mathbf{M})\eta \,\mathrm{d}\Omega. \tag{7.7}$$

Firstly, for the left hand side of the equation above, observe that we can integrate by parts to obtain

$$-\int_\Omega (\Delta\Phi)\eta \,\mathrm{d}\Omega = \int_\Omega \nabla\Phi \cdot \nabla\eta \,\mathrm{d}\Omega - \int_{\partial\Omega} (\nabla\Phi \cdot \mathbf{n})\eta \,\mathrm{d}\Gamma. \tag{7.8}$$

Since $\eta(\mathbf{r}) \in H_0^1(\Omega)$, the boundary integral vanishes, leaving only the volume integral.
Secondly, notice that $\mathbf{M}(\mathbf{r}) = \mathbf{M}(\mathbf{r})\mathbb{1}(\mathbf{r} \in \Omega_e)$, that is, $\mathbf{M}$ is restricted to the ellipsoid. Assuming $\mathbf{M}$ is continuously differentiable on the interior of Ω_e and continuous on the closure of Ω_e, we can write the right hand side of Equation 7.7 by firstly restricting the integral domain and thereafter applying the Divergence Theorem to obtain

$$-\int_\Omega (\nabla \cdot \mathbf{M})\eta \,\mathrm{d}\Omega = -\int_{\Omega_e} (\nabla \cdot \mathbf{M})\eta \,\mathrm{d}\Omega \tag{7.9}$$

$$= \int_{\Omega_e} \mathbf{M} \cdot \nabla\eta \,\mathrm{d}\Omega - \int_{\partial\Omega_e} (\mathbf{M} \cdot \mathbf{n})\eta \,\mathrm{d}S \tag{7.10}$$

where $\mathbf{n}$ is the normal vector, pointing outward from the ellipsoid. $\mathbf{n}(\mathbf{r})$ is known analytically, as was demonstrated in the chapter on the Ellipsoid formula and ellipsoids. This yields the final weak form of our problem: Find $\Phi \in H^1(\Omega)$ such that for all $\eta \in H_0^1(\Omega)$, we have

$$\int_\Omega \nabla\Phi \cdot \nabla\eta \, \mathrm{d}\Omega = \int_{\Omega_e} \mathbf{M} \cdot \nabla\eta \, \mathrm{d}\Omega - \int_{\partial\Omega_e} (\mathbf{M} \cdot \mathbf{n})\eta \, \mathrm{d}S. \tag{7.11}$$

We will now apply the Galerkin stratehy to find an approximation of Φ in a finite-dimensional subspace of the Hilbert space H^1, namely the space spanned by piecewise linear 'hat' functions on a predefined mesh.

7.2.3 Defining piecewise linear basis functions and applying the Galerkin procedure

In order to be able to use the Finite Element approach, Ω is subdivided in a finite number N_e of tetrahedral elements $e_k : 1 \leq k \leq N_e$, with N_n vertices $\mathbf{x}_j : 1 \leq j \leq N_n$. The Finite Element basis functions $\eta_j(\mathbf{x}) : 1 \leq j \leq N_n$ will be piecewise linear on elements, with the usual 'hat' property:

$$\begin{cases} \eta_i(\mathbf{x}_j) = \delta_{ij}, & \text{for all } i, j \in \{1, ..., N_n\} \\ \eta_i(\mathbf{x}) & \text{linear per element} \end{cases} \tag{7.12}$$

Now, expanding the sought solution $\Phi(\mathbf{r})$ in terms of these hat functions, we write

$$\Phi(\mathbf{r}) = \sum_{j=1}^{N_n} \phi_j \eta_j(\mathbf{r}) \tag{7.13}$$

where the summation includes the boundary node hat functions. These hat function satisfy $\eta_j \in H_1$, since their partial derivatives are piecewise constant functions on Ω. Their integrals as well as their gradients can be calculated analytically using well-known theorems and convenient formulas for tetrahedra. Since Dirichlet conditions are prescribed on $\partial\Omega$, it is useful to partition the set of nodes $\mathbf{x}_j : 1 \leq j \leq N_n$ into two subsets of nodes, namely

$$I_o = \{i \in \{1, ..., N_n\} : \mathbf{x}_i \in \Omega^\circ\} \tag{7.14}$$

$$I_b = \{i \in \{1, ..., N_n\} : \mathbf{x}_i \in \partial\Omega\}, \tag{7.15}$$

which allows us to write Equation 7.13 the following way:

$$\Phi(\mathbf{r}) = \sum_{j \in I_o} \phi_j \eta_j(\mathbf{r}) + \sum_{j \in I_o} \phi_j \eta_j(\mathbf{r}) \tag{7.16}$$

where for $j \in I_o$, the coefficients ϕ_j are known. Indeed, by combining Equation 7.4 and Equation 7.12, these coefficients are given by

$$\phi_j = -\mathbf{H}_a \cdot \mathbf{x}_j, \ j \in I_b \tag{7.17}$$

Now, employing the Galerkin strategy by inserting the above expansion Equation 7.16 in our weak form Equation 7.11 and choosing a basis function η_i with $i \in I_o$, such that it is a test

function in $H_0^1(\Omega)$, we transform the left hand side of the weak form Equation 7.11 to

$$
\begin{aligned}
-\int_\Omega \Delta\Phi\eta \,\mathrm{d}\Omega &= \int_\Omega \nabla\Phi\cdot\nabla\eta \,\mathrm{d}\Omega && (7.18)\\
&= \int_\Omega \nabla\left(\sum_{j=1}^{N_n}\phi_j\eta_j(\mathbf{r})\right)\cdot\nabla\eta_i(\mathbf{r})\,\mathrm{d}\Omega && (7.19)\\
&= \int_\Omega \nabla\left(\sum_{j\in I_o}\phi_j\eta_j(\mathbf{r})+\sum_{j\in I_o}\phi_j\eta_j(\mathbf{r})\right)\cdot\nabla\eta(\mathbf{r})\,\mathrm{d}\Omega && (7.20)\\
&= \sum_{j\in I_o}\phi_j\int_\Omega \nabla\eta_j(\mathbf{r})\cdot\nabla\eta_i(\mathbf{r})\,\mathrm{d}\Omega+\sum_{j\in I_b}\phi_j\int_\Omega \nabla\eta_j(\mathbf{r})\cdot\nabla\eta_i(\mathbf{r})\,\mathrm{d}\Omega && (7.21)\\
&= \sum_{j\in I_o}\phi_j\int_\Omega \nabla\eta_j\cdot\nabla\eta_i\,\mathrm{d}\Omega+\sum_{j\in I_b}\phi_j\int_\Omega \nabla\eta_j\cdot\nabla\eta_i\,\mathrm{d}\Omega && (7.22)\\
&=: \sum_{j\in I_o}\underline{\mathrm{K}}_{ij}\phi_j+\sum_{j\in I_b}\underline{\mathrm{K}}_{ij}\phi_j && (7.23)\\
& && (7.24)
\end{aligned}
$$

for $i\in I_o$. Since ϕ_j is known for all $j\in I_b$ because of Dirichlet boundary conditions, the above N_o statements contain N_o unknowns, which will have te be solved by equating the above statements to the right hand side of the weak form. We already notice the *stiffness matrix* $\underline{\mathrm{K}}$ appearing in the linear system above.
The right hand side is treated in the following way. Again, let $\eta(\mathbf{r})=\eta_i$ be an interior basis function, such that $\eta_i\in H_0^1(\Omega)$. Using integration by parts, we obtain

$$
\begin{aligned}
-\int_\Omega(\nabla\cdot\mathbf{M}(\mathbf{r}))\eta(\mathbf{r})\,\mathrm{d}\Omega &= -\int_{\Omega_e}(\nabla\cdot\mathbf{M}(\mathbf{r}))\eta(\mathbf{r})\,\mathrm{d}\Omega && (7.25)\\
&= \int_{\Omega_e}\mathbf{M}(\mathbf{r})\nabla\cdot\eta(\mathbf{r})\,\mathrm{d}\Omega-\int_{\partial\Omega_e}(\mathbf{M}(\mathbf{r})\cdot\mathbf{n}(\mathbf{r}))\eta(\mathbf{r})\,\mathrm{d}S && (7.26)\\
&= \int_{\Omega_e}\mathbf{M}\cdot\nabla\eta_i\,\mathrm{d}\Omega-\int_{\partial\Omega_e}(\mathbf{M}\cdot\mathbf{n})\eta_i\,\mathrm{d}S && (7.27)\\
&=: \boldsymbol{F}_i^M. && (7.28)
\end{aligned}
$$

We now observe the *load vector* $\boldsymbol{F}$ appearing.
Written out in components for readability, one obtains (by setting $\mathbf{M}(\mathbf{r})=(M_x(\mathbf{r}),\,M_y(\mathbf{r}),\,M_z(\mathbf{r}))^T$, and the from Ω_e outward pointing vector $\mathbf{n}(\mathbf{r})=(n_x(\mathbf{r}),\,n_y(\mathbf{r}),\,n_z(\mathbf{r}))^T$, and by omitting the coordinate $\mathbf{r}$, the elements of the load vector:

$$
\begin{aligned}
\boldsymbol{F}_i^M &= \int_{\Omega_e}\mathbf{M}\cdot\nabla\eta_i\,\mathrm{d}\Omega-\int_{\partial\Omega_e}(\mathbf{M}\cdot\mathbf{n})\eta_i\,\mathrm{d}S && (7.29)\\
&= \int_{\Omega_e}M_x\frac{\partial}{\partial x}\eta_i\,\mathrm{d}\Omega-\int_{\partial\Omega_e}M_xn_x\eta_i\,\mathrm{d}S && (7.30)\\
&+\int_{\Omega_e}M_y\frac{\partial}{\partial y}\eta_i\,\mathrm{d}\Omega-\int_{\partial\Omega_e}M_yn_y\eta_i\,\mathrm{d}S && (7.31)\\
&+\int_{\Omega_e}M_z\frac{\partial}{\partial z}\eta_i\,\mathrm{d}\Omega-\int_{\partial\Omega_e}M_zn_z\eta_i\,\mathrm{d}S && (7.32)
\end{aligned}
$$

for $i\in I_o$.
By employing the Holland-Bell theorem to integrate the linear basis function over their domains

and by employing a special case of Newton-Cotes quadrature to approximate the right-hand side integral (namely, the trapezoid rule), one arrives at a familiar linear equation. Indeed, by observing the above equations and by noting that the normal vector to the ellipsoid is known analytically on $\partial\Omega_e$, the load vector with the elements above, is linear in $\mathbf{M}(\mathbf{r})$, and the full system to be solved is given by

$$\underline{\mathrm{K}}\boldsymbol{\phi} = \boldsymbol{F}^M \tag{7.33}$$

$$= (\underline{\mathrm{D}}^M - \underline{\mathrm{E}}^M)\boldsymbol{M}, \tag{7.34}$$

where one observes the stiffness matrix $\underline{\mathrm{K}}$, containing the basis function gradient inner products integrated, the *unstructured divergence matrix* $\underline{\mathrm{D}}_M$, containing the linear coefficients of the volume integrals of Equation 7.29 and the *unstructured ellipsoid boundary matrix* $\underline{\mathrm{E}}_M$, containing the linear coefficients of the ellipsoid boundary integrals of Equation 7.29. These matrices are sparse, $\underline{\mathrm{K}}$ is even symmetric and positive definite, and we have

$$\underline{\mathrm{K}} \in \mathbb{R}^{N_n \times N_n},\ \boldsymbol{\phi} \in \mathbb{R}^{N_n},\ \underline{\mathrm{D}}^M, \underline{\mathrm{E}}^M \in \mathbb{R}^{N_n \times 3N_n},\ \boldsymbol{M} \in \mathbb{R}^{3N_n}. \tag{7.35}$$

where the vector $\boldsymbol{M}$ obeys the usual, node- and dimension dependent ordering

$$\boldsymbol{M} := \begin{pmatrix} M_x(\mathbf{x}_1) \\ M_y(\mathbf{x}_1) \\ M_z(\mathbf{x}_1) \\ \vdots \\ M_x(\mathbf{x}_{N_n}) \\ M_y(\mathbf{x}_{N_n}) \\ M_z(\mathbf{x}_{N_n}) \end{pmatrix} \tag{7.36}$$

One observes that because of the nature of the problem, but admittedly dependent on the meshing of the domain, many elements of the vector $\boldsymbol{M}$ will be zero, because many of the $\mathbf{x}_j$ will be located outside the ferromagnetic domain of the ellipsoid. The precise elements of the matrices involved, can be consulted by the author of this report.

7.2.4 Incorporating Dirichlet boundary conditions

The careful reader may have noticed that the matrices involved, give rise to N_n equations. However, our original system consisted of only N_o equations. Indeed, the system above is not finalized, because the equations of system Equation 7.34 still include the *known* coefficients $\phi_j : j \in I_b$. We eliminate the Dirichlet boundary conditions by employing an idea that is equivalent to the procedure from Vermolen et al. [18], Chapter 6.2.7, but is more general in the sense that the sets I_o and I_b can be arbitrary, as long as they are disjoint and $I_o \cup I_b = \{1, ..., N_n\}$. We start out by collecting the Dirichlet boundary values in one vector $\boldsymbol{R}$ of length N_b, ordered consistently. That is, if in the ordered set I_b we have $j \in I_b$ at 'position' $1 \leq j_b \leq N_b$, then

$$\boldsymbol{R}_{j_b} = -\mathbf{H}_a \cdot \mathbf{x}_j. \tag{7.37}$$

Observe moreover, that even this expression is linear to a great extent, in the sense that for $j \in I_b$, there exist a matrix $\underline{\mathrm{X}}_b \in \mathbb{R}^{N_b \times 3}$ such that

$$-\mathbf{H}_a \cdot \mathbf{x}_j = (\underline{\mathrm{X}}_b \mathbf{H}_a)_j \tag{7.38}$$

The existence of the first matrix is clear just by letting row j_b of $\underline{\mathrm{X}}_b$ be given by $\mathbf{x}_j^T$. This way, we can write the vector $\boldsymbol{R}$ from Equation 7.37 as

$$\boldsymbol{R} = \underline{\mathrm{X}}_b \mathbf{H}_a. \tag{7.39}$$

Next, we define the 'selection' matrix $\underline{\mathrm{B}} \in \mathbb{R}^{N_b \times N_n}$ such that the boundary conditions are implemented by the linear system

$$\underline{\mathrm{B}}\boldsymbol{\phi} = \boldsymbol{R} \tag{7.40}$$

by letting row j_b of $\underline{\mathrm{B}}$ be given by the transposed N_n-dimensional unit vector $\boldsymbol{e}_j$ such that $j \leftrightarrow j_b$.
Since, the matrix $\underline{\mathrm{B}}$ has such a simple form, the next steps are straightforward. We continue by forming the orthogonal complement-matrix $\underline{\mathrm{B}}_o \in \mathbb{R}^{N_n \times N_b}$ and the nullspace-matrix $\underline{\mathrm{B}}_n \in \mathbb{R}^{N_n \times (N_n - N_b)}$ associated to the matrix $\underline{\mathrm{B}}$. The columns of $\underline{\mathrm{B}}_o$ are per definition all orthogonal and even orthonormal to the rows of $\underline{\mathrm{B}}$ and the columns of $\underline{\mathrm{B}}_n$ are all contained in the kernel of $\underline{\mathrm{B}}$, so

$$\begin{cases} \underline{\mathrm{B}}\underline{\mathrm{B}}_n = \underline{0} \in \mathbb{R}^{N_b \times (N_n - N_b)} & \text{(the zero matrix, observe } N_n - N_b = N_o\text{)} \\ \underline{\mathrm{B}}\underline{\mathrm{B}}_o = \underline{\mathrm{I}}_{N_b} & \text{(the identity matrix)} \end{cases} \tag{7.41}$$

Having defined these matrices, we are ready to form the vector $\boldsymbol{\phi}_b \in \mathbb{R}^{N_n}$ such that the 'unknown indices' are still zero, while the boundary node indices are filled with their Dirichlet values according to Equation 7.17. This vector is simply given by

$$\begin{aligned} \boldsymbol{\phi}_b &= \underline{\mathrm{B}}_o \boldsymbol{R} && (7.42) \\ &= \underline{\mathrm{B}}_o \left(\underline{\mathrm{X}}_b \mathbf{H}_a\right) && (7.43) \end{aligned}$$

7.2.5 Deriving and solving the final, forward linear matrix system

Having found a way to formulate the Dirichlet boundary conditions in a convenient manner, we eliminate the known Dirichlet boundary values from the full system by defining the *reduced stiffness matrix and load vector*

$$\begin{cases} \underline{\mathrm{K}}_o &= \underline{\mathrm{B}}_n^T \underline{\mathrm{K}}\underline{\mathrm{B}}_n \in \mathbb{R}^{N_o \times N_o} \\ \boldsymbol{F}^o &= \underline{\mathrm{B}}_n^T (\boldsymbol{F}^M - \underline{\mathrm{K}}\boldsymbol{\phi}_b) \in \mathbb{R}^{N_o} \\ &= \underline{\mathrm{B}}_n^T ((\underline{\mathrm{D}}^M - \underline{\mathrm{E}}^M)\boldsymbol{M} - \underline{\mathrm{K}}\boldsymbol{\phi}_b) \end{cases} \tag{7.44}$$

We now solve for the unknown coefficients by solving the system

$$\underline{\mathrm{K}}_o \boldsymbol{\phi}^o = \boldsymbol{F}^o \tag{7.45}$$

which, by elimination of the boundary condition, is a very well-conditioned system. We obtain the complete solution, to be substituted in Equation 7.16 to find the FEM approximation to the potential Φ by adding the Dirichlet boundary conditions in the following way:

$$\boldsymbol{\phi} = \underline{\mathrm{B}}_n \boldsymbol{\phi}^o + \boldsymbol{\phi}_b. \tag{7.46}$$

Finally, the forward inhomogeneous system is written *symbolically* by the monstrous equation

$$\begin{aligned} \boldsymbol{\phi} &= \underline{\mathrm{B}}_n \underline{\mathrm{K}}_o^{-1} \boldsymbol{F}^o + \boldsymbol{\phi}_b && (7.47) \\ &= \underline{\mathrm{B}}_n \left[(\underline{\mathrm{B}}_n^T \underline{\mathrm{K}}\underline{\mathrm{B}}_n)^{-1} (\underline{\mathrm{B}}_n^T (\boldsymbol{F}^M - \underline{\mathrm{K}}\boldsymbol{\phi}_b)) \right] + \boldsymbol{\phi}_b && (7.48) \\ &= \underline{\mathrm{B}}_n \left[(\underline{\mathrm{B}}_n^T \underline{\mathrm{K}}\underline{\mathrm{B}}_n)^{-1} (\underline{\mathrm{B}}_n^T ((\underline{\mathrm{D}}^M - \underline{\mathrm{E}}^M)\boldsymbol{M} - \underline{\mathrm{K}}\boldsymbol{\phi}_b)) \right] + \boldsymbol{\phi}_b && (7.49) \\ &= \underline{\mathrm{B}}_n \left[(\underline{\mathrm{B}}_n^T \underline{\mathrm{K}}\underline{\mathrm{B}}_n)^{-1} (\underline{\mathrm{B}}_n^T ((\underline{\mathrm{D}}^M - \underline{\mathrm{E}}^M)\boldsymbol{M} - \underline{\mathrm{K}}(\underline{\mathrm{B}}_o (\underline{\mathrm{X}}_b \mathbf{H}_a))) \right] && (7.50) \\ &\quad + \underline{\mathrm{B}}_o \left(\underline{\mathrm{X}}_b \mathbf{H}_a\right) && (7.51) \end{aligned}$$

7.3 Obtaining H from Φ

Having obtained the FEM approximation to the sought inhomogeneous static potential, we have not arrived at our destination just yet. We are actually interested in the magnetic field $\mathbf{H}(\mathbf{r}) = -\nabla\Phi(\mathbf{r})$ in space, which requires another operation.

7.3.1 Magnetic field expansion in hat functions

Similar to the formulation of the unstructured divergence matrix $\underline{\mathrm{D}}^M$ and the unstructured ellipsoid boundary matrix $\underline{\mathrm{E}}^M$, we would like to derive some kind of unstructured gradient matrix $\underline{\mathrm{G}}$, such that $\boldsymbol{H} = -\underline{\mathrm{G}}\boldsymbol{\phi}$, where $\boldsymbol{H}$ obeys the same vector ordering as the familiar magnetization vector $\boldsymbol{M}$. In principle, this is possible by expanding the magnetic field itself as a sum of hat functions. This yields a linear system for the values of $\boldsymbol{H}$ at the nodes of the finite element mesh, and this way, one has obtained a full mapping $\boldsymbol{M} \to \boldsymbol{H}$ by firstly solving the weak problem to find an approximation to Φ and thereafter solving another weak, linear problem by means of a matrix inversion to find $\mathbf{H}$, indexed in the vector $\boldsymbol{H}$. This is very elegant, however, we have not succeeded in doing this, which will be made clear in the following. To make our attempted methodology clear, let us describe it very briefly here. We will only treat the x component of the magnetic field, the rest is analogous. Similar to the problem of finding $\boldsymbol{\phi}$, we are now looking for the vector $\boldsymbol{g}_x$, which also has some *known* values, namely the bounding box boundary values. $\boldsymbol{g}_x$ is defined as the vector containing minus the magnetic field values in the mesh nodes, following the indexing of the mesh. That is, we define

$$g^x(\mathbf{r}) := -\mathbf{H}(\mathbf{r}) = \frac{\partial\Phi(\mathbf{r})}{\partial x} \tag{7.52}$$

which leads to the vector

$$\boldsymbol{g}_j^x := \frac{\partial\Phi}{\partial x}(\mathbf{x}_j) = \frac{\partial\Phi}{\partial x}(\mathbf{x}_j) = -\mathbf{H}_x(\mathbf{x}_j) \tag{7.53}$$

We can now integrate the x-derivative of Φ, after multiplying it by a test function $\eta \in H_0^1$, yielding by partial integration

$$\int_\Omega g^x \eta \,\mathrm{d}\Omega = \int_\Omega \frac{\partial\Phi}{\partial x}\eta \,\mathrm{d}\Omega = -\int_\Omega \Phi\frac{\partial\eta}{\partial x}\,\mathrm{d}\Omega. \tag{7.54}$$

Now, since Φ is given in terms of the element-wise linear basis functions and boundary conditions by Equation 7.16, namely

$$\Phi(\mathbf{r}) = \sum_{j\in I_o}\phi_j\eta_j(\mathbf{r}) + \sum_{j\in I_o}\phi_j\eta_j(\mathbf{r}) \tag{7.55}$$

we can substitute this expansion in Equation 7.54. Moreover, we also expand g^x in terms of these basis functions:

$$g^x(\mathbf{r}) = \sum_{j\in I_o} g_j^x\eta_j(\mathbf{r}) + \sum_{j\in I_o} g_j^x\eta_j(\mathbf{r}) \tag{7.56}$$

Substituting the above expansions in equation (7.54), and picking the usual test function from the set of basis functions indicated previously, leads to a system of equations similar as in the previous section. Dirichlet boundary conditions for $\mathbf{H}_x$ can then be inserted to yield a well-conditioned system. By forming the matrices

$$\begin{cases} \underline{\mathrm{P}}_{ij} &= \int_\Omega \eta_i\eta_j \,\mathrm{d}\Omega \\ \underline{\mathrm{S}}_{ij}^x &= \int_\Omega \frac{\partial\eta_i}{\partial x}\eta_j \,\mathrm{d}\Omega \end{cases} \tag{7.57}$$

for $1 \leq i, j \leq N_n$ and by incorporating the same Dirichlet boundary indexing as before in the vector $\boldsymbol{g}_b^x$ (analogous to $\boldsymbol{\phi}_b$), the weak solution to finding the x-magnetic field at the nodes is given by firstly defining

$$\begin{cases} \underline{\mathrm{P}}_o & = \underline{\mathrm{B}}_n^T \underline{\mathrm{PB}}_n \\ \boldsymbol{G}^x & = \underline{\mathrm{S}}^x \boldsymbol{\phi} \\ \boldsymbol{G}_o^x & = \underline{\mathrm{B}}_n^T (\boldsymbol{G}^x - \underline{\mathrm{P}}) \end{cases} \tag{7.58}$$

and thereafter, symbolically

$$\underline{\mathrm{P}}_o = \underline{\mathrm{B}}_n^T \underline{\mathrm{PB}}_n \tag{7.59}$$

The reason why this has not succeeded in the end, is because of the fundamental flaw in the expansion Equation 7.56. It assumes that the magnetic field can be expanded in terms of hat functions, while mesh nodes are located on the interface between ellipsoid and air. Because the magnetic field is undefined there, the above procedure is invalid. However, it doe yield far-field results that are reasonable. More on this will be provided in the recommendations.

7.3.2 Magnetic field computation via interpolation

Because of the difficulties concerning the magnetic field at the boundary of the ellipsoid, rational thinking moved us in the following direction. Since the inhomogeneous models also have as defined output the signature values of the magnetized ellipsoid, it is a seemingly enough to calculate the magnetic field only there; in the remainder of the bounding box, it is of no use to go to great lengths to get an estimate of the magnetic field. However, to model the time evolution of the magnetization inside the ellipsoid using different hysteresis models, an estimate of the internal ellipsoid magnetic field is required. This is also done by interpolation, but extra caution must again be paid to the ellipsoid boundary. We thus propose the following straightforward method to calculate the magnetic field from the scalar potential. Firstly, choose a small number $\delta > 0$ a node $\mathbf{x}_j$. Since there exists a list of adjacent elements to each node, together with the tetrahedron domain that element inhabits, it is known which which element e_k satisfies the location $\mathbf{x}_j \pm \delta\hat{\mathbf{x}} \in e_k$, and similarly with $\mathbf{x}_j \pm \delta\hat{\mathbf{y}} \in e_k$ and $\mathbf{x}_j \pm \delta\hat{\mathbf{z}} \in e_k$. On these elements, the gradient of the FEM solution is known, since the coefficients $\boldsymbol{\phi}$ are known and the gradients of basis functions on elements are known exactly. We thereafter distinguish three different cases.

- If $\mathbf{x}_j \in \Omega_e^o$ or $\mathbf{x}_j \in \Omega \setminus \overline{\Omega}_e$, we approximate the magnetic field at node $\mathbf{x}_j$ by

$$\mathbf{H}(\mathbf{x}_j) \approx -\frac{1}{2\delta} \begin{pmatrix} \Phi(\mathbf{x}_j + \delta\hat{\mathbf{x}}) - \Phi(\mathbf{x}_j - \delta\hat{\mathbf{x}}) \\ \Phi(\mathbf{x}_j + \delta\hat{\mathbf{y}}) - \Phi(\mathbf{x}_j - \delta\hat{\mathbf{y}}) \\ \Phi(\mathbf{x}_j + \delta\hat{\mathbf{z}}) - \Phi(\mathbf{x}_j - \delta\hat{\mathbf{z}}) \end{pmatrix} \tag{7.60}$$

- If $\mathbf{x}_j \in \partial\Omega$, we have

$$\mathbf{H}(\mathbf{x}_j) = \mathbf{H}_a \tag{7.61}$$

- If $\mathbf{x}_j \in \partial\Omega_e$, we take the magnetic field to be the average of all adjacent, internal ellipsoid node magnetic fields. This heuristic measure has to be taken, because simply taking the central difference approximation yields unstable results in the forward simulation of the hysteretic evolution of the magnetization. Moreover, the magnetic field is not even *defined* boundary of the ellipsoid, so we have the freedom to assign a value to it there, provided that the result more or less resembles reality. Of course, there are formal boundary conditions, namely the familiar

$$\mathbf{n} \times (\mathbf{H}_2 - \mathbf{H}_1) = \mathbf{0}, \tag{7.62}$$

where $\mathbf{H}_1$ and $\mathbf{H}_2$ are the magnetic fields in- and outside the ellipsoid, and $\mathbf{n}$ is the ellipsoid surface normal vector. However, we have not been able to incorporate these boundary conditions in a rigorous way in our equations, which is why we have chosen to implement the averaging procedure above.

The above operations are denoted by the linear, global operation

$$\boldsymbol{H} = -\underline{\mathrm{G}}\boldsymbol{\phi} \tag{7.63}$$

which, in our implementations, is a `Matlab scatteredInterpolant()` object rather than a (sparse) matrix.

7.4 Towards inhomogeneous hysteresis: Deriving a time-stepping scheme from the static formulation

In this section, we try to derive a time-stepping algorithm to obtain an approximation of the quasi-static non-linear boundary value problem:

$$\begin{cases} \Delta\Phi(\mathbf{r},t) &= \nabla\cdot\mathbf{M}(\mathbf{r},t), \qquad \mathbf{r}\in\Omega \\ \mathbf{M}(\mathbf{r},t) &= \mathcal{M}_{hys}[\mathbf{H}_{eff}(\mathbf{H},\mathbf{M})(\mathbf{r},t),\theta(\mathbf{r},t)] \\ \mathbf{H}(\mathbf{r},t) &= -\nabla\Phi(\mathbf{r},t) \\ \Phi(\mathbf{r},t) &= \mathbf{r}\cdot\mathbf{H}_a(t), \qquad \mathbf{r}\in\partial\Omega \end{cases} \tag{7.64}$$

Having explained the inhomogeneous magnetostatic problem in detail in the previous chapter, we can transform it into a time-stepping scheme, analogous to the time-stepping case in the homogeneous ellipsoid models. There are some key differences, however.

1. Since the Ellipsoid Formula cannot be used any more, there is no way of relating of measuring the internal ellipsoid field by estimating $\mathbf{M}(\mathbf{r})$ when the hysteresis parameters are unknown. Later on, this prevents us from estimating the hysteresis parameters at an internal coordinate $\mathbf{r}_0$ by only looking at the $\mathbf{H}(\mathbf{r}_0) - \mathbf{M}(\mathbf{r}_0)$ curve. Rather, $\mathbf{H}(\mathbf{r})$ has to be found by solving the magnetostatic system of the previous section at each time step. In short, rather than finding the internal ellipsoid magnetic field by computing $\mathbf{H}(t) = \mathbf{H}_a(t) - \underline{\boldsymbol{N}}\mathbf{M}(t) = \mathbf{H}_e - \underline{\boldsymbol{\alpha}}\mathbf{M}(t)$, we have to solve the forward system to yield the scalar potential, which then has to be converted to the magnetic field via interpolation, keeping in mind the ellipsoid boundary effects that were discussed previously.

2. Since the magnetization vector is now defined on every ellipsoid node, inhomogeneous models are much more expensive to simulate than homogeneous models. At every proper time step, N_e magnetization updates have to be performed that are similar to the updates in the homogeneous model, increasing the simulation time by a factor of at least N_e. Moreover, to find the magnetic field, the system to find the scalar potential approximation has to be solved at every inner iteration also, drastically increasing the computation time. It is for this reason that the inverse inhomogeneous model is very expensive when using a genetic algorithm-approach. We will comment on this fact later.

These considerations together, yield our approach of the time evolution of the inhomogeneous steel ellipsoid under the influence of a uniform applied background field. The same way as in the homogeneous model case, choose ϵ, δ small and define the time steps $t_0, ..., t_T$, on which the applied uniform background field is defined beforehand.

Finally, the following pseudo code contains the procedure to simulate the homogeneous models with different underlying hysteresis models, simulated until a time value T. Choose $\varepsilon, \delta > 0$ small and take a maximum iteration number k_{end}. Then the following procedure yields a numerical approximation to the evolution of the ellipsoid magnetization. A Picard iteration, similar to the one used in the homogeneous model, is used to model the nonlinear, hysteretic magnetization steps through time. The forward model presented here, can incorporate location-dependent parameters. The input of the inhomogeneous model is given by a function in space $\mathbf{M}(\mathbf{r})$, a vector that indexes all (possibly location-dependent) variables and a list of applied background field vectors. For readibility, we have chosen to formulate quite a number of steps in words. Essentially, the main difference between homogeneous models and inhomogeneous models is the absence of demagnetization factors in the inhomogeneous case. One therefore needs to solve the static system Equation 7.45 at every time step.
Another very prominent difference is caused by the fact that in calculating the magnetic field, the demagnetization field is already accounted for. This causes the necessary inner iterations of the homogeneous forward model to be largely redundant in the inhomogeneous case; in the case of the inhomogeneous Rayleigh model, no iterations are needed at all because of the absence of the notion of the effective field.

Algorithm 2 Inhomogeneous Forward Model simulation

procedure nLAnH($\mathbf{M}_0(\mathbf{r})$, $\boldsymbol{\theta}$, $\mathbf{H}_a(t_n) : n = 0, 1, 2, ...$)
  $\mathbf{M}_0(\mathbf{r}) \to \boldsymbol{M}_0$
  $\mathbf{H}_a(t_0) \to \boldsymbol{\phi}_b$ ▷ Initialize boundary conditions
  Find $\mathbf{H}(\mathbf{r}, 0)$ by solving Equation 7.45 and interpolation
  Find $\mathbf{H}_{eff}(\mathbf{r}, 0)$ by definition
  for $1 \leq n \leq T$ **do** ▷ Outer, real-time loop
    Let $\mathbf{H}_a$ increment and calculate new boundary conditions
    for Every ellipsoid mesh node **do**
      for $1 \leq k \leq k_{end}$ **do** ▷ Inner, pseudo-time loop
        $$D_n^k = \frac{1}{2\delta} \begin{pmatrix} \mathcal{M}[\mathbf{H}_{eff,n}^k + \delta \mathbf{e}_x] - \mathcal{M}[\mathbf{H}_{eff,n}^k - \delta \mathbf{e}_x] \\ \mathcal{M}[\mathbf{H}_{eff,n}^k + \delta \mathbf{e}_y] - \mathcal{M}[\mathbf{H}_{eff,n}^k - \delta \mathbf{e}_y] \\ \mathcal{M}[\mathbf{H}_{eff,n}^k + \delta \mathbf{e}_z] - \mathcal{M}[\mathbf{H}_{eff,n}^k - \delta \mathbf{e}_z] \end{pmatrix}^T$$
        $$\mathbf{H}_{eff,n}^{k+1} = \left(\underline{\mathbf{1}} - \underline{\boldsymbol{\alpha}} D_n^k\right)^{-1} \left(\mathbf{H}(\mathbf{r}, t_{n-1}) + \underline{\boldsymbol{\alpha}}\right) \left(\mathcal{M}[\mathbf{H}_{eff,n}^k] - D_n^k \mathbf{H}_{eff,n}^k\right)$$
        if $\left\|\mathbf{H}_{eff,n}^{k+1} - \mathbf{H}_{eff,n}^k\right\| < \varepsilon \vee k = k_{end}$ **then**
          $k_{conv} = k$
          Exit inner loop
        end if
      end for
    end for
    $\mathbf{H}_{eff,n} = \mathbf{H}_{eff,n}^{k_{conv}}$ ▷ At every mesh node
    $\mathbf{M}_n = \mathcal{M}[\mathbf{H}_{eff,n}^{k_{conv}}]$ ▷ At every mesh node
    Make updated magnetization vector $\boldsymbol{M}$
    Find $\mathbf{H}(\mathbf{r}, t_n)$ by solving Equation 7.45 and interpolation
  end for
end procedure

It is important to notice from the above pseudo-code (and indeed, it is proper pseudo-code, since many details are left out) that the inner iterations are performed per node until convergence. One would expect the inner iterations also to require solving the main system Equation 7.45, but this is not necessary if one assumes that the magnetization and thus magnetic field does

not vary too wildly across the ellipsoid, which is a reasonable assumption.

7.5 Combining the FEM framework with analytical results

As will be apparent from the Results section, our implementation of forward inhomogeneous models yields a systematic error, which could be traced back to several different factors. It is for this reason that we have modified our forward finite element code by employing the linearity of the problem. That is, we write the magnetization distribution as a sum:

$$\mathbf{M}(\mathbf{r}) = \mathbf{M}^{HOM} + \mathbf{M}^{IHOM}(\mathbf{r}) \tag{7.65}$$

which gives a much more stable magnetization evolution. Indeed, by linearity $\Phi^{HOM}(\mathbf{r}, \mathbf{M}^{HOM})$ is the potential of the homogeneous problem with homogeneous magnetization $\mathbf{M}^{HOM}$, which automatically satisfies the applied field boundary conditions. In the heterogeneous case, we will view the term $\mathbf{M}^{HOM}$ as

$$\mathbf{M}^{HOM} = \int_{\Omega_e} \mathbf{M}(\mathbf{r})\, \mathrm{d}\Omega \tag{7.66}$$

which has to be understood component-wise. So in the inhomogeneous model, $\mathbf{M}^{HOM}$ is viewed as the mean magnetization vector.

Part IV

Model Inversion

Chapter 8

Inverse Ellipsoid Models

We now arrive at the subject of *inverse modelling*. That is, given certain measured model output data, can we reconstruct the inner workings, parameters and general unknowns of the forward simulation or experiment? This is a very large field in applied mathematics, with many insights from functional analysis (is the *inverse operator* well defined? [80]), numerical analysis, statistics and many other fields. More on inverse problems can be found for example in the thesis by Vijn [80], or in the book by Ramm [6], who discusses inverse problems from both a theoretical and applied standpoint.
In this chapter however, we will be very briefly touching upon theoretical considerations. Rather, we will discuss essentially three fairly different components of Inverse Ellipsoid Models, namely.

1. Estimating $\mathbf{M}(t)$ in the homogeneous case. This is an example of an *overdetermined* inverse problem, which is very well-posed;

2. Estimating $\mathbf{M}(\mathbf{r}, t)$ in the inhomogeneous case. Often, this is an example of an *underdetermined* inverse problem, which is therefore ill-posed. There are less data than parameters to be estimated, which makes a regularization step necessary, contrary to the homogeneous model case;

3. Estimating the hysteresis parameters $\boldsymbol{\theta}$ in both homogeneous and inhomogeneous models. Here, we consider one exception, namely *linear* and **IP**ellipsoid models, for which the 'hysteresis' parameter estimation can be performed can be performed quite straightforwardly. In the case of pure nonlinear hysteresis, we have to resort to genetic algorithms.

8.1 Estimating M in the homogeneous case

Firstly, let us consider the estimation of uniform magnetization in homogeneous models. As we have seen, the analytical result which is a solution to the infinite-domain Poisson equation assuming uniform magnetization, allows us to write

$$\mathbf{B}_s(\mathbf{r}_s) = \underline{\mathrm{A}}(\mathbf{r}_s)\mathbf{M} \tag{8.1}$$

where $\mathbf{r}_s \in \Omega \setminus \overline{\Omega}_e$. Now, inserting the *real* CLAViS sensor positions, we derived the expression of the homogeneous $\mathbf{M} - \boldsymbol{B}_s$ mapping by simply 'putting the $\underline{\mathrm{A}}$ - matrices on top of each other', where the ordering of the sensor positions is respected:

$$\boldsymbol{B}_s = \underline{\Lambda}_{SH}\mathbf{M} \tag{8.2}$$

which gives us the output vector of the model, indexed in the usual x, y, z manner. It would be tempting to just employ the Normal Equations on the above system. The above problem

is very well-posed and convex, which yields the Normal Equations to exhibit stable behaviour. However, we would like to minimize the static error

$$J_2(\boldsymbol{B}_s, \widehat{\boldsymbol{B}}_{\boldsymbol{s}}) = \frac{1}{2} \sum_{s=1}^{N_s} \left\| \mathbf{B}_s(\mathbf{r}_s) - \widehat{\mathbf{B}}_s(\mathbf{r}_s) \right\|_2^2 \tag{8.3}$$

which is different from just applying the normal equations to Equation 8.2. In this objective function definition, we denote the model realisation by the 'big hat' notation, whereas the signature to be approximated is denoted without superscript. Thus,

$$\begin{cases} \widehat{\boldsymbol{B}}_s = \underline{\Lambda}_{SH} \widehat{\mathbf{M}} & \text{Homogeneous Model Realisation} \\ \boldsymbol{B}_s & \text{Measured or Artifical Data} \end{cases} \tag{8.4}$$

To be clear, the above norm is indeed equivalent to the norm

$$\widetilde{J}_2(\boldsymbol{B}_s, \widehat{\boldsymbol{B}}_s) = \frac{1}{2} \left\| \boldsymbol{B}_s - \widehat{\boldsymbol{B}}_s \right\|_2^2 \tag{8.5}$$

which indeed would be minimized by applying the Normal Equations to Equation 8.2, but may exhibit different minimizing behaviour (and certainly has different numerical values in experiments). To minimize Equation 8.3, we compute the gradient with respect to the to be estimated homogeneous magnetization vector $\widehat{\mathbf{M}}$ to obtain

$$\nabla_M J_2 = \frac{1}{2} \sum_{s=1}^{N_s} \nabla_M \left\| \mathbf{B}_s(\mathbf{r}_s) - \widehat{\mathbf{B}}_s(\mathbf{r}_s) \right\|_2^2 \tag{8.6}$$

$$= \frac{1}{2} \sum_{s=1}^{N_s} \nabla_M \left\| \mathbf{B}_s(\mathbf{r}_s) - \underline{\mathrm{A}}(\mathbf{r}_s) \widehat{\mathbf{M}} \right\|_2^2 \tag{8.7}$$

$$= \sum_{s=1}^{N_s} \underline{\mathrm{A}}(\mathbf{r}_s)^T \mathbf{B}_s(\mathbf{r}_s) - \left(\sum_{s=1}^{N_s} \underline{\mathrm{A}}(\mathbf{r}_s)^T \underline{\mathrm{A}}(\mathbf{r}_s) \right) \widehat{\mathbf{M}}. \tag{8.8}$$

Setting the above expression to zero, one obtains

$$\left(\sum_{s=1}^{N_s} \underline{\mathrm{A}}(\mathbf{r}_s)^T \underline{\mathrm{A}}(\mathbf{r}_s) \right) \widehat{\mathbf{M}} = \sum_{s=1}^{N_s} \underline{\mathrm{A}}(\mathbf{r}_s)^T \mathbf{B}_s(\mathbf{r}_s) \tag{8.9}$$

with solution

$$\widehat{\mathbf{M}} = \left(\sum_{s=1}^{N_s} \underline{\mathrm{A}}(\mathbf{r}_s)^T \underline{\mathrm{A}}(\mathbf{r}_s) \right)^{-1} \sum_{s=1}^{N_s} \underline{\mathrm{A}}(\mathbf{r}_s)^T \mathbf{B}_s(\mathbf{r}_s) \tag{8.10}$$

$$= (\underline{\Lambda}_{SH}^T \underline{\Lambda}_{SH})^{-1} \underline{\Lambda}_{SH}^T \boldsymbol{B}_s. \tag{8.11}$$

This proves that J_2 is minimized with respect to the uniform magnetization vector by applying the Normal Equations to the combined system Equation 8.2. The above minimization is an example of a very well-posed system. It is very stable with respect to measurement noise; there are much more sensor data than unknowns to be estimated.

8.2 Estimating M(r) in the inhomogeneous case

In order to estimate the magnetization distribution in inhomogeneous ellipsoid models, one could try to directly invert the global static FEM model directly. That is, one could try to

estimate the vector $\boldsymbol{M}$ on the basis of measuring the vector $\boldsymbol{B}_s$ according to the forward FE model described in a previous chapter. Indeed, in the chapter on forward inhomogeneous models, we have derived a matrix $\underline{\Lambda}_{SF}$ such that

$$\boldsymbol{B}_s = \underline{\Lambda}_{SF}\boldsymbol{M} \tag{8.12}$$

where $\underline{\Lambda}_{SF} \in \mathbb{R}^{3N_s \times 3N_n}$. It is clear that $N_n >> N_s$, which makes the system above very ill-conditioned in general. However, significant reduction in system size can be achieved by using the fact that magnetization is only present on Ω_e (so many elements of the vector $\boldsymbol{M}$ are zero and do not need to be estimated), reducing the above system to

$$\boldsymbol{B}_s = \underline{\Lambda}_{SFe}\boldsymbol{M}_e \tag{8.13}$$

where now $\underline{\Lambda}_{SF} \in \mathbb{R}^{3N_s \times 3N_m}$, where N_m is the number of meshed ellipsoid domain nodes, and $\boldsymbol{M}_e$ is a vector containing the magnetization components of all ellipsoid mesh nodes. Still, the above system is very ill-conditioned, because in realistic and accurate meshes, $N_m >> N_s$. For example, in many of our computations we have $N_s = 112$ and $N_m = 8500$. Estimating 3×8500 free parameters using only 3×112 knowns, is an example of a classic underdetermined system. To get a grip on the situation, we have done the following.

- Firstly, we have tried to regularize the above system using three methods in literature. Classical Tikhonov regularization attempted as well as weighted Tikhonov regularization. Thereafter, we attempted to obtain useful estimates of $\boldsymbol{M}_e$ using iterated Tikhonov regularization. Lastly, we attempted to use Truncated Singular Value Regularization. However, there are simply too many free variables to be estimated. In common scenarios, this was reflected in the condition number of the above system, which takes a value of approximately 1×10^{26}.

- Since inversion of the above system is fairly impossible even when applying reliable methods of regularization, we haven chosen the path that was also taken by Baas [74]. This method is described below.

Roughly speaking, the inversion of Equation 8.13 can be interpreted as an estimation of the continuous field $\mathbf{M}(\mathbf{r})$, but parametrised as a superposition of 'hat' functions at every ellipsoid mesh node. In a certain sense then, the Finite Element approach of solving the Poisson equation consists of moving from a 'fine grid' ($\mathbb{R}^3$) to a coarser grid (our mesh). Suppose we move to an even coarser grid, now departing from our mesh grid. That is, suppose we express the components of $\mathbf{M}(\mathbf{r})$ in terms of basis functions that are capable of describing the magnetization distribution to a sufficient degree. Indeed, let us propose the expansion

$$\begin{cases} M_x(\mathbf{r}) &= c_1 M_{Hx} + \sum_{j=1}^{N_b} c_{3j+1} f_j^x(\mathbf{r}_j, \mathbf{r}) \\ M_y(\mathbf{r}) &= c_2 M_{Hy} + \sum_{j=1}^{N_b} c_{3j+2} f_j^y(\mathbf{r}_j, \mathbf{r}) \\ M_z(\mathbf{r}) &= c_3 M_{Hz} + \sum_{j=1}^{N_b} c_{3j+3} f_j^z(\mathbf{r}_j, \mathbf{r}). \end{cases} \tag{8.14}$$

This expansion is capable of producing a homogeneous ellipsoid magnetization by keeping only the first three numbers in the vector $\boldsymbol{c}$ nonzero. Moreover, it is able to model local perturbation in magnetization independently in the x, y, z components by requiring the functions $\{f_j^x, f_j^y, f_j^z\}$ to have small support or to be rapidly decaying around their N_b centers $\mathbf{r}_j$.
Continuing, we sequentially set the vector $\boldsymbol{c} \in \mathbb{R}^{3+3N_b}$, consisting of the basis function expansion coefficients $c_j,\ 1 \leq j \leq 3 + 3N_b$ to a unit vector. Sequentially then, we input the resulting magnetization distribution into the forward inhomogeneous static model and compute the signature. The signature vectors are collected in the matrix $\underline{\mathrm{C}} \in \mathbb{R}^{3N_s \times (3+3N_b)}$. By performing

this 'basis function impulse response' technique, we effectively construct a system to obtain the coefficients c back from measurements. This system can be viewed as a regularized, or coarse grid system with respect to the original full system Equation 8.13. In fact, the matrix $\underline{\mathrm{C}}$ contains weighted sums of the columns of $\underline{\Lambda}_{SFe}$ in such a way that the number of unknowns is greatly diminished to $N_c = 3 + 3N_b$. Finally therefore, the regularized mapping is given by

$$\boldsymbol{B}_s = \underline{\mathrm{C}}\boldsymbol{c} \tag{8.15}$$

In the Results section, we provide and discuss several realisations of this approach to finding the magnetization on the basis of the impulse response approach. We have proposed a variety of different 'blob' centers $\mathbf{r}_j$ as well as different blob shapes $\{f_j^x, f_j^y, f_j^z\}$.
The more blob centers one employs and the more spread out the blobs are, the more ill-conditioned the system Equation 8.15 becomes. This is a very interesting phenomenon and intuitively very clear. It is tempting to toy around with different numbers, locations and distributions of blobs and, in general, even other basis functions such as linear or parabolic components. However, one quickly runs into problems when adding to much blobs or generality in the expansion above. This is why we subsequently have used different regularization approaches when estimating the vector $\boldsymbol{c}$ from a measurement $\boldsymbol{B}_s$. These are presented below and are inspired from [86].

Iterated Tikhonov In Iterated Tikhonov regularisation, we employ the iterative scheme

$$\begin{cases} \boldsymbol{c}^{(0)} = 0, & \boldsymbol{r}^{(0)} = \boldsymbol{B}_s \\ \boldsymbol{c}^{(i)} = \boldsymbol{c}^{(i-1)} + (\underline{\mathrm{C}}^T\underline{\mathrm{C}} + h^2\underline{\mathrm{D}})^{-1}\underline{\mathrm{C}}^T\boldsymbol{r}^{(i-1)}, & \boldsymbol{r}^{(i)} = \boldsymbol{B}_s - \underline{\mathrm{C}}\boldsymbol{c}^{(i)} \end{cases} \tag{8.16}$$

for $i = 1, 2, ...$ Depending on the regularization matrix $\underline{\mathrm{D}}$ and the regularization parameter $h > 0$, one might achieve good estimates for $\boldsymbol{c}$ even when the original system is badly conditioned. Several examples of chosen regularization matrices and parameters are discussed in the Results section.

Truncated SVD In truncated singular value decomposition regularization, we assume that a singular value decomposition of $\underline{\mathrm{C}}$ exists:

$$\underline{\mathrm{C}} = \underline{\mathrm{U}\Sigma\mathrm{V}}^T \tag{8.17}$$

where $\underline{\mathrm{U}}$ and $\underline{\mathrm{V}}$ are orthogonal and $\underline{\Sigma} = \mathrm{diag}\,(\sigma_1, ..., \sigma_{N_c})$. For analytical derivations and proofs, we refer the reader to [86], but in short, the truncated SVD procedure consists of modifying the diagonal singular value matrix to a better behaved matrix by setting

$$\underline{\Sigma}_h = \mathrm{diag}\,(d_j),\ d_j = \begin{cases} 1/\sigma_j & \text{if} \sigma_j \geq h \\ 0 & \text{otherwise} \end{cases} \tag{8.18}$$

for a certain value of $h > 0$ to be determined ($h = 0$ yields the unregularized system, while h large yields the zero solution for $\boldsymbol{c}$). The regularized solution to Equation 8.15 is thereafter given by

$$\boldsymbol{c} = \underline{\mathrm{V}\Sigma_h\mathrm{U}}^T\boldsymbol{B}_s. \tag{8.19}$$

In the Results section, realisations and a discussion on the above regularization methods are also provided.

8.3 Hysteresis parameters estimation

In order to estimate the parameters of the hysteretic ellipsoid models, we employ genetic algorithms, since nonlinear behaviour is present and the number of free parameters is not too large in most cases. For *a realization* of a signature evolution, in the homogeneous case given by

$$\boldsymbol{B}_s(t_n) = \underline{\Lambda}_{SH}\mathbf{M}(t_n) \tag{8.20}$$

and in the inhomogeneous case given by (symbolically)

$$\boldsymbol{B}_s(t_n) = \underline{\Lambda}_{SF}\boldsymbol{M}(t_n) \tag{8.21}$$

under the influence of a pre-defined applied field $\mathbf{H}_a(t_n)$ according to the previously discussed homogeneous models, we introduce an objective function to be minimized, denoted by J_2^T, which is just the sum of the instantaneous sensor l_2 errors.

$$J_2^T(\boldsymbol{B}_s(t_0), ..., \boldsymbol{B}_s(t_T), \widehat{\boldsymbol{B}}_s(t_0), ..., \widehat{\boldsymbol{B}}_s(t_T)) = \sum_{n=0}^{T} J_2^T(\boldsymbol{B}_s(t_n), \widehat{\boldsymbol{B}}_s(t_n)) \tag{8.22}$$

$$= \frac{1}{2}\sum_{n=0}^{T}\sum_{s=1}^{N_s}\left\|\mathbf{B}_s(\mathbf{r}_s, t_n) - \widehat{\mathbf{B}}_s(\mathbf{r}_s, t_n)\right\|_2^2 \tag{8.23}$$

This objective function is called 'global' because of the summing over all times. Taking $T = 1$, yields a prediction or incremental interpretation of the error. Having defined this error measure, we can minimize the J_2^T error with respect to the hysteresis parameters in time. That is: We choose a hysteresis model. Given a model realisation or measured data $\boldsymbol{B}_s(t_n), n = 0, ..., T$ minimize J_2^T with respect to $\boldsymbol{\theta}$ and $\mathbf{M}_0$, where $\mathbf{M}_0$ can be estimated by applying the normal equations on the measured data $\boldsymbol{B}_s(t_0)$.
Let us firstly look into the inverse linear homogeneous model. In this case, direct estimation of the hysteresis parameter (the fixed susceptibility) can be performed. Thereafter, we take a look at the inverse nonlinear models. In that case, we employ genetic algorithms to obtain estimates of the hysteresis parameters.

8.3.1 The Homogeneous Linear Case

A particularly simple case is formed by the Linear Model, in which case there is an exact mapping from the applied background field to the sensor data. To derive the inverse model, observe that the effective susceptibility tensor relation is conveniently inverted:

$$\underline{\boldsymbol{\chi}}_a = \left(\underline{\mathbf{1}} + \underline{\boldsymbol{\chi}}\underline{\boldsymbol{N}}\right)^{-1}\underline{\boldsymbol{\chi}} \iff \underline{\boldsymbol{\chi}} = \underline{\boldsymbol{\chi}}_a\left(\underline{\mathbf{1}} - \underline{\boldsymbol{N}}\underline{\boldsymbol{\chi}}_a\right)^{-1}. \tag{8.24}$$

Provided that inverse in the above equation is well-defined, the material susceptibility can thus be deduced from the effective susceptibility via direct computation. To estimate the effective susceptibility from sensor measurements, notice that

$$\boldsymbol{B}_s = \underline{\Lambda}\underline{\boldsymbol{\chi}}_a\mathbf{H}_a \implies (\underline{\Lambda}^T\underline{\Lambda})^{-1}\underline{\Lambda}^T\boldsymbol{B}_s = \underline{\boldsymbol{\chi}}_a\mathbf{H}_a. \tag{8.25}$$

Now, the left had side of the right hand side equation above is known from the geometry of the setup and sensor data. The applied field is also known. Denoting the right hand side by $\boldsymbol{L}$, so

$$\boldsymbol{L} := (\underline{\Lambda}_{SH}^T\underline{\Lambda}_{SH})^{-1}\underline{\Lambda}_{SH}^T\mathbf{B}_s \tag{8.26}$$

one needs to estimate the 3×3 matrix $\underline{\boldsymbol{\chi}}_a$ from the two vectors $\mathbf{H}_a$ and $\vec{L}$ following the equation $\boldsymbol{L} = \underline{\boldsymbol{\chi}}_a\mathbf{H}_a$. It is mathematically impossible to obtain all elements of *a general* $\underline{\boldsymbol{\chi}}_a$ using only

one value of $\mathbf{H}_a$ and $\boldsymbol{L}$; one has to perform multiple measurements at different applied fields. This is perfectly intuitive, since rotational (off-diagonal) anisotropy is only visible when rotation of some sort is applied. In case of isotropic or diagonally anisotropic material however, one measurement suffices to estimate the material susceptibility, since element-wise inversion can be employed in that case. Contrary to the derivation in the diagonally (an)isotropic case, the fully anisotropic and thus most general linear homogeneous inverse needs multiple measurements along multiple directions. Moreover, in practice one does not know in advance whether some material exhibits only diagonal (an)isotropy. The general anisotropic parameter estimation procedure is discussed presently.
Consider applying 3 different external magnetic fields, which are supposed to be linearly independent vectors: $\mathbf{H}_a^{(1)}, \mathbf{H}_a^{(2)}, \mathbf{H}_a^{(3)}$. One can calculate the 3 (hopefully different) values of the sensor data vectors $\boldsymbol{L}^{(1)}, \boldsymbol{L}^{(2)}, \boldsymbol{L}^{(3)}$ by measurements or running a forward simulation. One obtains a system of equations, capable of correctly estimating the effective susceptibility tensor under the conditions above, by forming the matrices $\underline{\mathrm{X}} \in \mathbb{R}^{3\times 3}$ and $\underline{\mathrm{Y}} \in \mathbb{R}^{3\times 3}$, defined by

$$\underline{\mathrm{X}} := [\mathbf{H}_a^{(1)}, \mathbf{H}_a^{(2)}, \mathbf{H}_a^{(3)}], \ \underline{\mathrm{Y}} := [\boldsymbol{L}^{(1)}, \boldsymbol{L}^{(2)}, \boldsymbol{L}^{(3)}] \tag{8.27}$$

to obtain an estimate of the effective susceptibility

$$\underline{\mathrm{Y}} = \underline{\boldsymbol{\chi}}_a \underline{\mathrm{X}} \implies \underline{\boldsymbol{\chi}}_a = \underline{\mathrm{Y}}\underline{\mathrm{X}}^T(\underline{\mathrm{X}}\underline{\mathrm{X}}^T)^{-1} \tag{8.28}$$

after which the right hand side of Equation (8.24) can be employed to arrive at the estimate for the material susceptibility of the ellipsoid. The relative permeability can be calculated by the relation $\underline{\boldsymbol{\mu}}_r = \underline{\boldsymbol{\chi}} + \underline{\mathbf{1}}$.
The above procedure is possible, because all fields and unknowns can be expressed in terms of each other analytically. In the nonlinear situation, this is no longer the case. Rather, we have to employ algorithms that can estimate a limited number of parameters (less than 20) to achieve at an estimate of the hysteresis parameter vector $\boldsymbol{\theta}$. This is achieved by employing genetic algorithms.

8.3.2 The General Case

In order to minimize J_2^T with respect to the free parameters, we essentially run the forward models many times, and via the procedures of genetic algorithms (in `Matlab`), we keep the evaluations with lowest error, we update the parameter pool and keep simulating many realizations of the homogeneous forward models until a satisfactory small error is obtained. There are many possible choices in selecting genetic algorithms. For example, Baas [74] has employed the so-called Shuffled Frogs Leaping Algorithm (at least, one can conjecture that the field of nonlinear inverse modelling is a great inspiration for zoological nomenclature). In our research, we have employed the intrinsic `Matlab` genetic algorithm `ga()` to minimize J_2^T. The algorithm was initialized by firstly estimating $\mathbf{M}_0$ from the data, using the Normal Equations. By running the forward models many times, with parameters in a preselected domain, one can obtain an increasingly good estimate of the hysteresis parameters. The algorithm stops when the error stops decreasing for several iterations, or when a specific maximum iteration number is reached. Different degrees of anisotropy can be allowed by increasing or decreasing the parameter space and thus the dimension of $\boldsymbol{\theta}$.

Part V

Results, Discussion, Conclusions and Recommendations

Chapter 9

Results and Discussion

The present chapter will provide a summary of results which were obtained using the models described in previous chapters. To do this, we have used the research subquestions and the order of model description throughout the report. We will provide a wide variety of figures, mostly signature plots and hysteresis loops, to illustrate the behaviour of ellipsoid models and their specific properties. The structure of the current chapter is as follows.
Firstly, we will take a look at real, measured signature data using the CLAViS.
Secondly, we will discuss the homogeneous models and their specific properties. Anisotropy is illustrated using different models. Hysteresis model-specific results are analysed and we compare the hysteresis models along different axes of performance. To communicate the performance of our inverse algorithms, we follow the chapter by providing and discussing results on a wide variety of (identical) twin experiments. We finish the part on homogeneous model by looking at measured data and estimating the hysteresis parameters of the real ellipsoid, which, after all, is the purpose of the present project.
Thirdly, we move to the heterogeneous ellipsoid models by discussing the performance of our self-written Finite Element models. We compare these FE - based approximations of the ellipsoid signature and magnetization to the results of the homogeneous models and discuss the added difficulties of not having an exact solution to the ellipsoid magnetization and signature in the FE-case. We investigate a number of factors that could contribute to the observed behaviour. Furthermore, one added difficulty in the FE-case is the intrinsic ill-posedness of inverse problem: the ellipsoid magnetization is now described by a large vector (depending on the mesh resolution, up to tens of thousands of semi-free real numbers), while the number of sensors is limited to 112. This impacts the difficulty of the inverse algorithm severely, as will be shown in the current chapter. After having discussed this, we turn to (identical) twin experiments. Our forward heterogeneous models have the capacity to simulate the ellipsoid magnetization with location-dependent, anisotropic parameters. Unfortunately, the number of hysteresis parameters in such a case is too great a freedom for our inverse algorithms to handle and for our twin experiments, we have taken the parameters to be constant and unchanging throughout the ellipsoid. This means that the only cause of having a nonuniform magnetization and thus magnetic field, is formed by the initial or permanent magnetization of the ellipsoid.

All of the before is needed to (partially) provide answers to our original subquestions or subgoals:

- Develop a flexible and general forward model
- Identify and understand the physical and mathematical significance of model parameters
- Investigate a flexible, general and reliable method of model inversion and parameter estimation

- Quantify the impact of hysteresis, (an)isotropy and (in)homogeneity
- Improve the model using data assimilation and real-time control

Now, let us commence by looking at signature measurement data. One thing to be noted in the current chapter, is that the units of many parameters and quantities are not included to increase readability.

9.1 Measuring the ellipsoid signature using the CLAViS

We have measured the ferromagnetic behaviour of the prolate steel ellipsoid in real life, using a device built by Lepelaars. More information on the CLAViS can be found in the documentation by Lepelaars. The calibration algorithms of the CLAViS convert raw data to measures magnetic flux densities at the sensor array, previously described. A series of Helmholtz coils produces an (almost) uniform background field. When measuring, we have used the following field, using 342 time steps.

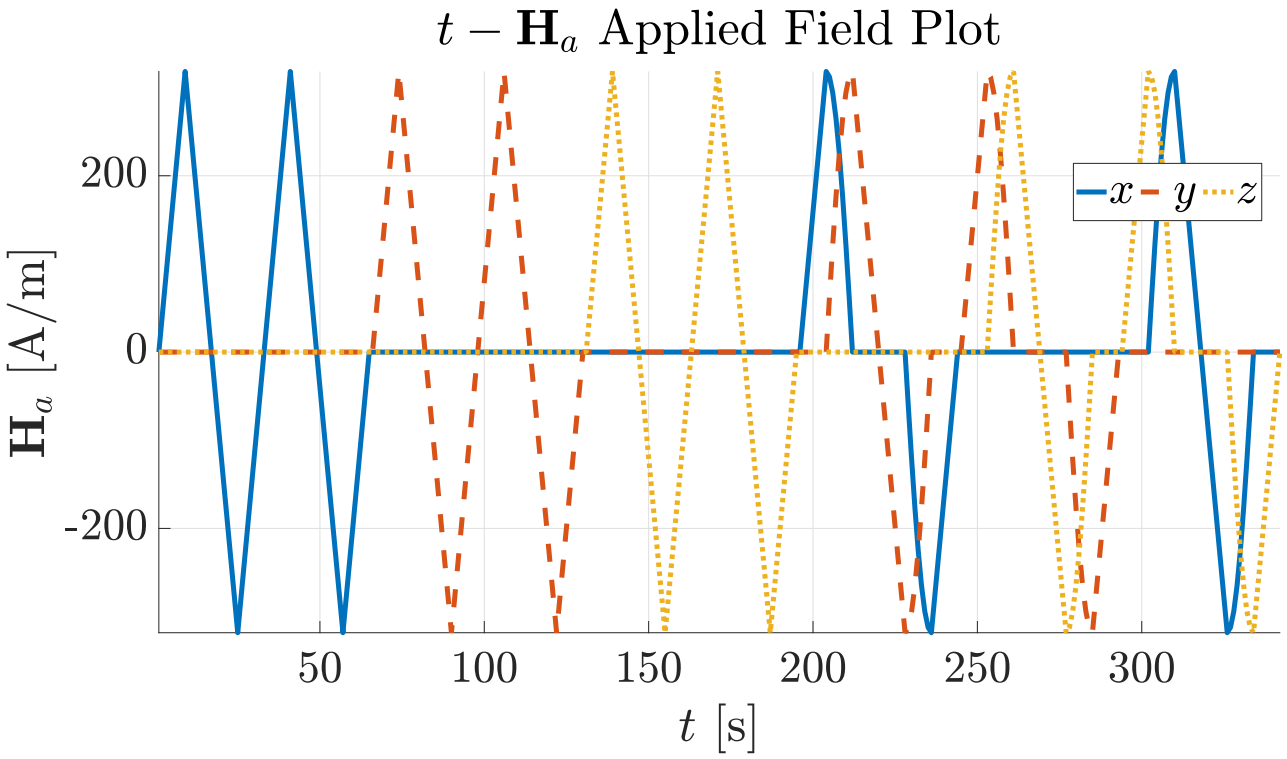

Figure 9.1: The applied magnetic field that was used to obtain the CLAViS data.

Changing the background field according to the above figure and measuring the sensor signature, one obtains a sequence of signatures. These signatures are caused by the magnetization distribution inside the ellipsoid only, since the background field is subtracted from the total field that is measured. An example of a measured signature can be observed in Figure 9.2. There, we plot the three components of the reduced flux density, which is the signature, together with the norm of the signature at the sensor locations. The figure was made at time step 100 with the applied field above.

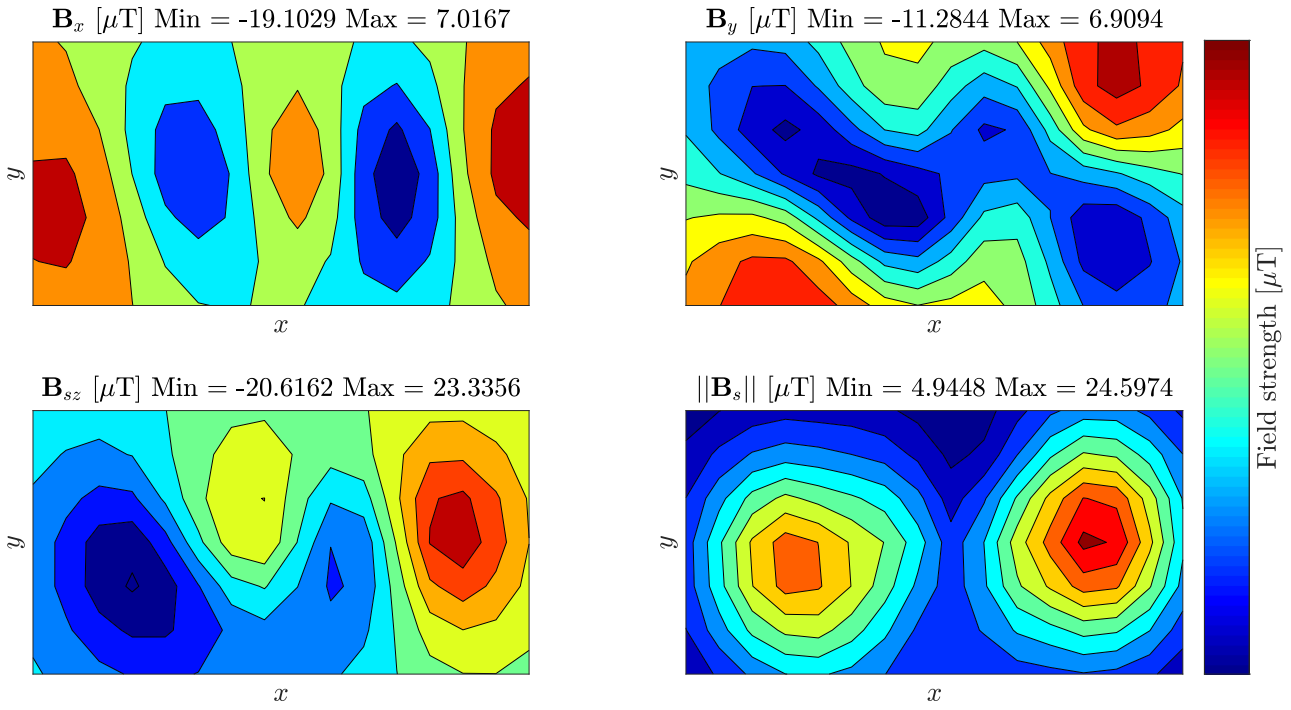

Figure 9.2: The measured signature at using the CLAViS at time step 100. At that time, the applied field was given by $\mathbf{H}_a(t_{100}) \approx (0,\ 80,\ 0)^T \mathrm{A\,m^{-1}}$.

In the present chapter, all builds up to one goal: Estimating all relevant quantities - magnetization evolution, initial condition, and hysteresis parameters - that govern the process generated by the above depicted signal Figure 9.1 and producing the signature output that is observed - in one time instance - in the signature contour plot depicted above Figure 9.2.
Let us look in more detail at the raw data themselves. Can, for example, hysteresis be seen? Below, two figures are placed to illustrate the 'semi-raw' data generated by the CLAVis.

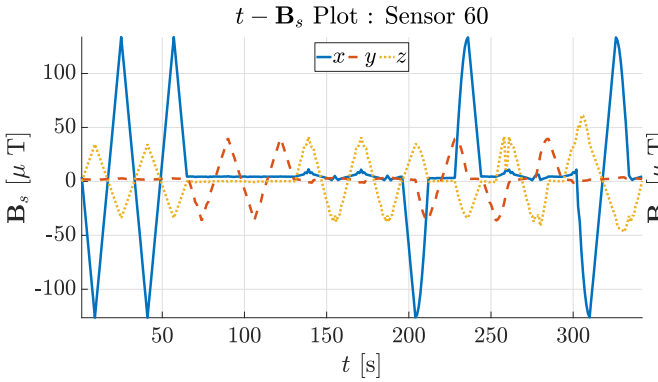

Figure 9.3: A plot of the measured signature in time, at sensor 60.

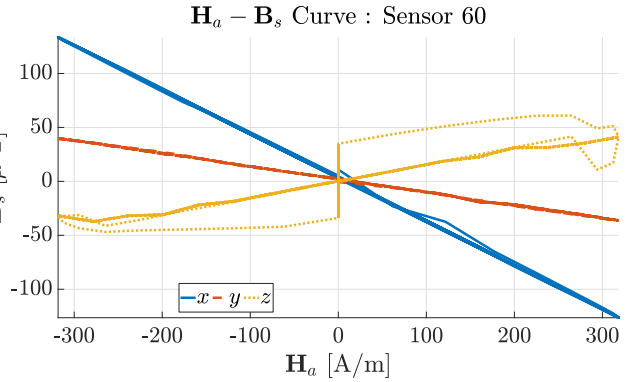

Figure 9.4: A semi-hysteresis curve, measured at sensor 60.

The left hand side figure depicts the magnetic induction field measured by sensor 60 in time, while the right hand side depicts the same measurement, but plotted against the applied field $\mathbf{H}_a$ from Figure 9.1. Note that in that case, $\mathbf{B}_s$ is under the influence of the spatial mapping to map $\mathbf{M}(\mathbf{r})$, the ellipsoid magnetization distribution, to the sensor array. This causes the 'material to seem anisotropic', because the spatial mapping when analysed, is not diagonal. In fact, not much can be concluded about the right-hand side figure above. We need real model inversion. But firstly, let us examine various homogeneous forward models and their properties.

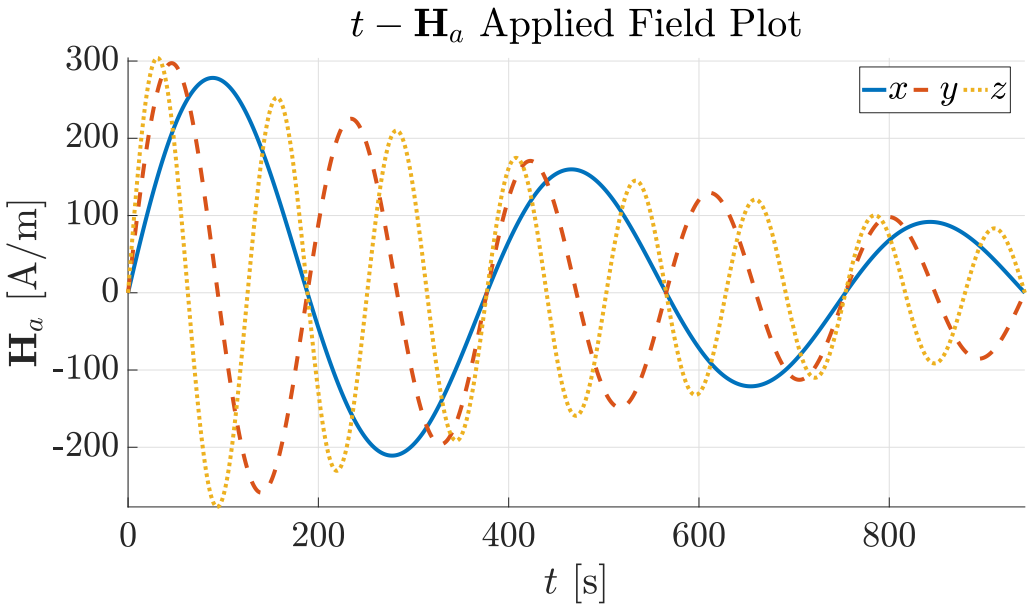

Figure 9.5: The applied magnetic field Equation 9.1 that was used in most or our homogeneous forward simulations.

9.2 Results of specific homogeneous ellipsoid models

In order to provide figures, hysteresis loops and signature plots of realizations of the homogeneous ellipsoid models, we firstly have to choose an applied field that functions as the underlying driving force. We have chosen this field to be the following:

$$\mathbf{H}_a(t) = \frac{400\,\mu\mathrm{T}}{\mu_0}\frac{1}{2}^{(t/T_1)}\begin{pmatrix}\sin(t/T_1)\\ \sin(t/T_2)\\ \sin(t/T_3)\end{pmatrix} \tag{9.1}$$

where $T_1 = 360$, $T_2 = 180$ and $T_3 = 120$, in seconds. We discretize this signal using 1500 equidistant time points. If an explicit ODE solver were used, this time step would have been too large. But since we are employing an iterative method to obtain both the increments in the magnetization and the (effective) magnetic field inside the ellipsoid iteratively, the process is simulated stably. A plot of applied field in time can be observed in the following figure. The reason that this field is used, is not for inversion purposes or reflection of realistic situations. Rather, it is to show the behaviour of the hysteresis models in an as clear as possible manner. If, in this section, another applied field is utilised, we will comment on it.
Furthermore, the initial condition of our simulation will, unless otherwise indicated, always be the demagnetized state, that is,

$$\mathbf{M}_0 = \mathbf{0}. \tag{9.2}$$

9.2.1 The Homogeneous IPEllipsoid Model

Below, two figures displaying the $\mathbf{H}$ versus $\mathbf{M}$ curve and the $\mathbf{H}_a$ versus $\mathbf{M}$ curve can be seen. The simulations were done using an isotropic susceptibility of 99 and using $\mathbf{M}_{per} = \mathbf{0}$.

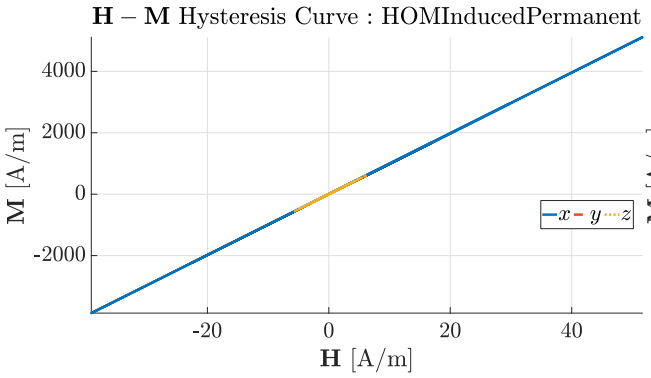

Figure 9.6: nLIH - $\mathbf{IPH}_a - \mathbf{M}$ curve.

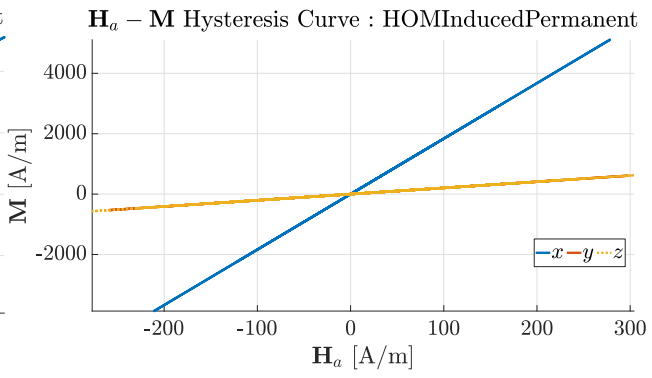

Figure 9.7: nLIH - $\mathbf{IPH}_a - \mathbf{M}$ curve.

The nature of the **IP**model becomes apparent. The linear relation between $\mathbf{M}$ and $\mathbf{H}$ is clear. The demagnetization tensor is apparent: Although the applied field is more or less equal in maximum magnitude in all three directions, the $\mathbf{H}_a - \mathbf{M}$ curve shows the difference in magnetization response due to the easy x-axis of the ellipsoid. Now, adding anisotropy (the left hand side figure) and furthermore setting $\mathbf{M}_{per} = (2 \ \ -1 \ 4)^T$, one observes the following two 'hysteresis' curves, which were made using:

$$\underline{\boldsymbol{\chi}} = \begin{pmatrix} 99 & 20 & 50 \\ 20 & 149 & 30 \\ 50 & 30 & 129 \end{pmatrix}. \tag{9.3}$$

The curves are depicted below.

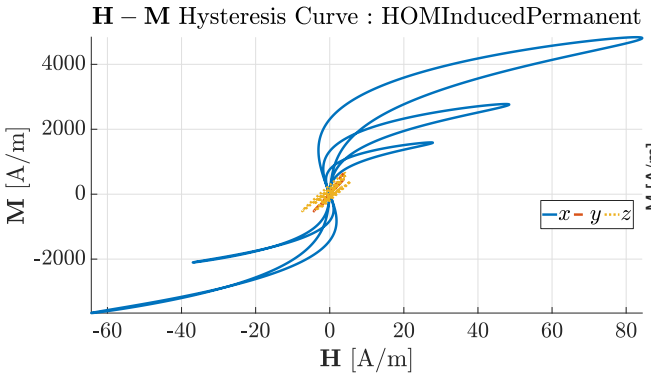

Figure 9.8: nLAH - $\mathbf{IPH}_a - \mathbf{M}$ curve.

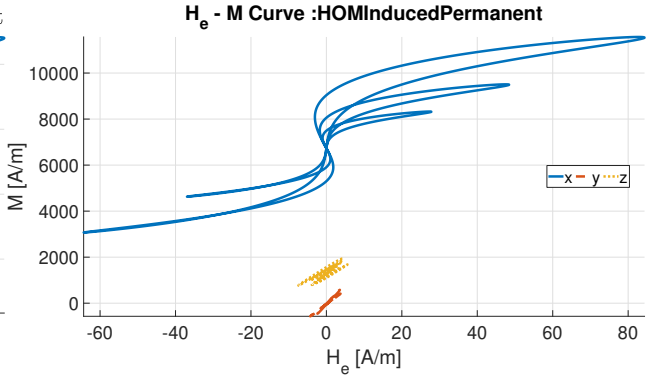

Figure 9.9: nLAH - $\mathbf{IPH}_a - \mathbf{M}$ curve.

The two above figures are interesting. One could mistake the **IP**model for a nonlinear hysteresis model by just taking the above figures at face value. Furthermore, the inclusion of $\mathbf{M}_{per}$, and even a very small value compared to the actual magnetization, introduces wildly different behaviour of the ellipsoid magnetization. The above behaviour is the case in very anisotropic materials, which rarely occur in the field of ferromagnetism. However, the simulations show the capacity of the **IP**model to model a wide range of curves.

9.2.2 The Homogeneous RAEllipsoid Model

Let us now take a quick look at the behaviour of the Rayleigh model in the homogeneous case. Simulating the Rayleigh model using the applied field Equation 9.1, zero initial conditions and isotropic parameters of $\chi = 99$ and $\alpha_R = 20$, one obtains

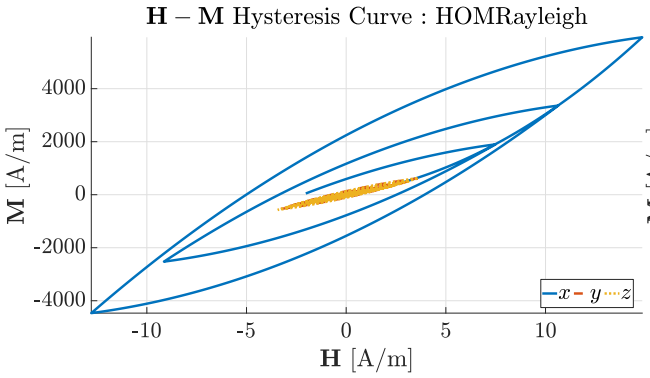

Figure 9.10: nLIH - **RAH** – **M** curve.

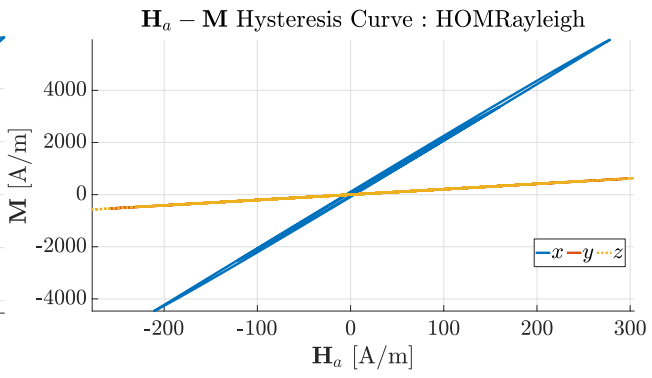

Figure 9.11: nLIH - **RAH**$_a$ – **M** curve.

Under the influence of the ellipsoid demagnetization factors, the parabolic shape of the Rayleigh curves is still present. The same behaviour as in the **IP**model is encountered when looking at the $\mathbf{H}_a - \mathbf{M}$ curves, although the x - curve exhibits a notable hysteresis gap even when 'compressed' by the demagnetization tensor. Introducing anisotropy by letting the linear Rayleigh parameter be given by $\underline{\boldsymbol{\mu}}_i = \underline{\mathbf{1}} + \underline{\boldsymbol{\chi}}$ with the susceptibility as in Equation 9.3 and keeping α_R unchanged, one obtains the following figures.

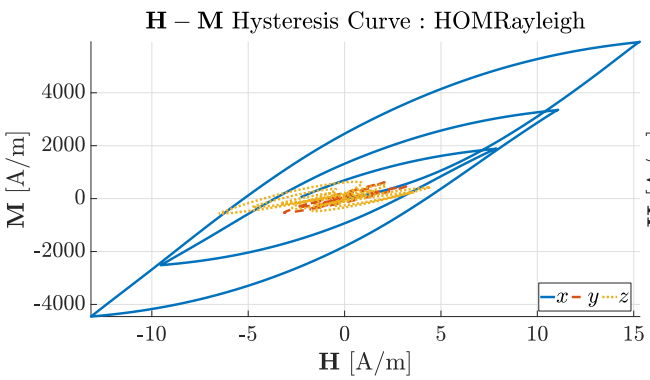

Figure 9.12: nLAH - **RAH**$_a$ – **M** curve.

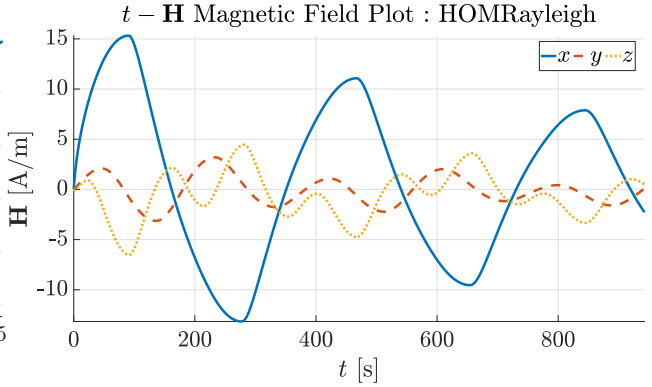

Figure 9.13: nLAH - **RA**t – **H** curve.

One notices that the concentric parabolic shapes are still visible, but with slight distortion. Also, the y and z components of the hysteresis curve exhibit more distortion than the x-component, as can also be observed in Figure 9.13.
One fact that was noticed about the homogeneous **RA**models is the following. When initializing the process at a very 'wild' magnetization, the iterative solving of the ODE tends to stabilize the magnetic field and magnetization evolution. For example, initializing above depicted anisotropic model by letting $\mathbf{M}_{per} = (500 \;\; -100 \;\; 60)^T$, one obtains the following hysteresis curve: More on this can be found in the current chapter, on the section of modelling choices in the homogeneous model.

9.2.3 The Homogeneous JAEllipsoid Model

Let us now turn to have a quick look at different realizations of the Jiles-Atherton ellipsoid magnetization model in the homogeneous case. The **JA**model takes as input five parameters, which can all be extended to include anisotropy. A sixth parameter used to close minor loops, has been omitted in the present research. The reason that this parameter is needed, becomes apparent in the current discussion. But firstly, let us look at some realizations of the **JA**model in the case of perfectly normal isotropic parameters, namely some of the original parameters

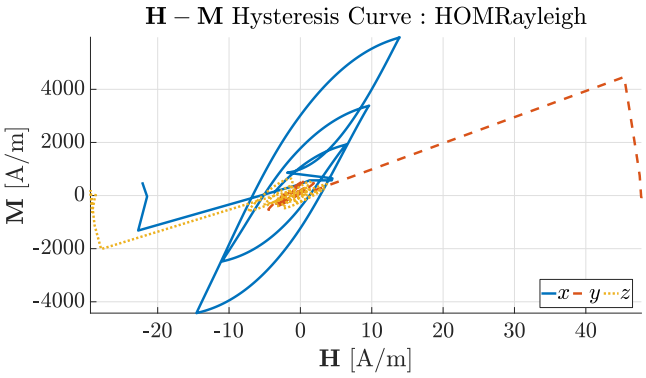

Figure 9.14: nLAH - **RAH** – **M** curve using an unrealistic initial condition. When time progresses, the curve approximates the curve in Figure 9.12.

discussed in the original **JA**introduction paper [21]. These are given by $M_s = 1.6 \times 10^6\,\mathrm{A\,m^{-1}}$, $A = 1100\,\mathrm{A\,m^{-1}}$, the Weiss parameter $\alpha = 1.6 \times 10^{-3}$, $k = 400$ and $k = 400$. This yields the following.

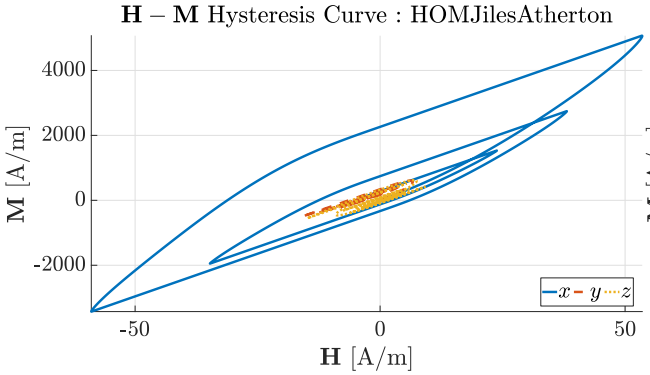

Figure 9.15: nLIH - **JAH** – **M** curve.

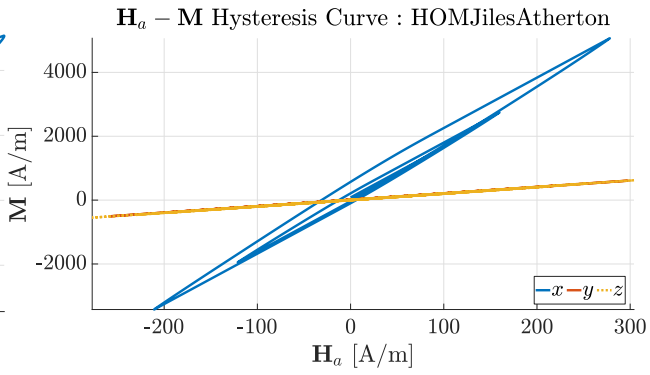

Figure 9.16: nLIH - **JAH**$_a$ – **M** curve.

Again, one can observe the influence of the demagnetization tensor on the hysteresis curve. The y and z components of the magnetization are much more 'damped' out. Now, adding anisotropy by letting $A = 1100$, $\alpha = 1.6 \times 10^{-3}$ and letting the anisotropic parameters and tensors be given by

$$\boldsymbol{M_s} = 1.6 \times 10^6 \begin{pmatrix} 0.1 \\ 1 \\ 1 \end{pmatrix} \quad \text{and} \quad \underline{\boldsymbol{k}} = 400 \begin{pmatrix} 0.8 & 0.1 & 0.2 \\ 0.1 & 1 & 0.1 \\ 0.2 & 0.1 & 0.8 \end{pmatrix} \quad \text{and} \quad \underline{\boldsymbol{c}} = \frac{1}{100} \begin{pmatrix} 2 & 0 & 0 \\ 0 & 1 & 0 \\ 0 & 0 & 1 \end{pmatrix}, \tag{9.4}$$

one obtains the following anisotropic **JA**model curves.

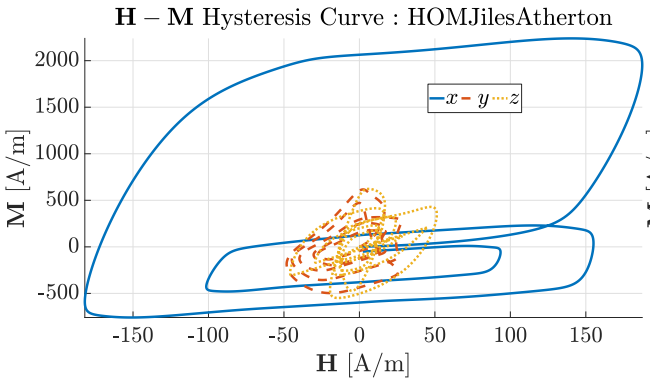

Figure 9.17: nLIH - **JAH** – **M** curve.

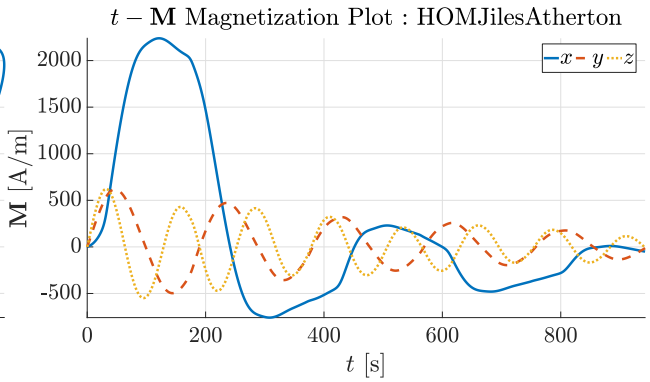

Figure 9.18: nLIH - **JAH**$_a$ – **M** curve.

Again, it is apparent that the homogeneous, anisotropic ellipsoid models are capable of simulating ferromagnetic behaviour that appears to differ greatly from the classical **JA**model as introduced by Jiles and Atherton themselves [21].

9.2.4 The Homogeneous EVEllipsoid Model

The homogeneous **EV**ellipsoid model is the most complex of all models discussed in the present section on homogeneous models. This is reflected in the simulation time and parameter space, but also in the fact that the **EV**model appears to be the most stable of the models discussed here. One can take large increments in the applied field, such that the **RA**and **JA**model would diverge, but the **EV**model shows stable behaviour in most cases. In this short summary of **EV**forward model results, we firstly show some general behaviour of the model. Thereafter, we highlight specific properties of the model, discuss the influence of the number of cells Let us firstly look at a realization of the isotropic **EV**model with $N_c = 41$ cells. The Weiss mean field parameters was set to a value found in literature on the **EV**model, $\alpha = 8.8 \times 10^{-5}$. The model weights ω_i are all chosen equal, with varying isotropic weight tensors, linearly increasing from 0 to $k_{max} = 2$. One might be a bit surprised by the small magnitude of this k_{max}. However, due to the strong internal ellipsoid demagnetization, the geometry of the ellipsoid itself can be viewed as a 'frictional force', resisting magnetization increase along its axes.

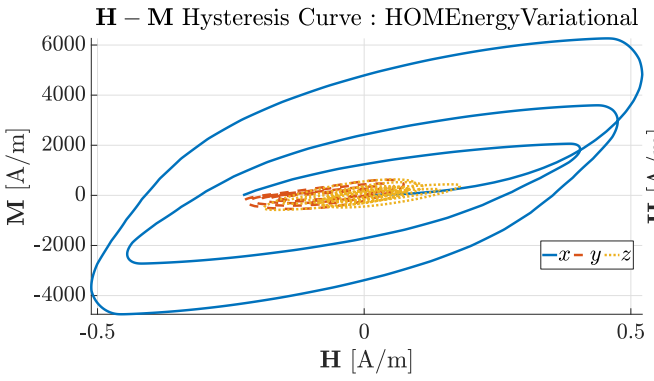

Figure 9.19: nLIH - **EV**$\mathbf{H} - \mathbf{M}$ curve.

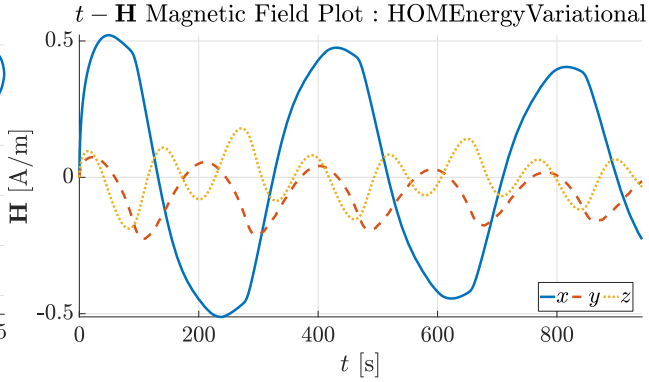

Figure 9.20: nLIH - **EV**$t - \mathbf{H}$ plot.

Secondly, we have simulated the **EV**model using anisotropic parameters. Keeping all other parameters unchanged, we have set

$$\underline{\boldsymbol{k}}_i = \frac{k_{max}(i-1)}{3(N_c-1)} \begin{pmatrix} 3 & 1 & 1 \\ 1 & 3 & 1 \\ 1 & 1 & 3 \end{pmatrix} \tag{9.5}$$

for $1 \leq i \leq N_c$. This yields the following.

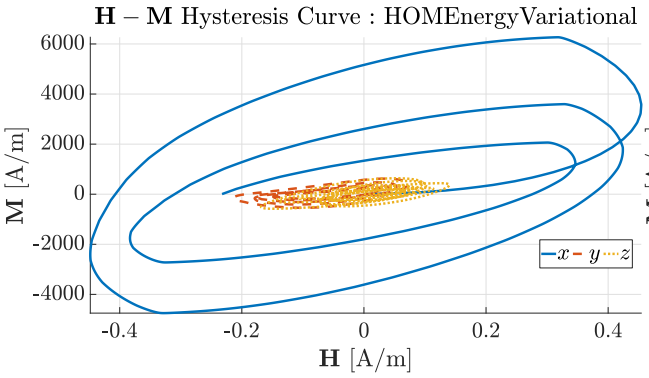

Figure 9.21: nLAH - **EVH** − **M** curve.

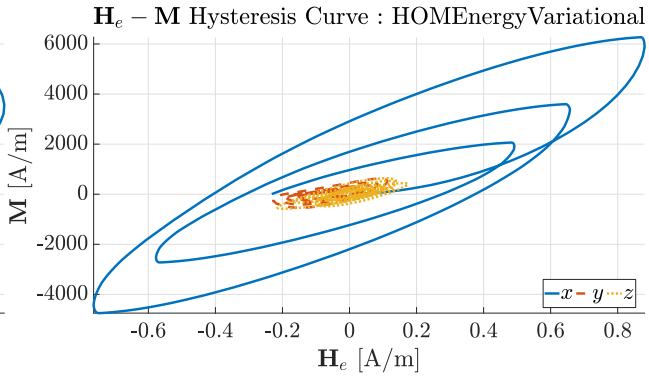

Figure 9.22: nLAH - **EVH** − **M** plot.

Comparing the two results above is interesting. In the **JA**model, the difference between a $\mathbf{H}-\mathbf{M}$ curve and a $\mathbf{H}_e-\mathbf{M}$ is 'very small', even if the Weiss mean field parameter is relatively large. In the **EV**model however, we observed that the Weiss mean field parameter is very critical. Changing it by a small amount, leads to very different behaviour. We conjecture that this has to do with the intrinsic nature of the **EV**model. Looking at the range of **H** in the **JA**model versus in the **EV**model (see Figure 9.15 and Figure 9.19), we conclude that using these sets of parameters, the incremental susceptibility is much higher in the case of the **EV**model, even though the parameters that were used are in some sense 'very normal'. Very high susceptibility yields the $\underline{\boldsymbol{\alpha}}\mathbf{M}$ term dominant in the Weiss effective field description, behaviour which is very much related to the actual value of $\underline{\boldsymbol{\alpha}}$.
All of this could be tweaked such that the models exhibit roughly the same behaviour. This 'cross-over' between hysteresis models will be commented upon in the section on homogeneous (identical) twin experiments.

9.3 Empirical Comparison of the Homogeneous Ellipsoid Models

So far, we have roughly observed that the ellipsoid models are cast in increasing order of complexity and range as follows (where the anisotropic notation 'A' includes the isotropic cases 'I') : LAH, nLAH-**IP**, nLAH-**RA**, nLAH-**JA**, nLAH-**EV**. This is true also in terms of the number of parameters. Let us make these observations more precise in the following table.

	IP	**RA**	**JA**	**EV**
Orders of physics included	1st order	2nd order	∞th order	∞th order
Temperature dependencies	No	No	Yes	Yes
Hysteresis behaviour	No	Yes	Yes	Yes
Anistropy extensions	Yes	Yes	Yes	Yes*
Number of parameters (scalar)	1	2	5	$2+2N_c$
Computational burden	low	limited	high	very high

Table 9.1: Assessment of the four models for ferromagnetic behaviour.

To illustrate this table, we have run the four forward homogeneous models (**IP**, **RA**, **JA**, **EV**) many times with different parameters, driven by the background field Equation 9.1. In terms

of computation time, we have found the following.

9.4 Homogeneous Sensor Mapping and Measurement Noise

In the homogeneous model, we solve for the magnetization evolution $\mathbf{M}(t)$ at discrete time steps t_n. As discussed earlier, the exact solution to the magnetostatic Poisson equation allows for an analytical derivation of the magnetic flux density both in- and outside the ellipsoid, and thus an analytical expression of the ellipsoid signature. As discussed before, the relation between uniform ellipsoid magnetization and the signature outside the ellipsoid is given by the equations

$$\mathbf{B}_s(\mathbf{r}, t) = \mathbf{B}(\mathbf{r}, t) - \mu_0 \mathbf{H}_a(t) = \underline{\mathrm{A}}(\mathbf{r})\mathbf{M}(t). \tag{9.6}$$

Now, since the number of sensors in the CLAViS is 112 and because of the ordering choice discussed in **??**, the above linear mapping can be extended to form one linear mapping for all sensors. This yields for the discrete time stepping points

$$\boldsymbol{B}_s(t_n) = \underline{\Lambda}\mathbf{M}(t_n). \tag{9.7}$$

This formulation was chosen because in the end, it is in the same form as the (processed) output of the CLAViS. Some typical signature plots can be observed in the figure below.

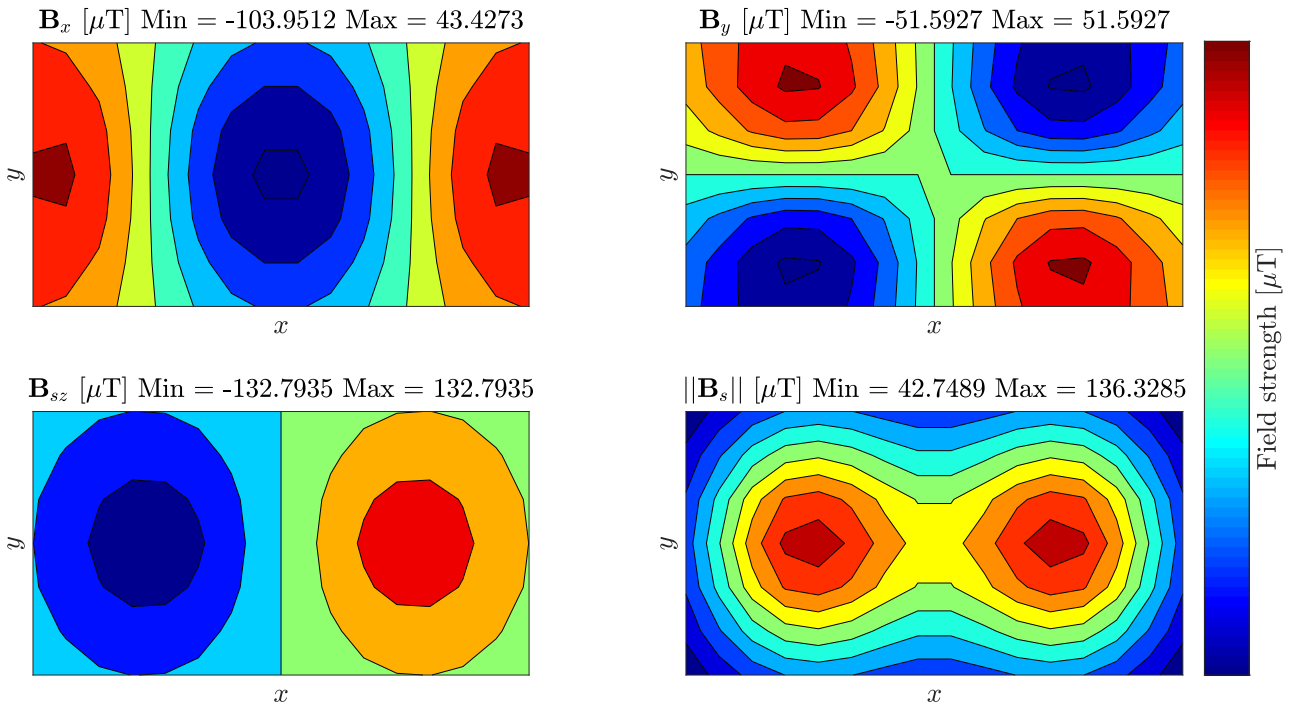

Figure 9.23: An ellipsoid signature plot, produced by an uniform ellipsoid magnetization of $\mathbf{M} = (6000, 0, 0)^T$ using equation Equation 9.7.

Another example is depicted in the next figure, which is an example of a signature plot with off-axes uniform magnetization.

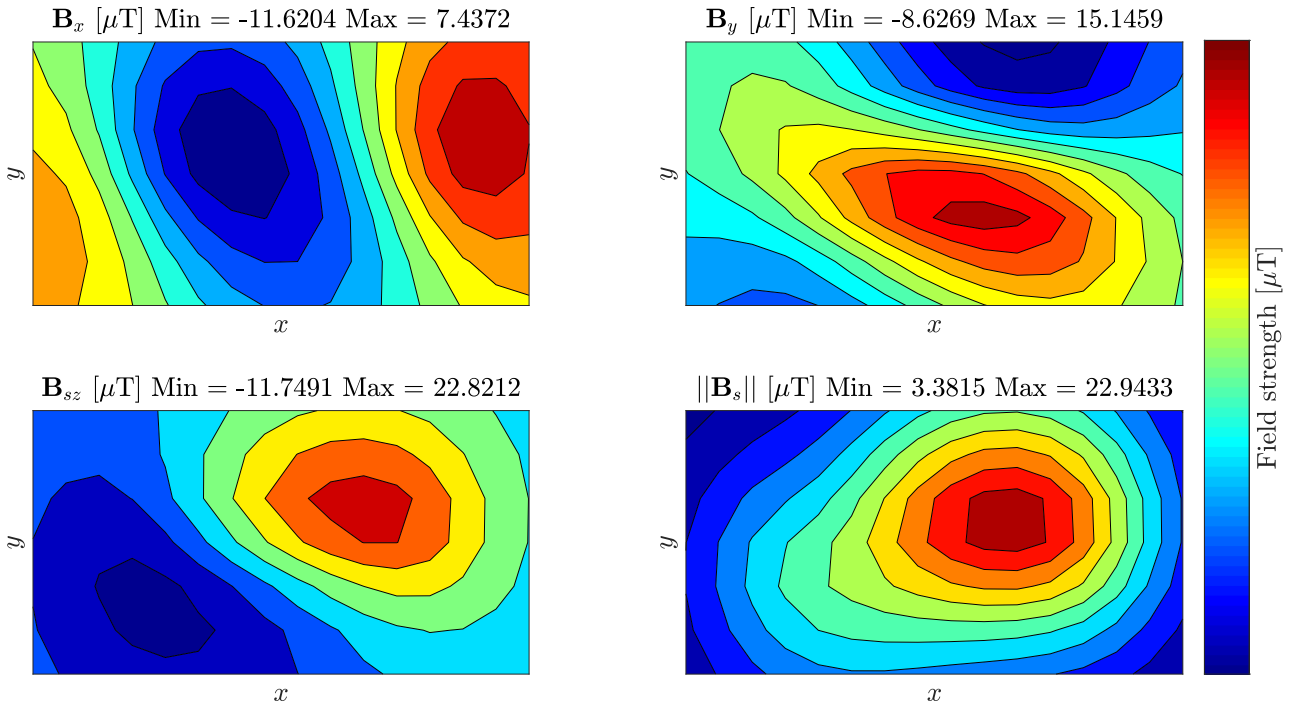

Figure 9.24: An ellipsoid signature plot, produced by an uniform ellipsoid magnetization of $\mathbf{M} = (600, -300, 200)^T$ using equation Equation 9.7.

Now that the nature of the mapping Equation 9.7 has been made visible, we are ready to introduce the concept of noise. One is obliged to admit that the field of noise modelling is an entire research field on its own. We have looked at several causes effects that *could be regarded as system noise*, such as

1. The uncertainty in sensor positions;
2. The intrinsic measurement error of sensors;
3. Barkhausen noise [5];
4. CLAViS calibration biases or imperfections;
5. Fundamental sensor imperfections and random extreme measurements;
6. Uncertainty in the uniformity or magnitude of the applied field;
7. Uncertainty in the position of the ellipsoid;
8. In the case of the homogeneous model, a very obvious source of something that could be perceived as noise *in the homogeneous model* would be the non-uniformity of the ellipsoid magnetization. This will be treated in more detail later on in the current report.

It is beyond the scope of the current research to model all these noise sources using rigorous arguments. Rather, we have postulated that all the noise discussed above can be modelled by perturbing the signature output of models and experiments by a normally distributed vector $\boldsymbol{\varepsilon} \sim \mathcal{N}(0, \Sigma)$, where Σ is the covariance matrix of the noise. Having discussed perturbing signature data, we continue by discussing various twin experiments that were performed during our research.

9.5 Homogeneous Twin Experiments

A twin experiment is essentially the following: We run a forward model and thereafter use the output of that model to estimate the parameters that were used in the forward simulation. Since the forward simulation was done on a computer, all *real* parameters are known. This procedure can be extended to include measurement noise. Unfortunately, we have not been able to devise new ideas to invert the hysteresis models. The genetic algorithms discussed in the section on inverse homogeneous models, is a kind of 'brute force' approach, which maybe lacks a bit of aesthetic value. Surely it is possible to derive incremental algorithms that estimate the homogeneous hysteresis parameters by looking at the relation between d$\mathbf{M}$ and d$\mathbf{H}$ at each time step. These are related by the incremental susceptibility, which in turn is directly related to the hysteresis parameters. In the homogeneous case, the big advantage over the inhomogeneous models is that the magnetic field is known through the ellipsoid formula, making these types of inversion algorithms possible.
In short, our twin experiments demonstrate that the chosen forward models are stable and that inversion is stable with respect to noise addition.

9.6 Homogeneous Parameter Estimation Using CLAViS Data

Let us return to the CLAViS measurement, introduced at the beginning of the current chapter. As discussed before, Equation 9.7 allows for finding the uniform magnetization estimate that minimizes the 2-norm error of the signature within the homogeneous model, by employing the normal equations. It is a severely overdetermined system, giving a very robust estimation of the (in the homogeneous model assumed) uniform magnetization. Solving the normal equations that are associated to Equation 9.7, we find the following estimation of the homogeneous ellipsoid magnetization, magnetic field and hysteresis curves.

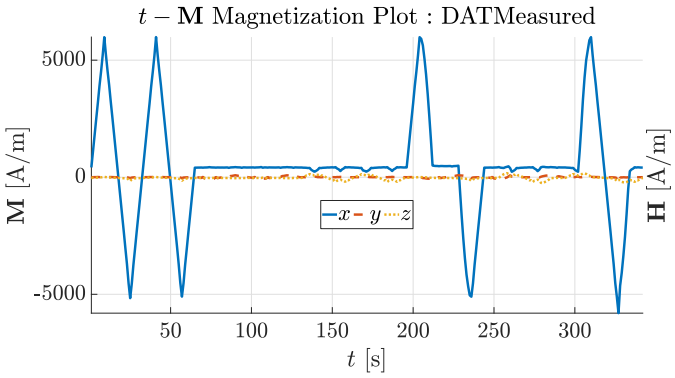

Figure 9.25: Estimation of the ellipsoid internal magnetic field using the normal equations .

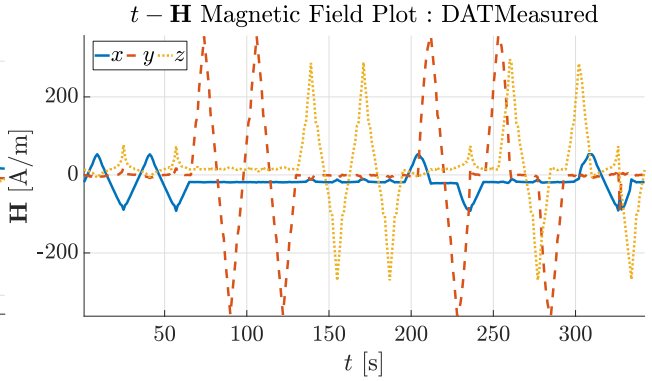

Figure 9.26: Estimation of the ellipsoid internal magnetic field using the Ellipsoid Formula.

The estimations depicted above, lead to the following hysteresis curves.

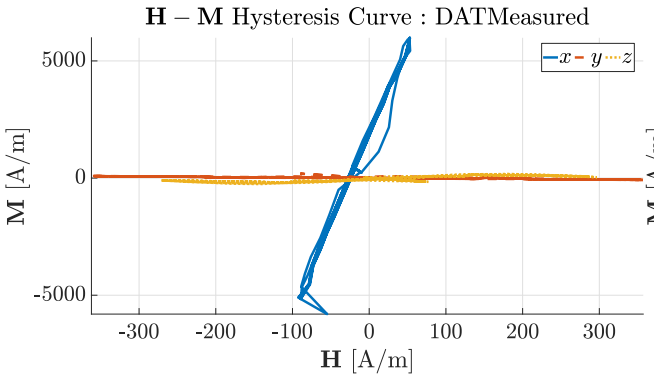

Figure 9.27: The CLAViS $\mathbf{H} - \mathbf{M}$ loop.

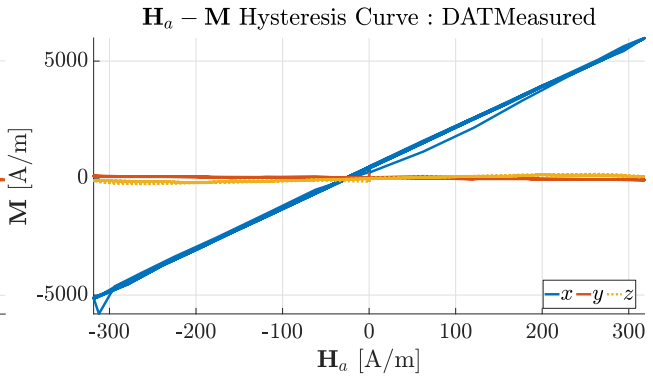

Figure 9.28: The CLAViS $\mathbf{H}_a - \mathbf{M}$ loop.

We are now ready to fit several homogeneous forward models to the measured CLAViS data. The table below represents the outcomes that were observed when running our genetic algorithms with the applied field that was used in the CLAViS measurements.

Table 9.2: A subset of estimated hysteresis parameters using real measurement data.

Homogeneous Ellipsoid Models: Parameters			
	Isotropic	Uniaxial Anisotropic	Fully Anisotropic
Linear	$\mu_r = 72.36$	$\underline{\boldsymbol{\mu}}_r = \begin{pmatrix} 81 & 0 & 0 \\ 0 & 0.82 & 0 \\ 0 & 0 & 1.49 \end{pmatrix}$	$\underline{\boldsymbol{\mu}}_r = \begin{pmatrix} 76 & 0.3 & 0.84 \\ 0.3 & 0.62 & 0.19 \\ 0.84 & 0.19 & 1.07 \end{pmatrix}$
IP	$\mathbf{M}_{per} = \begin{pmatrix} 0.43 \\ 1.85 \\ -2.86 \end{pmatrix}$	$\mathbf{M}_{per} = \begin{pmatrix} 0.27 \\ 2.1 \\ -2.9 \end{pmatrix}$	$\mathbf{M}_{per} = \begin{pmatrix} 0.45 \\ 3.4 \\ -2.4 \end{pmatrix}$
	$\mu_r = 72.36$	$\underline{\boldsymbol{\mu}}_r = \begin{pmatrix} 81 & 0 & 0 \\ 0 & 0.82 & 0 \\ 0 & 0 & 1.49 \end{pmatrix}$	$\underline{\boldsymbol{\mu}}_r = \begin{pmatrix} 70 & 0.4 & 2.9 \\ 0.4 & 0.74 & 0.26 \\ 2.9 & 0.26 & 0.32 \end{pmatrix}$
RA	$\mu_r = 72.35$	$\underline{\boldsymbol{\mu}}_r = \begin{pmatrix} 73.23 & 0 & 0 \\ 0 & 0.82 & 0 \\ 0 & 0 & 1.49 \end{pmatrix}$	$\underline{\boldsymbol{\mu}}_r = \begin{pmatrix} 73 & 0.16 & 0.04 \\ 0.16 & 0.74 & 0.43 \\ 0.04 & 0.43 & 1.05 \end{pmatrix}$
	$\alpha_R = 0.012$	$\underline{\boldsymbol{\alpha}}_R = \begin{pmatrix} 8 \times 10^{-5} & 0 & 0 \\ 0 & 0.05 & 0 \\ 0 & 0 & 1.5 \end{pmatrix}$	$\underline{\boldsymbol{\alpha}}_R = \begin{pmatrix} 0.031 & 0 & 0 \\ 0 & 1.4 & 0 \\ 0 & 0 & 0.6 \end{pmatrix}$
JA	$M_s = 1.1 \times 10^6$ $A = 1.3 \times 10^3$ $\alpha = 4.8 \times 10^{-5}$ $k = 592$ $c = 0.29$		

A wise question is now as follows: Do these parameter estimations actually *mean* anything? We are obliged to say that the parameter estimation for Rayleigh and Jiles-Atherton models is very unstable. That is, the scalar model approximation does arrive at consistent estimates of parameters, and can thus be regarded as reliable. However, when anisotropic parameters are used, our algorithms often end up at varying estimates. It is worth noting that the **IP**model is capable of approximating measurements the best (by far). The Uniaxial **IP**model manages to achieve a global sensor error of at least 10 times lower than all other models that have been fitted. Moreover, one could say that the estimate of the linear part of the linear model, **IP**and **RA**are very stable, even in anisotropic cases. We also point out that the anisotropic models

arrive at a very low relative permeability in the y and z direction. This solidifies the conjecture that more data are needed to fit anisotropic models, since the achieved estimates are just very unrealistic in complex models.
The above estimates were all performed using 'gene pools' of 1000 parameter sets and by running the homogeneous forward models for many epochs.
Unfortunately, we have not been successful in inverting the **EV**model, due to planning reasons. In their original paper however, Prigozhin et al. provide a multi-step way of inverting the **EV**model. However, this makes use of intrinsic `Matlab` functions such as `fminunc()`, which is comparable to our current approach using `ga()`, in the sense that it requires many forward model runs.

9.7 Results of specific inhomogeneous ellipsoid models

In the current chapter, we formulate our results for inhomogeneous Ellipsoid Models. The sections within the current chapter are structured as follows:

1. Firstly, we take a short look at the performance of our magnetostatic Finite Element implementation, and discuss some observations. We discuss the difference between the full-FEM approach and the mixed-FEM approach and try to formulate possible explanations for the discrepancy in results. This is combined with an analysis choices that were made in our FEM-implementation, including computation time, mesh size, condition numbers and boundary condition choices.

2. Secondly, we discuss the procedure to find $\mathbf{H}$ from Φ and compare it to the 'weak form gradient' method.

3. Thirdly, we discuss the performance of our procedure to estimate the magnetization distribution, based on sensor data. We compare several approaches in terms of reliability and

4. Fourthly, we provide some results on inhomogeneous forward models, in particular the inhomogeneous **RA**model. Since these models are quite complex to run on our standard PC's, we have not been able to estimate the (possibly inhomogeneous) hysteresis parameters. More on this will be said in the Recommendations section.

5. Finally, we again turn to our CLAViS data to see if there are 'chunks' of permanent magnetization to be found. As said previously, we have not been able to obtain the hysteresis parameters in the inhomogeneous case, which is mostly due to time limitation.

9.8 The static forward problem

We have run many static forward problems using our FEM implementation. In doing this, we have made use of the following mesh sizes:

Table 9.3: Summary of used `Comsol` mesh data, in ascending order of complexity.

Name	Nodes	Elements	Condition number of $\underline{K}_o$	Mean system solving time
M1	1279	6729	1.44×10^3	1.6×10^{-2} s
M2	4654	25302	2.36×10^3	4.4×10^{-2} s
M3	10227	57341	6.06×10^3	1.2×10^{-1} s
M4	32707	189847	6.67×10^3	5.5×10^{-1} s
M5	38142	220895	4.02×10^4	9.4×10^{-1} s
M6	91527	530355	2.98×10^4	5.8 s

The condition number of M5 is higher than the system condition number of M6, which is interesting. In fact, M5 was manipulated to be very fine inside the ellipsoid, and less fine in the airbox. We conclude that the domain-dependent meshing algorithms used by `Comsol` have integrated features that attempt to minimize system condition numbers.
Let us firstly observe two inhomogeneous model realizations. However, we apply a homogeneous $\mathbf{M}$ distribution of $(2000, 200, -300)^T$ A m^{-1}. This gives a measure of how well our FEM implementation performs, since the homogeneously magnetized ellipsoid potential and field are known analytically. We observe the following.

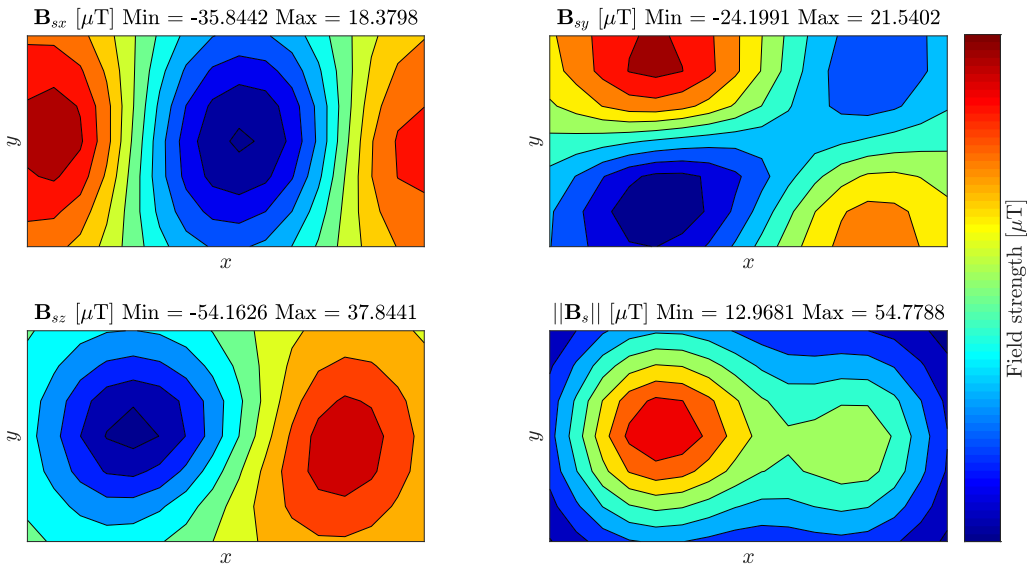

Figure 9.29: Homogeneously magnetized ellipsoid signature using the homogeneous sensor mapping.

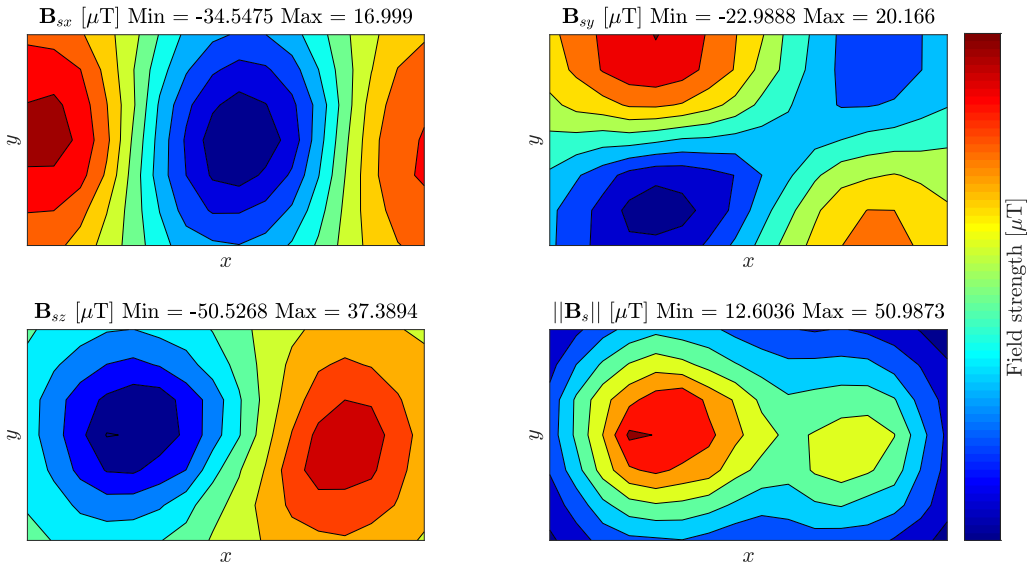

Figure 9.30: Homogeneously magnetized ellipsoid signature using the purely FEM sensor mapping.

One can see that there is a difference in the signature of a homogeneously magnetized ellipsoid. This difference is already caused by a fundamental difference in Φ and subsequently also for the magnetic field, which is derived from the potential approximation via interpolation. What is the cause of this? We have come up with several possible explanations.

- In discretizing the FE domain using tetrahedral elements, we introduce a fundamental reduction of complexity.

- Scalar potential intrinsic instability in regions of high variation is often discussed in literature. Indeed, on the boundary of the ellipsoid and in a neighbourhood thereof, there exists wildly chaotic behaviour in the FEM solution.

- Newton-Cotes integration of ellipsoid boundary elements and normal vectors, might induce an error that spreads out throughout the computation domain.

- The intrinsic `Matlab` backslash solver for large sparse linear systems, might produce errors by for example having too high a tolerance.

Further research is required to investigate this behaviour of the inhomogeneous model. *This is the reason* why we have chosen to modify our implementation according to the procedure described in the FEM chapter of the current report. That is, the magnetization is always written as a *sum of a homogeneous part and an inhomogeneous perturbation.* A cross-sectional example of this inhomogeneous perturbation can be observed below.

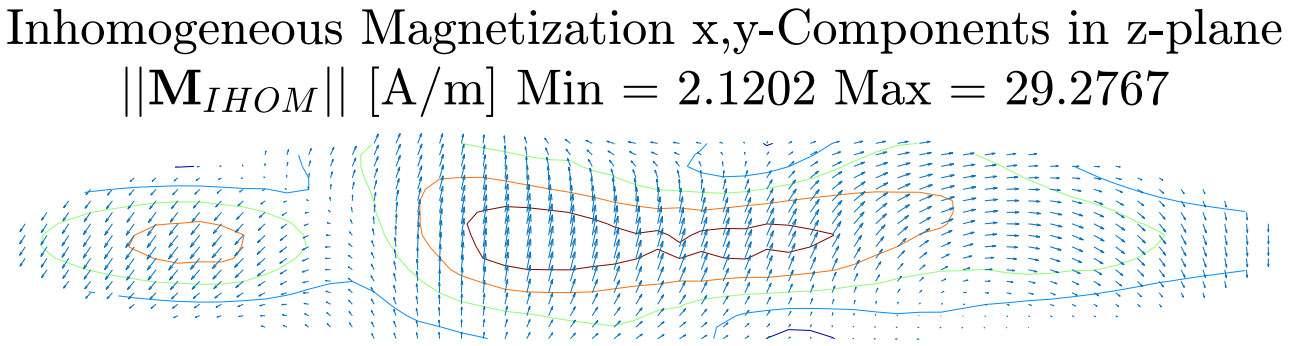

Figure 9.31: Cross-sectional depiction of a superimposed inhomogeneous magnetization component.

Since the solution to the homogeneous problem is known analytically, FEM errors damp out drastically if the inhomogeneous magnetization component is assumed to be small. Below, we provide some figures that depict the signatures of both homogeneous and inhomogenously magnetized ellipsoids. One can see that an inhomogeneously perturbed ellipsoid magnetization carries with it a small effect on the sensor array, that needs to be estimated in the inverse static inhomogeneous model.

9.9 The Inverse Static Problem

We now turn to the problem of estimating the inhomogeneous magnetization distribution $\mathbf{M}(\mathbf{r})$ from measured data. As discussed before, we employ an impulse-response method by expanding the magnetization into a homogeneous component with several 'blobs' superimposed, functioning as imhomogeneous magnetization areas. An example of internal magnetization that can be achieved this way, can be seen in the following cross-sectional plot:

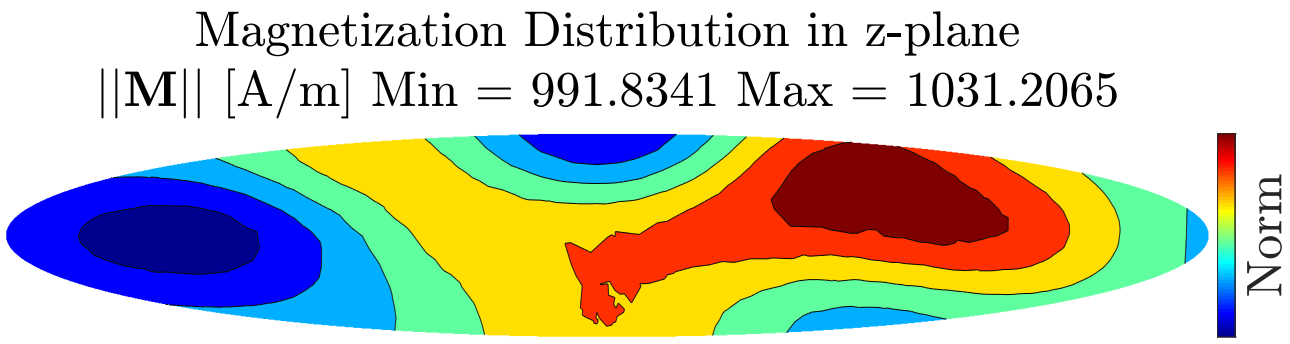

Figure 9.32: An example of a possible internal inhomogeneous magnetization distribution. The magnetization norm is plotted.

In the current section, it is our aim to 'decompose' variations of the above magnetization distribution in components. We have performed the following experiments to achieve this.

- (E1) Trying to estimate the $\mathbf{M}$-distribution directly using direct inversion and regularization. This is practically impossible due to singular values of order 1×10^{-26} in our equations.

- (E2) Trying to estimate the $\mathbf{M}$-distribution on the basis of sensor data, using more or less homogeneously distributed 'blob centers' on the ellipsoid and by using generalized

normal blobs on these centers as inhomogeneous basis functions. In this case, the basis functions were of the form, for $\mathbf{r} = (x, y, z)^T$

$$f_j(\mathbf{r}_j, \mathbf{r}) = A \exp\left(-\frac{1}{2}\left(\frac{x - x_j}{\sigma_x}\right)^{2p_x} - \frac{1}{2}\left(\frac{y - y_j^2}{\sigma_y}\right)^{2p_y} - \frac{1}{2}\left(\frac{z - z_j}{\sigma_z}\right)^{2p_z} \right). \tag{9.8}$$

We took $\sigma_x = 0.01a$, and $\sigma_y = \sigma_z = 0.01b$, where a and b are the semidiameters of the ellipsoid, and we took $p = 1$ for all dimensions. Also, the coefficient A is chosen such that $f_j(\mathbf{r}_j, \mathbf{r}_j) = 1$.

- (E3) Trying to estimate the **M**-distribution on the basis of sensor data, using equally spaced 'blob centers' along the x-axis and by using generalized normal blobs on these centers as inhomogeneous basis functions. In this case, the basis functions were of the same shape as in experiment (E2), but in this case we only used six equally spaced points on the x-axis and took $\sigma_x = \sigma_y = \sigma_z = 0.02a$, where a is the x-semidiameter of the ellipsoid. Moreover, we took $p_x = 2$ and $p_y = p_z = 1$, together yielding a system size with 21 unknowns to solve.

The ellipsoidal normal blob locations of experiment (E2) are chosen with the help of prolate spheroidal coordinates in order to have a 'nice' distribution. Their locations can be observed below.

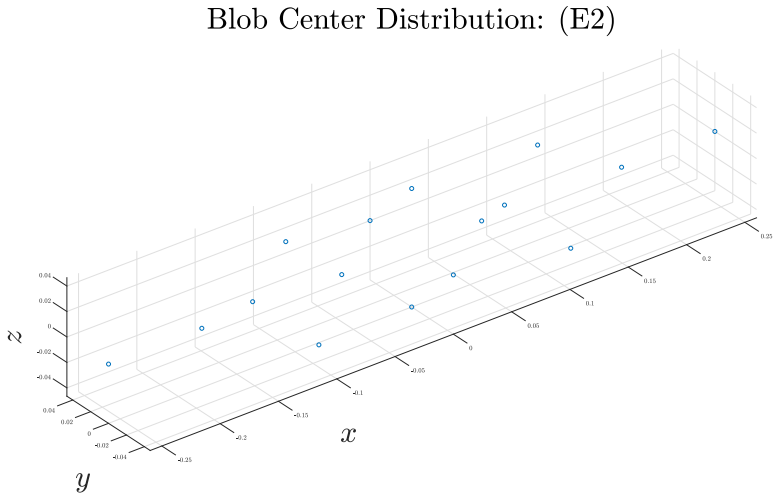

Figure 9.33: Locations of the normal blob centers in experiment (E2).

To see the shape of a general blob function in experiment (E2), let us look at a cross-sectional plot of the magnetization norm in the z plane, where the magnetization is given by only one basis function. The basis function is centered on the ellipsoid major axis.

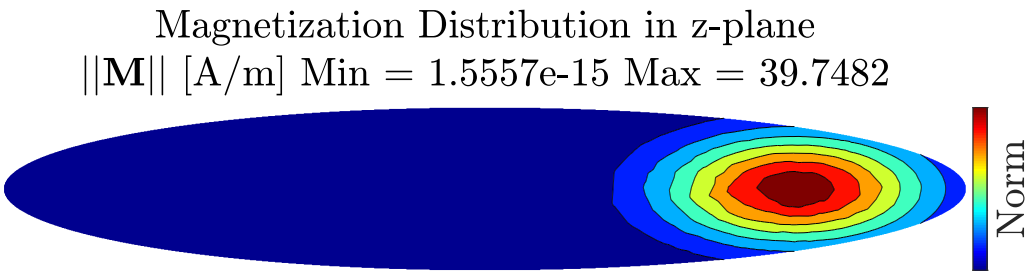

Figure 9.34: The magnetization caused by letting $c_7 = 40$ in the coarse grid system. This is equivalent to taking an ellipsoidal normal distribution of magnetization in the x-direction, located at $\mathbf{r}_7 = (0.18cm, 0, 0)^T$.

The magnetization blob depicted above, yields the following signature:

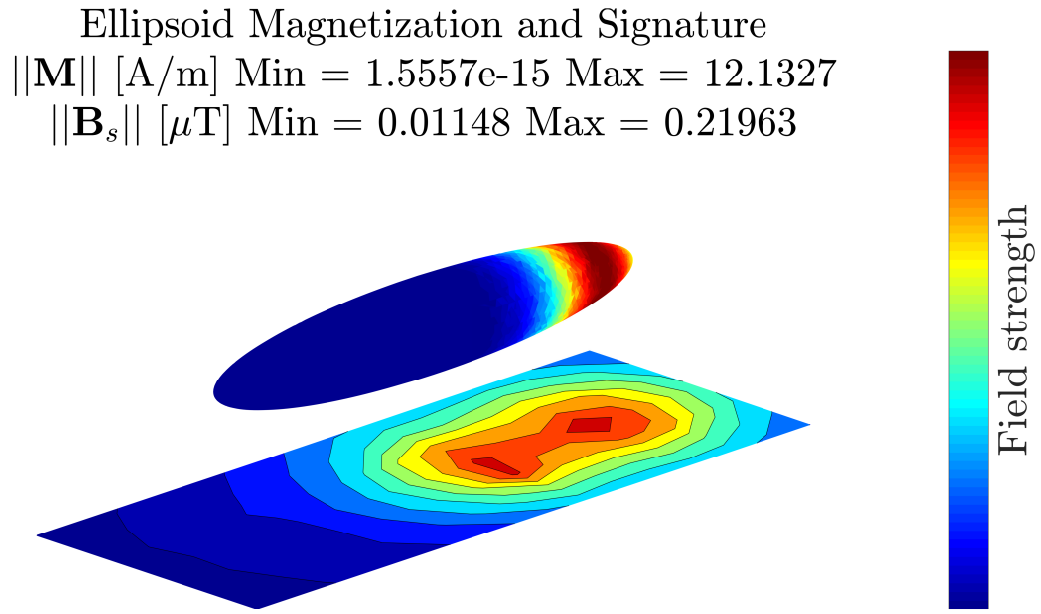

Figure 9.35: The magnetization caused by letting $c_7 = 40$ in the coarse grid system, combined with the produced signature plot.

An example of the range of magnetization distributions (E2) can take is given below.

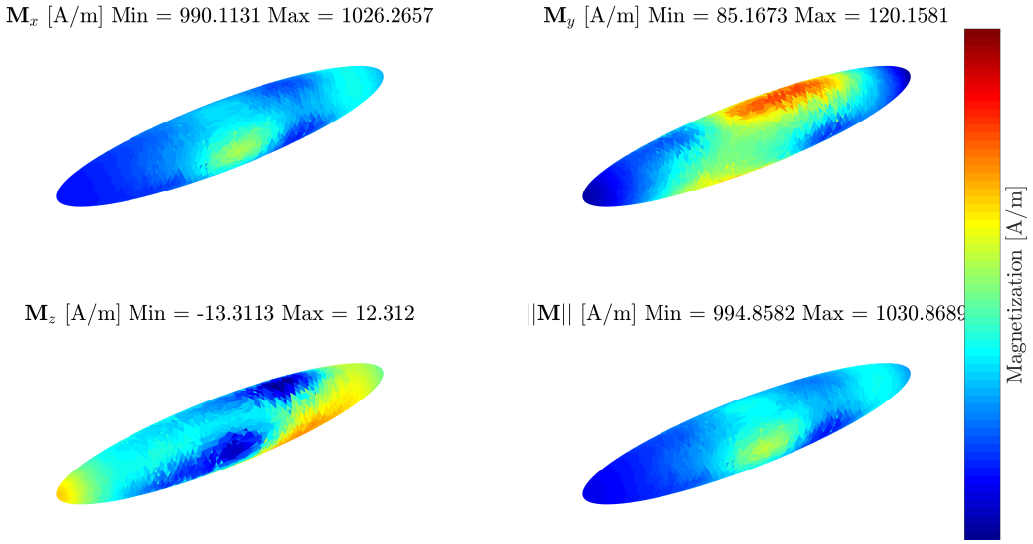

Figure 9.36: Nonuniform ellipsoid magnetization by initializing an inhomogeneoud Ellipsoid Model using a homogeneous magnetization of $\mathbf{M}_{HOM} = (1000, 100, 0)^T$ an by using normally distributed coefficients for the normal ellipsoidal blobs.

As stated previously, the system

$$\underline{\mathrm{C}}\boldsymbol{c} = \boldsymbol{B}_s \tag{9.9}$$

needs to be solved for the basis function coefficients $\boldsymbol{c}$. Now, in (E1), the condition number of the above system was of the order 1×10^{19}. For (E2), the condition number was roughly 1.6×10^4 and for the third experiment, the condition number was given by 688. Since the condition number of the second experiment is still quite large, even when using the coarse grid approach, we have employed regularization techniques to solve the above system efficiently. To

see the subtle difference in signatures to be accounted for in our inverse estimations, let us compare the difference in sensor output between to magnetized ellipsoids. The first ellipsoid is homogeneously magnetized, whereas the second ellipsoid is homogeneously magnetized but given a small perturbation in magnetization on top. Below, the two signature outputs are compared and the difference is visualized.

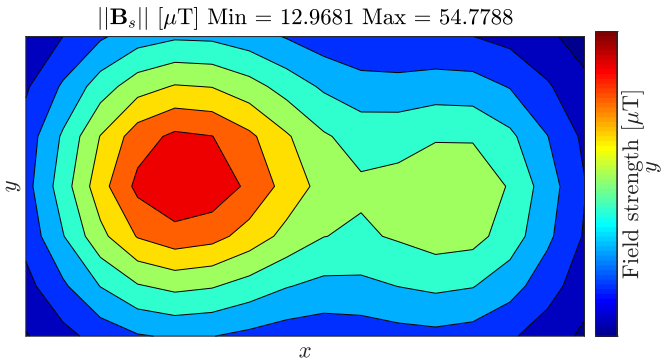

Figure 9.37: Signature norm of a homogeneously magnetized ellipsoid with magnetization $\mathbf{M} = (2000, 200, -300)^T$.

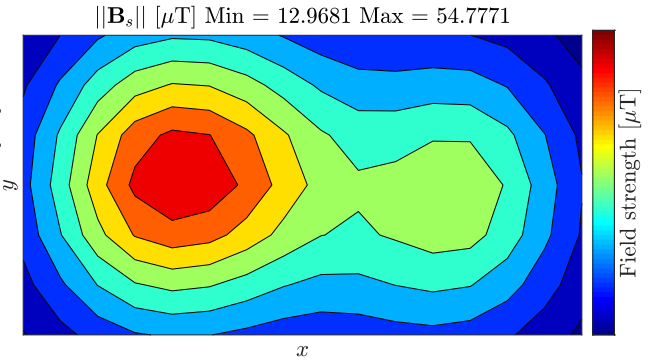

Figure 9.38: Signature norm of a homogeneously magnetized ellipsoid with magnetization $\mathbf{M} = (2000, 200, -300)^T$, perturbed with a normal blob of amplitude 5 in the z-direction.

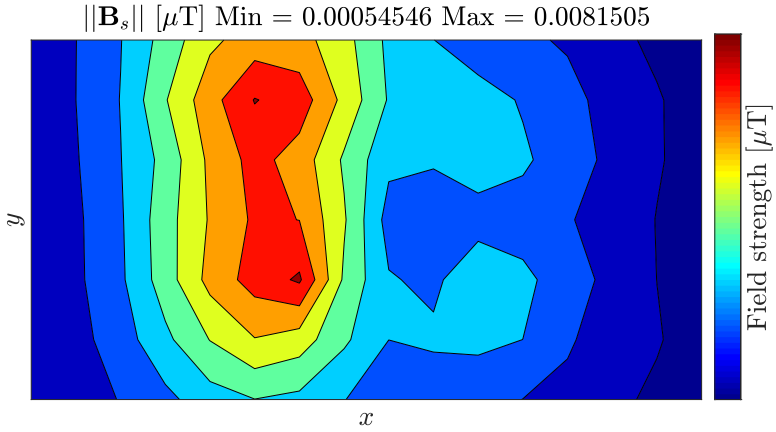

Figure 9.39: Difference between the two signatures above. Once one has grasped the vastly different scales that are present in the model, one sees the need for regularization, which is investigated in the next section of this Results chapter.

9.10 Estimating M(r): Regularization and Twin Experiments

We now turn to the estimation of the ellipsoid magnetization using regularization. We also analyze the robustness of our inversion when different levels of noise are added, and we look at estimations of optimal regularization parameters. In our experiments, we observe that truncated SVD regularization outperformed iterated Tikhonov regularization almost always, an observation that is warranted also by Neumaier [86]. Using the SVD is intrinsically a more 'complex' form of regularization that is capable of capturing certain aspects of the inversion problem and eliminating precisely the noise in the 'difficult' areas of the linear system.
Now, let us firstly solve

$$\underline{\mathrm{C}}\boldsymbol{c} = \boldsymbol{B}_s \tag{9.10}$$

using a direct approach and SVD regularization using noise-contaminated measurements. From now on, we only focus on truncated SVD as our regularization method. The results of estimating $\boldsymbol{c}$ are depicted in the following figure. In that experiment, we have initialized a large homogeneous magnetization and superimposed small perturbations.

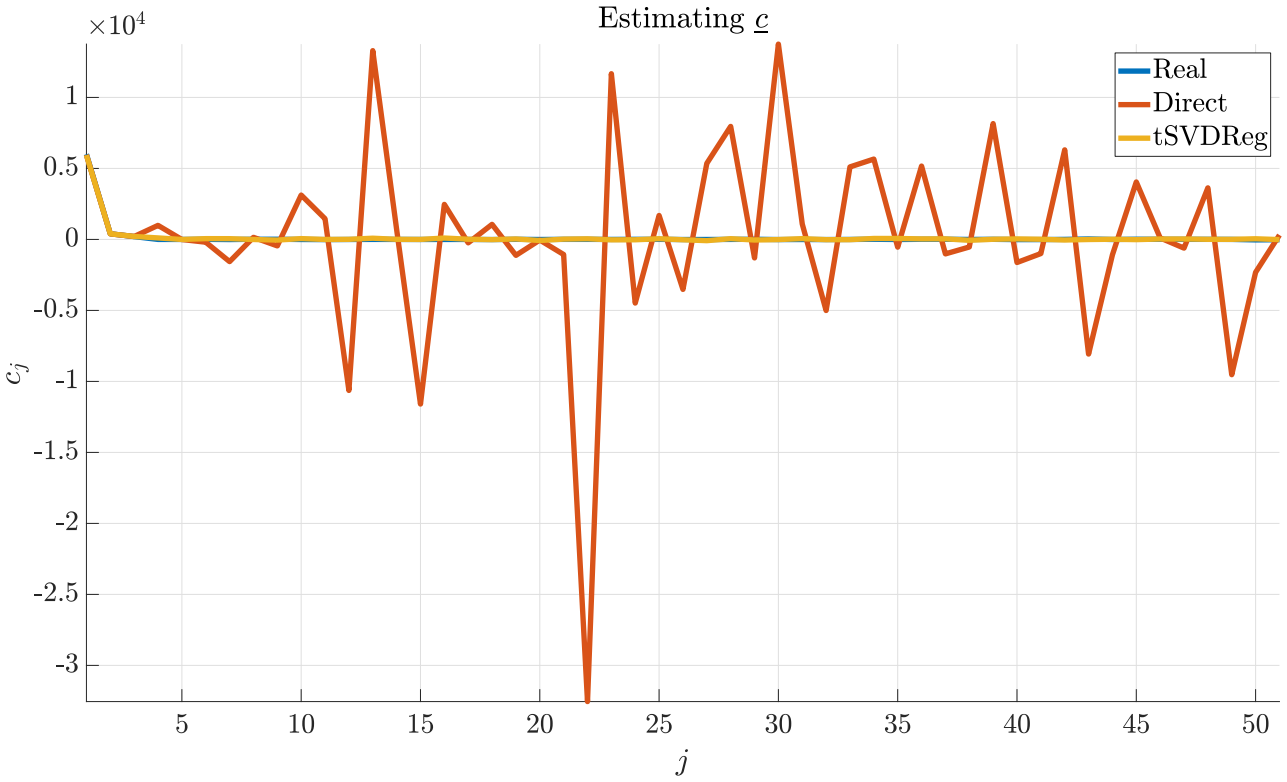

Figure 9.40: Influence of SVD regularization on the estimation of $\boldsymbol{c}$ in experiment (E2) which has quite a high condition number and 51 free blob amplitudes to estimate. We have found an optimal value for the SVD regularization parameter by inspecting different error measures on different parameters and by iteratively raising or lowering the parameter. In this experiment, we have added noise to the signature data with 50 signal to noise ratio. One can see that the homogeneous magnetization components are easily deduced by the inverse estimation.

Experiment (E3) is much better conditioned. This is reflected in the relative performance of direct inversion and SVD inversion, as can be observed in the following left figure. The figure on the right is visualizing the estimation of $\boldsymbol{c}$ on with a small homogeneous magnetization component and a relatively large measurement noise to perturb the data (20 signal to noise ratio). Although the SVD regularization procedure still performs better than direct inversion, adding a lot of noise simply makes it impossible for any smart procedure to arrive at 'the' best estimate.

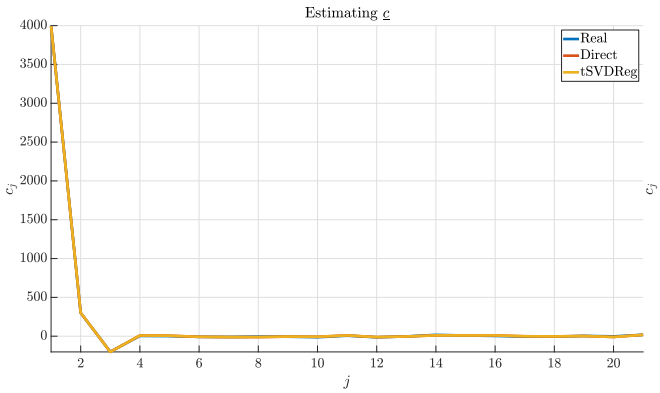

Figure 9.41: Estimating $\boldsymbol{c}$ in the well-conditioned situation (E3), with 50 signal to noise ratio.

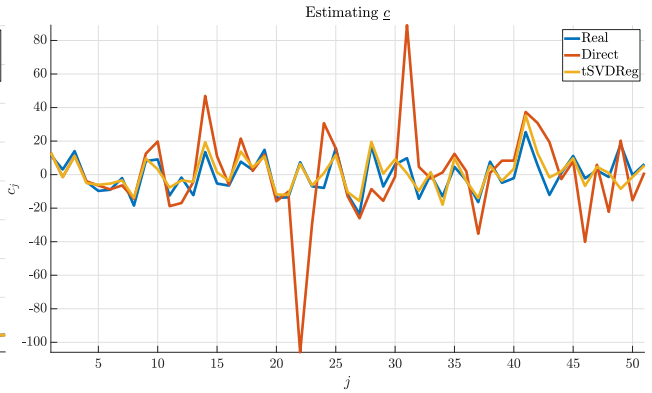

Figure 9.42: Estimating $\boldsymbol{c}$ in the experiment (E2), with 20 signal to noise ratio and a small homogeneous component.

The right hand side figure above was also used to visualize the estimated magnetization and signature using SVD and direct inversion, which yielded the following. The 'real' situation was given by

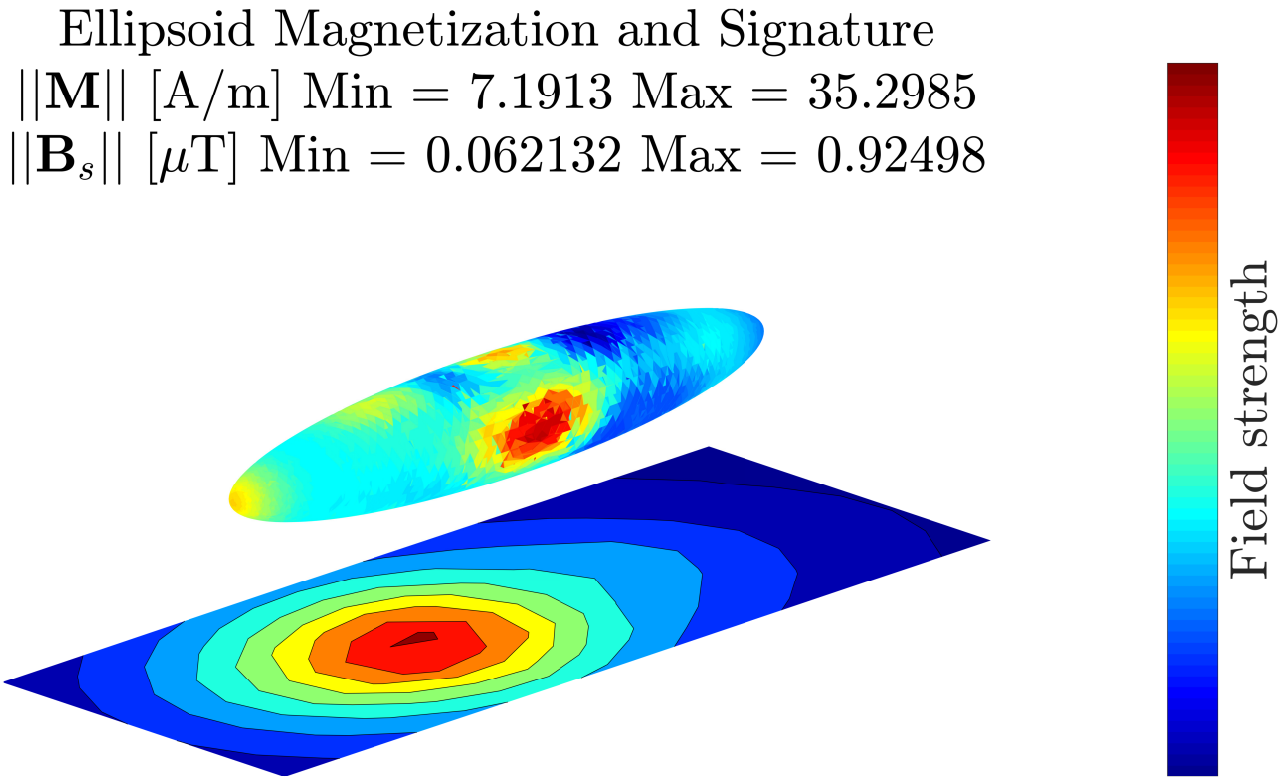

Figure 9.43: Twin experiment reference situation.

After adding normally distributed noise at the sensor locations, with variance that equalled 0.05 times the norm of that particular sensor measurement, we inverted the (E2) model on these perturbed data. SVD regularization clearly yields a more reliable inversion.

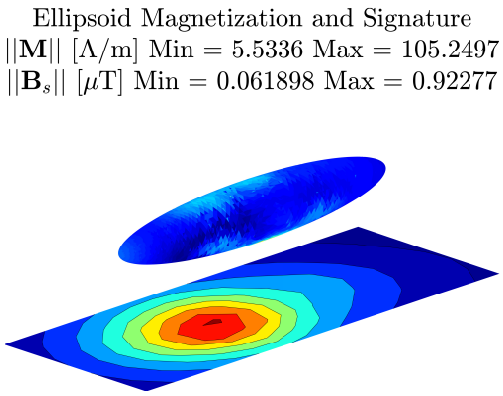

Figure 9.44: Direct estimation in the perturbed twin experiment.

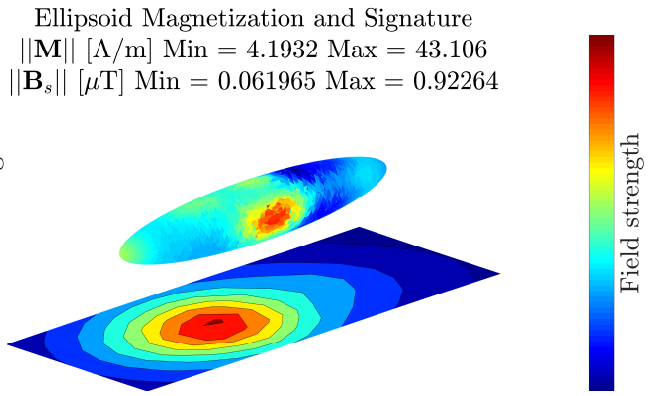

Figure 9.45: SVD-regularized estimation in the perturbed twin experiment.

From the three figures above, one can indeed conclude that the *signature* of the three situations does not differ all that much. However, the magnetization distribution does, which is a typical fact in ill-posed inverse modelling.

Chapter 10

Conclusions and Recommendations

10.1 Conclusions

In the current Conclusions chapter, we attempt to formulate answers to the original goals and questions of the research. To freshen up our memory a bit, these were given by:

'Formulate, motivate, design, implement, verify and improve a model of the magnetic behaviour of a ferromagnetic steel ellipsoid, taking into account hysteresis, anisotropy and inhomogeneity, moreover, quantify the impact of these three aspects.'

We attempted to reach this goal by formulating the following sub-goals.

- Develop a flexible and general forward model
- Identify and understand the physical and mathematical significance of model parameters
- Investigate a flexible, general and reliable method of model inversion and parameter estimation
- Quantify the impact of hysteresis, (an)isotropy and (in)homogeneity

We have set up our research as follows. Firstly, we have examined a class of models known as *homogeneous ellipsoid models*, which are very conveniently coupled to four different nonlinear hysteresis models: The Induce-Permanent model, the Rayleigh model, the Jiles-Atherton model and the Energy-Variational model. Using genetic algorithms, three out of four homogeneous hysteresis models, with the exception of the Energy-Variational model, have been fitted to measured data. We have quantified the prediction error that was made by approximating the magnetic behaviour of the real ellipsoid by our simplified models. The homogeneous models, which have the property of only requiring time integration, are able to describe the ellipsoid magnetization only up to a uniform level. On the one hand, this makes estimating the magnetization 'distribution' very straightforward and overdetermined, on the other hand, it induces a larger prediction error, since measurements indicate that the magnetization of the experimental ellipsoid is not uniform. Using a signature-based mean squared error optimization algorithm, we have been able to estimate the optimal ellipsoid parameters, but not in all cases; more data are required to fit more complex models to the measured data.

Resorting to the inhomogeneous models, which are able to describe non-uniform magnetization distributions and their signatures, one has considerably more freedom to estimate the realistic magnetization distribution, yielding a lower prediction error. By using a heuristic method of regularization that effectively drastically reduces the number of unknowns but nevertheless is

able to model a wide range of magnetization distributions, we have been able to estimate the magnetization distribution through time that minimizes the global squared signature error. Unfortunately, we have not been able to estimate hysteresis parameters in the inhomogeneous case.

From our results, we can conclude that the ellipsoid exhibits all three aspects that were a priori established as interesting variations of models. This is concluded on the basis of the signature prediction error decreasing with model complexity increasing; indeed, the more flexible the model is in terms of both spatial and temporal range, the more accurately it can describe the very complex behaviour of the experimental steel ellipsoid.

Most of our knowledge in the current research, honesty compels us to say, has been *experiential*. That is, by tweaking and modifying several classes of models bit by bit, we have been able to get a thorough understanding of them and the role of underlying parameters. This is why the 'quantifiable' aspect of our main research goal lacks a bit of substance. However, the apparatus is there to perform many model simulations, twin experiments and model extensions.

This brings us to the subject of Recommendations.

10.2 Recommendations

During this research, we encountered many uncertainties and have made many choices leading to this final report. It is hard to guess the evolution of such a research beforehand, which has been a very sobering but also enlightening experience. Let us discuss our recommendations in the same order as the topics covered in the current thesis.

10.2.1 Homogeneous models

Effectively, we have formulated and analyzed five different forward ellipsoid models, of which one is linear and four are nonlinear (**IP**, **RA**, **JA**and **EV**). One aspect of the forward homogeneous models that has not received much attention, is the initialisation of these models. Although unnecessary in the linear and **IP**model, the other three models all have some sort of 'compatibility criterion' at the start: Indeed, in the real world, the start of an hysteresis model is not really the starting point at all. Rather, the material at hand has probably already undergone several hysteresis loops. We have some thoughts on initialising homogeneous models by applying a 'negative-time' applied field, such that the model arrives at a coherent and physical situation, where the three interdependent quantities $\mathbf{H}$, $\mathbf{M}$ and $\mathbf{H}_a$ are physically realistically interrelated. In the **EV**model, we have already implemented this because of the necessity of the **EV**model to build forth on realistic previous cell magnetizations.
We recommend investigating more efficient inversion algorithms for inverting homogeneous models. Instead of minimizing the total sum of signature errors, one could employ an increments-based procedure, which adjusts estimates real-time. Moreover, in all models except the **EV**model, adjoint parameter estimation procedures have been proposed, since the gradient of the magnetization evolution with respect to the model parameters is relatively easily derived numerically by incrementing parameters locally and computing the magnetization increment. We have contemplated these routes, but nevertheless chose the relatively less efficient method of genetic algorithms. However, these genetic algorithms have the big advantage of being able to escape local minima. Further investigation is required.
Strictly speaking, we have not proven the validity of the incremental ellipsoid formula as well

as the validity of the ellipsoid formula in anisotropic circumstances. Perhaps the proof is relatively straightforward, but it would be reassuring to know that our approach is also warranted mathematically.
The **EV**model has not been inverted, although over the course of the current project, some ideas came up, which the original authors had not mentioned. The **EV**model is built on the principle of a weighted superposition of elementary magnetized cells, which tempts us to think that there should exist some kind of decomposition technique to estimate the weights and friction parameters of the **EV**model more directly.
The **EV**model was found to have great potential in terms of flexibility but also in terms of extendibility. That is, since the **EV**model starts from an energy balance, principally other energy terms related to magnetism could be added, for example stress-related terms or temperature. These could be related to material magnetization and magnetic fields, yielding different equations but perhaps very elegant model evolutions.

10.2.2 Inhomogeneous models

Our FEM implementation of the ellipsoid magnetization, exhibits a systematic error that would not vanish. We recommend anyone familiar with the FEM to look at our procedure. Perhaps, an interface boundary condition was neglected, or similar problems should be analysed using the vector magnetic potential rather than the scalar potential. In the Results and Discussion chapter, we also proposed some plausible explanations of this persistent annoyance.
Experiment with different basis functions in order to find a reliable set with good generalisation properties.
Look into more complex regularization techniques.
Investigate more reliable solvers than the standard `Matlab` backslash solver.
Develop more realistic boundary conditions by matching the FEM boundary conditions to infinite domain or multilayer techniques.
Use higher order elements or radically different elements to model the region that is close to the ellipsoid boundary.

10.2.3 General recommendations

Investigate the use of another signature error objective function on the basis of real research on concrete naval mines.
Perform research on magnetic meso-domains in order to propose a realistic set of inhomogeneous magnetization basis functions to estimate the non-uniform magnetization.
Perform many more measurements using the CLAViS.
Rather than point estimates of optimal parameters, use the spatial linear and incrementally nonlinear magnetization evolution to develop a Bayesian framework for parameter density estimation.
In order to estimate a density of hysteresis parameters, employ adjoint approaches such as in weather forecasting.

10.2.4 Outlook towards Data-Assimilation and Degaussing

The models that we have implemented, can be extended to include data assimilation and the possibility of non-uniform background fields. Indeed, for an evolving magnetic signature, one can estimate the hysteresis parameters based on previous increments. With knowledge of the applied background field, an estimate can be made about the next system state. By using

signature measurements, this same state can be estimated by inverse static magnetization estimations. Combining these two approaches, yields a reliable way of predicting the magnetization - and thus signature evolution of the ellipsoid. This way, incrementally improving the estimation of both hysteresis parameters, magnetization distribution and thus the complete state of the model, the data assimilation dream is reached.
Inhomogeneous background fields can be analysed by employing the discretized unstructured divergence operator on the (then extra) term $\nabla \mathbf{H}_a$. This way, degaussing coils produce such non-uniform fields that are included in the finite element computations. Then, a model prediction can be performed using the previously described data-assimilation approach. This model prediction can be internally corrected by applying a sequence of non-uniform applied fields, which is a step towards active signature minimization.

Bibliography

[1] Eugene P. Wigner. The unreasonable effectiveness of mathematics in the natural sciences. richard courant lecture in mathematical sciences delivered at new york university, may 11, 1959. *Communications on Pure and Applied Mathematics*, 13(1):1–14, 1960.

[2] John David Jackson. *Classical Electrodynamics*. John Wiley and Sons, Inc., 1999.

[3] Joao Pedro A. Bastos and Nelson Sadowski. *Magnetic Materials and 3D Finite Element modelling*. CRC Press, Taylor and Francis Group, 2014.

[4] Daniela Calvetti and Erkki Somersalo. *Introduction to Bayesian Scientific Computing*. Springer, 2007.

[5] J.M.D. Coey. *Magnetism and Magnetic Materials*. Cambridge University Press, 2009.

[6] Alexander G. Ramm. *Inverse Problems: Mathematical and Analytical Techniques with Applications to Engineering*. Springer, 2004.

[7] Victor Isakov. *Inverse Problems for Partial Differential Equations*. Springer, 2017.

[8] David Jiles. *Introduction to Magnetism and Magnetic Materials*. Chapman and Hall, 1991.

[9] Richard Phillips Feynman. *The Feynman Lectures on Physics*. Basic Books, the millennium edition edition, 2011.

[10] J.J. Holmes. *Modelling a Ship's Ferromagnetic Signatures*. Springer US, 2007.

[11] J.J. Holmes. *Reduction of a Ship's Magnetic Field Signatures*. Springer US, 2008.

[12] J.J. Holmes. *Exploitation of a Ship's Magnetic Field Signatures*. Springer US, 2006.

[13] Steven H. Simon. *The Oxford Solid State Basics*. Oxford University Press, 01 2013.

[14] Jianming Jin. *The Finite Element Method in Electromagnetics*. IEEE Press, 2002.

[15] Yu Zhu and Andreas Cangellaris. *Multigrid Finite Element Methods for Electromagnetic Field Modeling*. IEEE Press, 2006.

[16] J Dunning-Davies. *Concise thermodynamics: Principles and applications in physical science and engineering*. Albion Thermodynamics Science Series, 01 2008.

[17] Sushin Chikazumi and Stanley H. Charap. *Physics of Magnetism*. Robert E. Krieger Publishing Company, 1964.

[18] J. van Kan, A. Segal, and F.J. Vermolen. *Numerical Methods in Scientific Computing*. Delft Academic Press / VSSD, 2014.

[19] Philip M. Morse and Herman Feshbach. Methods of theoretical physics. *American Journal of Physics*, 22(6):410–413, 1954.

[20] James Clerk Maxwell. A dynamical theory of the electromagnetic field. *Philosophical Transactions of the Royal Society of London.*, 155(1):459–512, 1865.

[21] D.C. Jiles and D.L. Atherton. Theory of ferromagnetic hysteresis. *Journal of Magnetism and Magnetic Materials*, 61(1-2):48–60, 1986.

[22] F. Preisach. Uber die magnetische nachwirkung. *Zeitschrift für Physik*, 94:277–302, 1935.

[23] Lord Rayleigh. On the behaviour of iron and steel under the operation of feeble magnetic forces. *Philos. Mag.*, 23(225), 1887.

[24] M. Kachniarz and R. Szewczyk. Study on the rayleigh hysteresis model and its applicability in modelling magnetic hysteresis phenomenona in ferromagnetic materials. *12th SMMM*, 2016.

[25] Faycal Ikhouane Mohammed Ismail and Jose Rodellar. The hysteresis bouc-wen model, a survey. *Arch. Comput. Methods Eng*, 16:161–188, 2009.

[26] J. D. Jackson. From lorenz to coulomb and other explicit gauge transformations. *American Journal of Physics*, 70(9):917–928, 2002.

[27] J. A. Osborn. Demagnetizing factors of the general ellipsoid. *Phys. Rev.*, 67:351–357, Jun 1945.

[28] Alessandra Manzin Oriano Bottauscio, Mario Chiampi. Homogenized magnetic properties of heterogeneous anisotropic structures including nonlinear media. *IEEE Transactions on Magnetics*, 45(10):3946–3949, 2009.

[29] R. Szewczyk, C. Zielinski, and M. Kaliczynska. *Recent Advances in Automation, Robotics and Measuring Techniques*. Springer International Publishing Sqitzerland, 2014.

[30] Peter G. Lelievre and Douglas W. Oldenburg. Magnetic forward modeling and inversion for high susceptibility. *Geophys. J. Int.*, 166:76–90, 2006.

[31] Diego Takahashi and Vanderlei C. Oliveira Jr. Ellipsoids: 3d magnetic modelling of ellipsoidal bodies. *Geoscientific Model Development*, 10:3591–3608, 2017.

[32] Leonid Prigozhin and Vladimir Sokolovsky. Fft-based solution of 2d and 3d magnetization problems in type-ii superconductivity. *Superconductor Science and Technology*, 31(5), 2018.

[33] Emanuelle Lima, Andrei Irimia, and John Wikswo. The magnetic inverse problem. *The SQUID Handbook Vol. 2*, 2:139–267, 12 2006.

[34] Marius Birsan. Recursive bayesian method for magnetic dipole tracking with a tensor gradiometer. *IEEE Transactions on Magnetics*, 47(2), 2011.

[35] Riccardo Scorretti, Ruth Sabariego, Fabien Sixdenier, Benjamin Ducharne, and Marie Raulet. Integration of a new hysteresis model in the finite elements method. *Proceedings of the 18th Conference on the Computation of Electromagnetic Fields*, 07 2011.

[36] Pedro Melo and Rui Araújo. An overview on preisach and jiles-atherton hysteresis models for soft magnetic materials. In *Technological Innovation for Smart Systems*, pages 398–405, 03 2017.

[37] Anders Bergqvist. Magnetic vector hysteresis model with dry friction-like pinning. *Physica B: Condensed Matter*, 233(4):342 – 347, 1997. Hysteresis Modeling and Micromagnetism.

[38] V. Francois-Lavet, F. Henrotte, L. Stainier, L. Noels, and C. Geuzaine. Vectorial incremental nonconservative consistent hysteresis model. *Fifth International Conference on Advanced Computational Methods in Engineering*, 47(2), 2011.

[39] L. Prigozhin, V. Sokolovsky, J. W. Barrett, and S. E. Zirka. On the energy-based variational model for vector magnetic hysteresis. *IEEE Transactions on Magnetics*, 52(12):1–11, Dec 2016.

[40] A. J. Bergqvist. A simple vector generalization of the jiles-atherton model of hysteresis. *IEEE Transactions on Magnetics*, 32(5):4213–4215, Sep. 1996.

[41] Jean V. Leite, Abdelkader Benabou, and Nelson Sadowski. Accurate minor loops calculation with a modified jiles-atherton hysteresis model. *COMPEL - The international journal for computation and mathematics in electrical and electronic engineering*, 28(3):741–749, 2009.

[42] Xuefeng Zhao, Jia Lu, and Madhavan L. Raghavan. Identifying heterogeneous anisotropic properties in cerebral aneurysms: a pointwise approach. *Biomech Model Mechanobiol.*, 10:177–189, 2011.

[43] P Queffelec, David Bariou, and Philippe Gelin. A predictive model for the permeability tensor of magnetized heterogeneous materials. *Magnetics, IEEE Transactions on*, 41:17 – 23, 02 2005.

[44] G. Lei, P. C. Dong, S. Y. Mo, S. Yang, Z. S. Wu, and S. H. Gai. Calculation of full permeability tensor for fractured anisotropic media. *Journal of Petroleum Exploration and Production Technology*, 5(2):167–176, Jun 2015.

[45] N. Demerdash, T. Nehl, and F. Fouad. Finite element formulation and analysis of three dimensional magnetic field problems. *IEEE Transactions on Magnetics*, 16(5):1092–1094, Sep. 1980.

[46] A. Benabou, S. Clénet, and F. Piriou. Comparison of preisach and jiles–atherton models to take into account hysteresis phenomenon for finite element analysis. *Journal of Magnetism and Magnetic Materials*, 261(1):139 – 160, 2003.

[47] Krzysztof Chwastek. Higher order reversal curves in some hysteresis models. *Archives of Electrical Engineering*, 61(4):455 – 470, 2012.

[48] D. C. Jiles, J. B. Thoelke, and M. K. Devine. Numerical determination of hysteresis parameters for the modeling of magnetic properties using the theory of ferromagnetic hysteresis. *IEEE Transactions on Magnetics*, 28(1):27–35, Jan 1992.

[49] Nicusor Pop and Ovidiu Caltun. Jiles-atherton magnetic hysteresis parameters identification. *Acta Physica Polonica Series a*, 120, 09 2011.

[50] Sergey E. Zirka, Yuriy I. Moroz, Robert G. Harrison, and Krzysztof Chwastek. On physical aspects of the jiles-atherton hysteresis models. *Journal of Applied Physics*, 112(4):043916, 2012.

[51] Grzegorz Szymański and Michał Waszak. Vectorized jiles–atherton hysteresis model. *Physica B: Condensed Matter*, 343(1):26 – 29, 2004. Proceedings of the Fourth International Conference on Hysteresis and Micromagnetic Modeling.

[52] Mohammad Asif Zaman, Paul C. Hansen, Lars T. Neustock, Punnag Padhy, and Lambertus Hesselink. Adjoint method for estimating jiles-atherton hysteresis model parameters. *Journal of Applied Physics*, 120(9):093903, 2016.

[53] Y. Vuillermet, O. Chadebec, J. Coulomb, L. Rouve, G. Cauffet, J.P. Bongiraud, and L. Demilier. Scalar potential formulation and inverse problem applied to thin magnetic sheets. *IEEE Transactions on Magnetics*, 44(6):1054–1057, June 2008.

[54] O. Biro, K. Preis, and K. R. Richter. On the use of the magnetic vector potential in the nodal and edge finite element analysis of 3d magnetostatic problems. *IEEE Transactions on Magnetics*, 32(3):651–654, May 1996.

[55] Colleen M. Witzenburg and Victor H. Barocas. A nonlinear anisotropic inverse method for computational dissection of inhomogeneous planar tissues. *Computer Methods in Biomechanics and Biomedical Engineering*, 19(15):1630–1646, 2016. PMID: 27140845.

[56] Gabriella Bolzon and Marco Talassi. An effective inverse analysis tool for parameter identification of anisotropic material models. *International Journal of Mechanical Sciences*, 77:130 – 144, 2013.

[57] Jonas Adler and Ozan Öktem. Solving ill-posed inverse problems using iterative deep neural networks. *Inverse Problems*, 33(12):124007, nov 2017.

[58] Fioralba Cakoni and David Colton. A uniqueness theorem for an inverse electromagnetic scattering problem in inhomogeneous anisotropic media. *Proceedings of the Edinburgh Mathematical Society*, 46(2):293–314, 2003.

[59] E.S.A.M. Lepelaars, S.A. Synnes, and P.A. Brodtkorb. Representing the ship magnetic field using prolate spheroidal harmonics - a comparative study of methods. *IEEE Transactions on Magnetics*, 47(2), 2011.

[60] Aad Vijn, Eugene Lepelaars, Johan Dubbeldam, Martin van Gijzen, and Arnold Heemink. Magnetic susceptibility estimation for magnetostatics. *IEEE Transactions on Magnetics*, 55(3):1–9, 2019.

[61] Rafal Biedrzycki, Dorota Jackiewicz, and Roman Szewczyk. Reliability and efficiency of differential evolution based method of determination of jiles-atherton model parameters for x30cr13 corrosion resisting martensitic steel. *Journal of Automation, Mobile Robotics and Intelligent Systems*, 8(4), 2014.

[62] Muzaffar Eusuff, Kevin Lansey, and Fayzul Pasha. Shuffled frog-leaping algorithm: a memetic meta-heuristic for discrete optimization. *Engineering Optimization*, 38(2):129–154, 2006.

[63] J Baldwin Jr. Rayleigh hysteresis—a new look at an old law. *Magnetics, IEEE Transactions on*, 14:81 – 84, 04 1978.

[64] A. Magni, C. Beatrice, G. Durin, and G. Bertotti. Stochastic model for magnetic hysteresis. *Journal of Applied Physics*, 86(6):3253–3261, 1999.

[65] R. G. Harrison. A physical model of spin ferromagnetism. *IEEE Transactions on Magnetics*, 39(2):950–960, March 2003.

[66] M. Bosack, J. Kollmer, B. Niemoczynski, and S. Biswas. Closed loop control of hysteretic magnetization. In *2014 7th International Symposium on Resilient Control Systems (ISRCS)*, pages 1–6, Aug 2014.

[67] P. Palmesi, L. Exl, F. Bruckner, C. Abert, and D. Suess. Highly parallel demagnetization field calculation using the fast multipole method on tetrahedral meshes with continuous sources. *Journal of Magnetism and Magnetic Materials*, 442:409 – 416, 2017.

[68] Franz Lang and Stephen J. Blundell. Fourier space derivation of the demagnetization tensor for uniformly magnetized objects of cylindrical symmetry. *Journal of Magnetism and Magnetic Materials*, 401:1060 – 1067, 2016.

[69] Dmitri Chernyshenko and Hans Fangohr. Computing the demagnetizing tensor for finite difference micromagnetic simulations via numerical integration. *Journal of Magnetism and Magnetic Materials*, 381:440 – 445, 2015.

[70] S. Tandon, M. Beleggia, Y. Zhu, and M. De Graef. On the computation of the demagnetization tensor for uniformly magnetized particles of arbitrary shape. part ii: numerical approach. *Journal of Magnetism and Magnetic Materials*, 271(1):27 – 38, 2004.

[71] R Moskowitz and Edward Della Torre. Theoretical aspects of demagnetization tensors. *Magnetics, IEEE Transactions on*, 2:739 – 744, 01 1967.

[72] A. V. Farahani and A. Konrad. An iterative method to obtain nonuniform field distribution in magnetic substrates. *IEEE Transactions on Magnetics*, 41(10):3316–3318, Oct 2005.

[73] Ian Berkman. Ferromagnetic hysteresis in ship's steel, analysis of the preisach and jiles-atherton models. TNO Internship Report, December 2017.

[74] O.C.O. Baas. Nonlinear behaviour of ferromagnetic steel. Msc thesis, TU Delft, 2018.

[75] Radoslav Jankoski. *Stochastic modelling of Magnetic Properties by Using Random Fields*. PhD thesis, Technische Universität Darmstadt, 2012.

[76] Massimiliano d'Aquino. *Nonlinear Magnetization Dynamics in Thin-films and Nanoparticles*. PhD thesis, Universita degli studi di Napoli, 2004.

[77] M. d'Aquino, G. Rubinacci, A. Tamburrino, and S. Ventre. Efficient numerical solution of magnetic field problems in presence of hysteretic media for nondestructive evaluation. *IEEE Transactions on Magnetics*, 49(7):3167–3170, July 2013.

[78] Sarah Hamilton, Matti Lassas, and Samuli Siltanen. A direct reconstruction method for anisotropic electrical impedance tomography. *Inverse Problems*, 30, 02 2014.

[79] Andrew J. Newell, Wyn Williams, and David J. Dunlop. A generalization of the demagnetizing tensor for nonuniform magnetization. *Journal of Geophysical Research: Solid Earth*, 98(B6):9551–9555, 1993.

[80] A.R.P.J. Vijn. Inverse modelling for magnetic signature monitoring of naval ships. Msc thesis, TU Delft, 2016.

[81] Zoltan Nagy. Numerical approaches to 3d magnetic mems. Msc thesis, ETH Zürich, 2006.

[82] A.C. Lumadjeng. Determination of the magnetic background field on naval ships, 2017. BSc Thesis TU Delft.

[83] M.W. Schaaphok. A data-driven model for magnetostatics, 2018. BSc Thesis.

[84] Ji-Ming Peng. Equivalence of variational inequality problems to unconstrained minimization. *Mathematical Programming*, 78(3):347–355, Sep 1997.

[85] J. J. Moreau. Application of convex analysis to the treatment of elastoplastic systems. In Paul Germain and Bernard Nayroles, editors, *Applications of Methods of Functional Analysis to Problems in Mechanics*, pages 56–89, Berlin, Heidelberg, 1976. Springer Berlin Heidelberg.

[86] Arnold Neumaier. Solving ill-conditioned and singular linear systems: A tutorial on regularization, 1994. Lecture Notes.

[87] John K. Hunter. Notes on partial differential equations. Lecture Notes in a course by Mark Veraar at TU Delft.

[88] Jan Willem Polderman. Optimal control: Course notes, 2004. MSc Course TU Enschede.

[89] Aad Vijn. Macroscopic hysteresis model for the general ellipsoid, 2018. Private Notes.

[90] E.S.A.M. Lepelaars. Static magnetic signature variation, 2011. TNO Internal Restricted Report.

[91] H.W.L. Naus. Magnetic signatures of ships, 2011. TNO Overview Report.

[92] D Bekers and E.S.A.M. Lepelaars. Degaussing system design optimization, 2013.